ELECTRICAL PROPERTIES

AND

DEFECT STRUCTURE

OF

UO_2-CeO_2 SOLID SOLUTIONS

by

Thomas George Stratton

B.A.,Concordia College,Moorhead MN
(1978)

Submitted to the Department of
Material Science and Engineering
in Partial Fulfillment of the Requirements
for the Degree of

DOCTOR OF PHILOSOPHY

at the

MASSACHUSETTS INSTITUTE OF TECHNOLOGY

Febuary 1984

Signature of Author .....
Department of Materials Science and Engineering,
13 January 1984

Certified by.....
H.L.Tuller, Thesis Supervisor

Accepted by.....
Chair, Departmental Committee on Graduate Students

ELECTRICAL PROPERTIES AND DEFECT STRUCTURE OF UO_2-CeO_2 SOLID SOLUTIONS

by
Thomas G. Stratton

Submitted to the Department of Material Science and Engineering on January 13,1984 in partial fulfillment of the requirements for the Degree of Doctor of Philosophy in Ceramics

ABSTRACT

Following an extensive study of electrical properties of compositions including $Ce_{.999}U_{.001}O_{2\pm x}$, $Ce_{.99}U_{.01}O_{2\pm x}$, $Ce_{.95}U_{.05}O_{2\pm x}$, $Ce_{.05}U_{.95}O_{2\pm x}$, $Ce_{.031}U_{.969}O_{2\pm x}$, and $Ce_{.015}U_{.985}O_{2\pm x}$ coupled with a development of a detailed chemical model an extensive series of defect parameters has been determined, which establish the generation of both intrinsic and defect formation energies formed during deviation from stoichiometry. For example, the reaction constants for both oxidation and reduction have been dertermined. Although analysis of the urania rich members of this solid solution is complicated by signifigant defect association, a model is proposed to qualitatively fit the experimental results.

Electrical transport characteristics have been discussed. Furthermore, electronic transport by electrons or holes was characterized by polaron conduction. This was established by measurment of a thermally activated mobility:

$\mu = (226/T) \exp(-0.31\pm.05 \text{ ev}/k_bT)$ ceria rich

$\mu = (1.46/T) \exp(-.31\pm.05 \text{ ev}/k_bT)$ urania rich

This corresponds to a value of 0.01 (cm^2/Vs)for ceria rich and 0.068 (cm^2/Vs) for urania rich at 1000°C.

Analysis has been performed by TEP vs ln in the region of partially occupied bands. Extrema of the curves are predicted and this is compared with experiment. Parameters used to obtain a fit to experiment suggest that polaron-polaron site exclusion is substantial in ceria rich compositions. On the other hand, in urania rich materials no similar observation was made. In uranis rich compositions a simple relation for the slope of the TEP vs. ln is observed at low doping concentration.

Thesis Supervisor: Dr. H.L. Tuller
Title: Associate Professor of Ceramics

CONTENTS

LIST OF FIGURES

LIST OF TABLES

ACKNOWLEDGEMENTS

I would like to thank Professor Harry Tuller for his encouragment and support during my five years as a reserch assistant in his group. I would also like to thank Pat Kearney for his help and advise whhich greatly facilitated experimental work. I would like to thank my wife Bev for her continual support and encouragement. I would also like to thank my parents who have helped in every way they could.

Several People have provided stimulating discussions about both science and the world in general:

Mike Barsoum
Dunbar Bernie
Dan Button
Dan Goldschmidt
Wayne Hasz
Asif Iqubal
Anna McHale
Stan Rotman
Mike Wargo
Brian Zelinski

and many others.

Several groups have helped make life at MIT enjoyable:

The Lutheran Minisry in Higher Education at MIT

The Ceramics Graduate Students
The Cape Cod Cubs
The Brotaslava Bruins
The Skinned Knees
Cobles Creepers

The work of the following people is greatly appreciated:

Technical Typists: Linda Sayegh and Susan Rosevear.
Proof Reader: Missy Daniels.

I INTRODUCTION

Defects in solids play a critical role in determining many materials properties. Electrical conductivity, dielectric constant and breakdown strength, magnetic properties, optical properties, ionic diffusion, and corrosion resistance are all affected by the concentration and type of defects. Tailoring a material to fit a particular application, therefore, requires a detailed understanding of the defect chemistry and the relations between the defects and the property of interest. Some important aspects of the defect chemistry of a material include the conditions necessary to establish a given stoichiometry; e.g., temperature and atmosphere, the concentration of intrinsic defects at stoichiometry, the band gap energy, and the primary current carrying defects.

Even though the importance of defects has been known for more than 20 years, a complete and detailed description of the defect equilibria is not available for any material. This is a result of (a) the tendency for materials to be either readily reduced or oxidized, thereby becoming either oxygen deficient or excess; and (b) the existence of low intrinsic defect concentrations in typical ceramics resulting in the masking of intrinsic properties by impurities. A prime objective of this thesis will be to demonstrate that I have been able to overcome these limitations in the urania-ceria solid solution system and thereby uniquely provide a detailed picture of the defect

equilibria both close and far removed from stoichiometry. This was made possible by combining two systems which individually tend to deviate from stoichiometry in the direction of oxygen excess (UO_{2+x}) and the direction of oxygen deficiency (CeO_{2-x}).

Aside from the nature of the defects, the issue of electron transport is of considerable interest given the nature of the bands derived from f-orbitals in both ceria and urania. This study has confirmed and characterized small polaron motion in this system and examined in some detail the results of combined electrical conductivity and thermoelectric power data.

Urania is an extensively studied material with the fluorite crystal structure. The material is of great technological importance as a nuclear fuel and has also been suggested as an electrode material for fuel cells and as an oxygen selective membrane[1]. Ceria has also been studied for its high oxygen ion conductivity.[2] It has not been observed at stoichiometry because of its strong tendency to become oxygen deficient.

The urania-ceria system has several characteristics which together make it a unique model system for a study of the defect structure and electronic transport. At the urania rich end, the material tends to be oxygen rich and a p type semiconductor. At the ceria rich end, on the other hand, the material becomes oxygen deficient and an n type

semiconductor. Both end members tend to be highly non-stoichiometric. CeO_2 and UO_2 form a complete solid solution at elevated temperatures. This combination, therefore, provides a unique system in which to examine the defect chemistry of both oxygen deficient and oxygen excess compositions, and both n-type and p-type conduction in a single crystal structure.

This study makes use of previously published spectroscopic data to determine the relative ionization levels for cerium and uranium in the UO_2-CeO_2 solid solutions and relates them to the resultant electrical properties. Special emphasis is placed on observing the ceria-urania system on both sides of stoichiometry. To accomplish these tasks, measurements of the electrical conductivity and thermoelectric power as a function of PO_2, temperature, and composition were made. Although these are techniques which do not directly provide information about the ionic defects in solids, important information about these ionic defects may be derived from defect models developed for these systems. In the following section, I review the literature concerned with structure, defects and electrical properties of the ceria and urania end members.

LITERATURE REVIEW

A CRYSTAL AND DEFECT STRUCTURE

The crystal structure of a material has significant influence on the defect chemistry and the electrical properties. The local ionic coordination affects the energy of defect formation and ionization. Also the overall crystal stucture may be perturbed locally by the existence of defects and defect associations. The following section examines previous work on the crystal structure of CeO_2, UO_2, and the solid solution.

The defect structure of the end members gives insight to the expected defects in the solid solution. The following section also examines previous work on the defect structure of the ceria and the urania systems.

CRYSTAL STRUCTURE OF URANIA AND CERIA

The crystal structure of both urania and ceria is the well-known fluorite structure, Figure II.A.1. This structure can be represented as a simple cubic anion lattice with every other interstitial position filled with a cation. This results in a fairly open structure capable of supporting large concentrations of defects. Both urania and ceria exhibit large deviation from stoichiometry.[3-8] Examination of the respective phase diagrams demonstrates that ceria exhibits oxygen deficiency with x in CeO_{2-x} as large as 0.3 at 1000C,(Figure II.A.2[9]) while

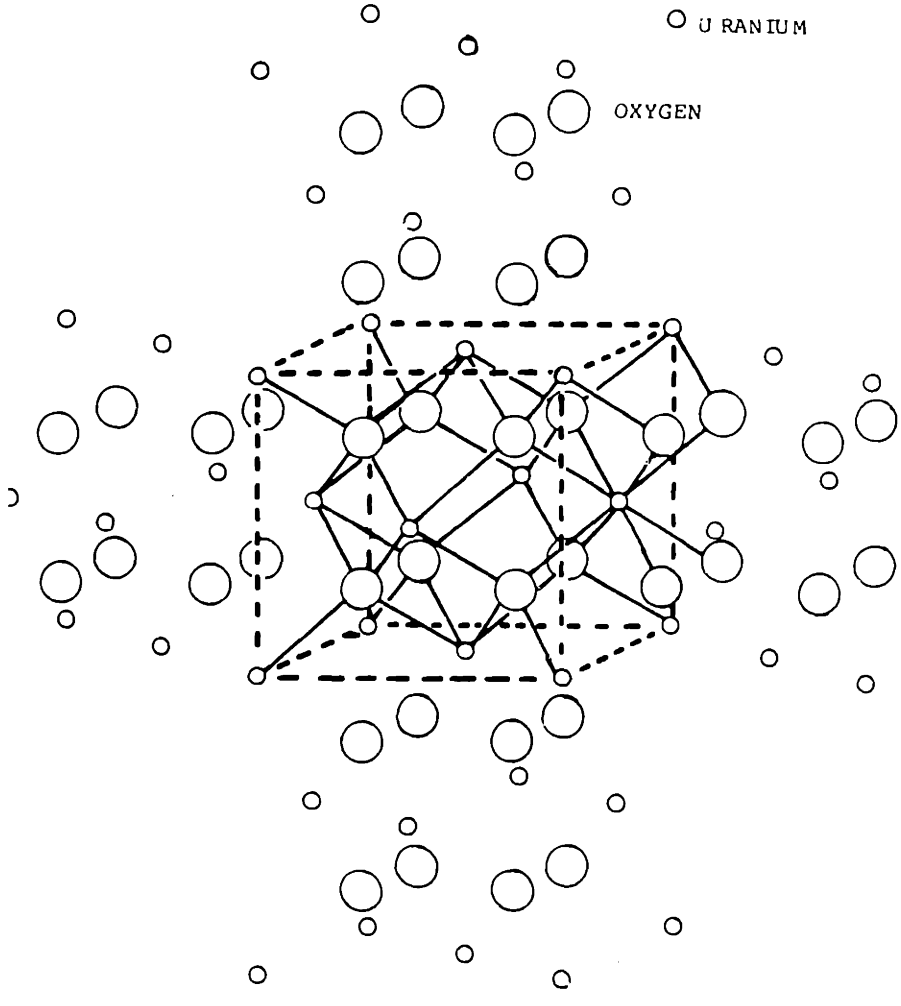

Figure II.A.1 Fluorite crystal sructure.

urania exhibits oxygen excess with x in UO_{2+x} as large as 0.25 at 1200C,(Figure II.A.3[10]).

DEFECTS AND DEFECT INTERACTIONS IN URANIA AND CERIA

At large concentrations of defects, clusters form in both urania and ceria.[6,11] The Bevan cluster, Figure II.A.4[13], is composed of two oxygen vacancies on opposite corners of a cube with a cerium ion in the center. The Willis cluster present in urania is shown in Figure II.A.5[1]. This cluster consists of one or more oxygen interstitial ions displaced from the 1/2,1/2,1/2 position along the [110] axis and lattice oxygen ions displaced along the [111] direction forming two oxygen vacancies and two oxygen interstitials. The cluster is usually denoted (a:b:c) where a is the number of [111] and b the number of [110] oxygen interstitials, and c is the number of vacant oxygens. For example the (2:1:2) cluster has 2 interstitials displaced along the [111] direction, 2 vacant oxygen sites, and 1 interstitial displaced along the [110] direction. Associated with such a cluster are charge compensating holes on the uranium cations.

The thermodynamic data for UO_2 related to deviation from stoichiometry was extensively reviewed by Kroger[13] some time ago, who concluded that no single defect chemical model could account for all the data. Catlow[14] has since performed theoretical calculations on defects in UO_2 which suggest that excess oxygen is present as fully charged

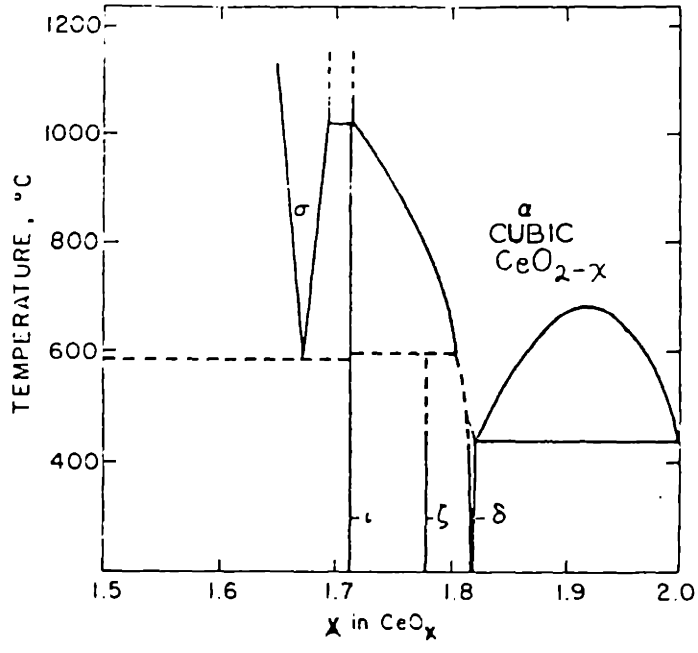

Figure II.A.2 Phase diagram for CeO_{2-x}[9].

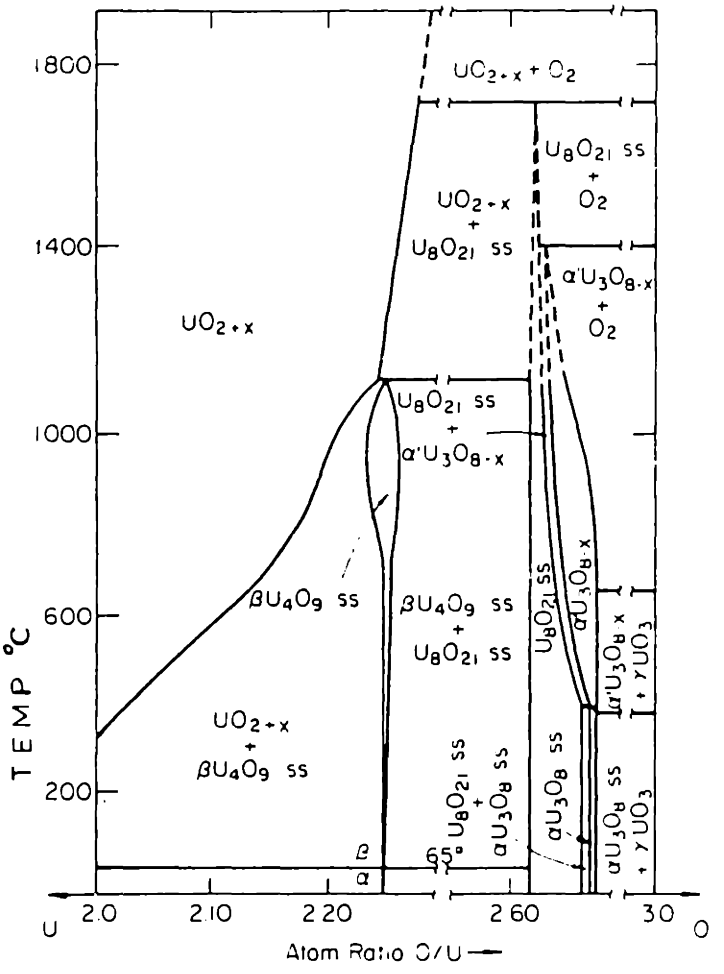

Figure II.A.3 Phase diagram for UO_{2+x}[10].

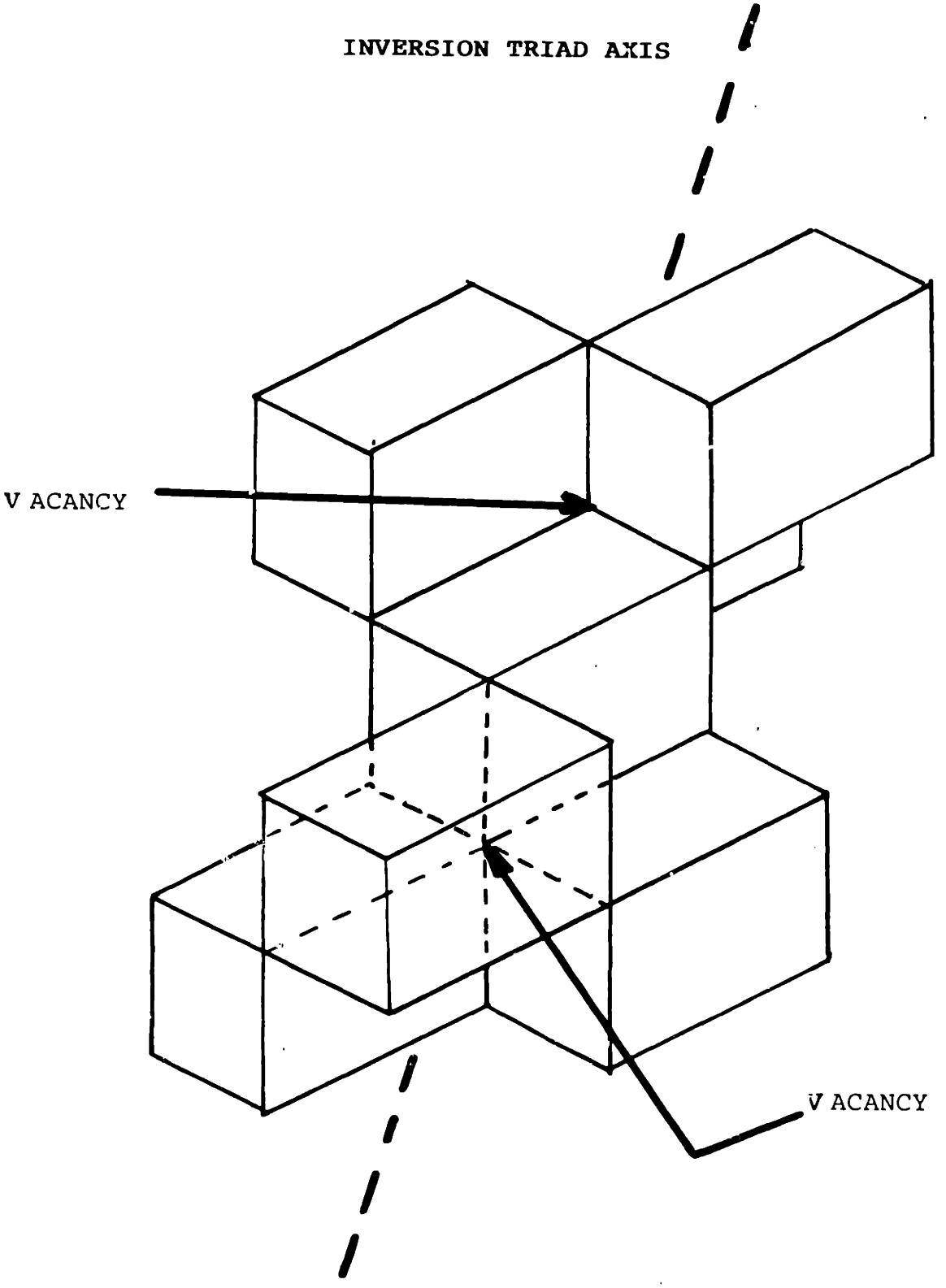

Figure II.A.4 Diagram of a Beven Cluster[7]

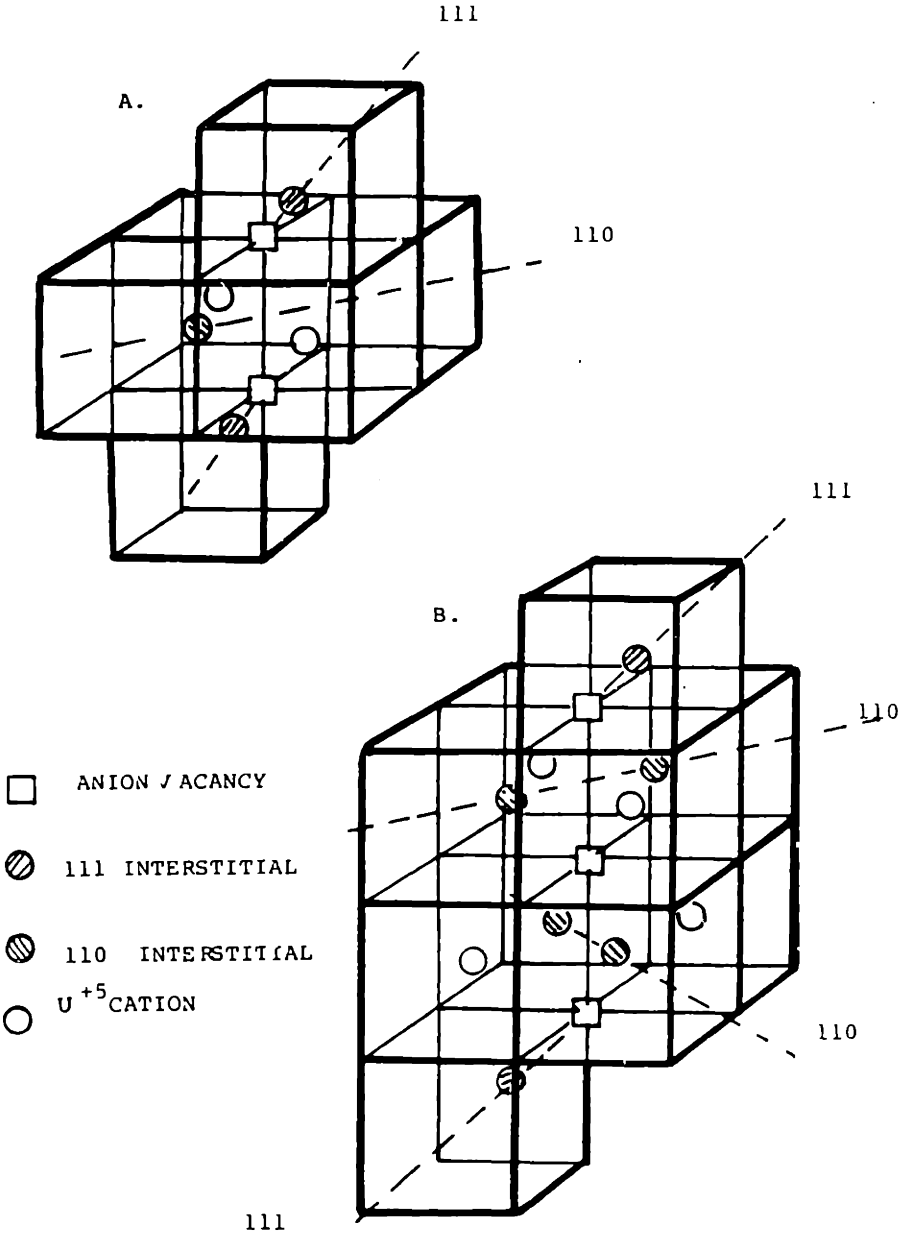

Figure II.A.5 Diagram of two types of Willis clusters[1].
A. (2:1:2).
B. (4:3:2).

oxygen interstitials; and that the band gap is about 2ev, the same value as used by Kroger. Catlow, however, suggested that the oxygen interstitial lies below the valence band in UO_2. Catlow also calculated relative energies for different Willis clusters concluding that the (2,1,2) cluster predominates for interstitial concentrations of about 1m/o.

ELECTRICAL PROPERTIES OF URANIA

Several authors have reported measurements of the electrical conductivity of UO_2[15-25]. Willardson et al.[15] measured electrical conductivity and thermoelectric power (TEP) of poly-crystalline samples over the temperature range of 25 to 600°C. The oxygen partial pressure was not well controlled, and the samples were not in equilibrium as was evident by the change of the TEP of some samples from n type conduction to p type on subsequent equilibration above 200C. The calculated activation energy of conduction for the p-type sample was about 0.37ev, a questionable value given the lack of equilibration.

Nagels et al.[16] measured the electrical conductivity of single crystal UO_2 over the temperature range from 20 to 800°C. Again, the PO_2 was not well controlled and irreversible changes occured at low temperatures. At higher temperatures, the activation energy for conductivity was between 0.34 and 0.19ev with the activation energy decreasing with increasing conductivity, a consequence of

increased oxygen content. Attempts to measure a Hall voltage were unsuccessful, thereby placing an upper bound on the Hall mobility of $0.015 cm^2 v^{-1} s^{-1}$. All measurements were made as a function of temperature assuming that the composition of each sample remained constant and temperature independent.

Aronson et al.[17] measured the electrical conductivity and TEP of sintered pellets over the temperature range from 500 to 1150°C. The results were interpreted in terms of an electron hopping model with data fitting the following relations

$$\sigma \text{ (ohm cm)}^{-1} = [(3.8e6)(2x)(1-2x)\exp(-0.3\pm0.03ev/(kT)))]/T$$

and

$$TEP = (k/e)\ln((1-2x)/2x)$$

Again, these measurements were also performed as a function of temperature assuming a constant composition. Measurements performed at even higher temperatures[25] have shown a change of the activation energy from about 0.3 to about 1.0ev with a transition temperature of 1000-1200C. The higher activation energy was correlated with intrinsic electron-hole generation with no account being made for possible contributions from nonstoichiometry. This change in activation energy has also been linked to a change of

the conduction mechanism from p to n-type.

The conductivity of UO_{2+x} was measured by Ishii et al.[22] as a function of PO_2 and temperature. The incorporation of oxygen as doubly ionized interstitials was confirmed by correlation of electrical conductivity with weight change data. The results showed a very steep PO_2 dependence of the conductivity and were interpreted in terms of interstitial molecular oxygen with holes hopping between these defects.

Killeen[23] measured the electrical conductivity and TEP of pure and Nb_2O_5 doped UO_2 over a temperature range of from 25 to 1520°C with the PO_2 controlled with H_2/H_2O mixtures. As a result, all data was obtained at very low PO_2's. The conductivity data shows significant hysterysis below 700°C during changes of temperature at the same H_2/H_2O ratio. The TEP was measured as a function of temperature in dry H_2. A p to n transition is observed as the temperature is raised with the transition temperature decreasing from about 1050°C in pure UO_2 to about 800°C in 0.5% doped UO_2. This data is interpreted as indicating that pure urania is characterized by hole type small polaron transport below about 1100°C and and n type semiconduction above 1100C. Again, it should be emphasized that the data was taken under very reducing conditions at constant H_2/H_2O ratio which is unlikely to result in constant composition.

Dudney et al.[24] measured the conductivity of pure

and yttria doped UO_2 as a function of PO_2 at temperatures in the range of 800 to 1401°C. Their results show that the p type conductivity of urania is enhanced by the addition of yttria. For doping levels below 1m/o, the conductivity at low PO_2 is directly related to the yttria concentration; and the mobility of the holes is 0.06 to 0.085 cm^2/Vs with an activation energy of about 0.2ev. Dudney et al.[26] also confirmed that the p type conduction of UO_2 had no significant contribution from ionic conduction.

From the above results, the following observations may be made. UO_2 is a p type semiconductor in the temperature range from 800 to 1100C. Conduction occurs by an activated process with a mobility consistent with small polaron theory. Above 1100°C a mechanism change occurs resulting in an increase of the apparent activation energy for conduction.

ELECTRICAL PROPERTIES OF CERIA

The electrical properties of CeO_2 have been investigated by Tuller and Nowick[27] and by Naik and Tien[28]. Tuller and Nowick measured the electrical conductivity as a function of PO_2 over a temperature range of from 625 to 1500°C. These results, confirmed by Naik and Tien, show that CeO_2 is an n type semiconductor with electrons compensating for singly or doubly charged oxygen vacancies, depending on temperature and oxygen partial pressure. The electrical conductivity was found to be

consistent with a small polaron mechanism with the electron mobility equal to 2.2×10^{-3} to 8.1×10^{-3} cm^2/Vs at 1000C. The activation energy for mobility was found to have a value of about 0.39 ev at low x and increased to about 0.5ev at large deviations from stoichiometry. Tuller and Nowick [29] also measured the TEP of CeO_2 with fixed deviation from stoichiometry and found it to be independent of temperature. Given the activated nature of the conductivity under identical conditions, this demonstrated that the mobility was activated.

At very large deviations from stoichiometry, the conductivity of CeO_2 decreases with increasing deviation from stoichiometry. This was explained by Tuller and Nowick as being the result of oxygen vacancy trapping of electrons resulting in a decrease in the effective concentration of carriers. Tuller and Nowick also observed a decrease of the TEP at high PO_2 which they attributed to an ionic contribution due to vacancies, a conduction mechanism wellknown to be important for CeO_2 doped with lower valent cations.

Naik and Tien[30] also measured the electrical conductivity of CeO_2 doped with Nb_2O_5 as a function of PO_2 over a temperature range of from 805 to 1420°C. Their results indicate that Nb_2O_5 enhances the electronic conductivity. Weight change measurements made on the same compositions indicate that oxygen interstitial compensation

for the Nb_2O_5 is important at high PO_2. However, comparison with results of Tuller and Nowick for pure CeO_2 indicates that if oxygen interstitial incorporation is as important as the weight change data indicate, then a region of PO_2 dependent conductivity should have been seen at high PO_2 and low temperature. No such region was observed. Furthermore, measurable weight change which should have occured at $PO_2 \gtrsim$ latm was not observed.

URANIA CERIA SOLID SOLUTION PHASE DIAGRAM

Urania and ceria are materials with the same crystal structure and similar cationic radii, (Ce^{+4}=1.01A, U^{+4}=.97A)[31], and it is thus not surprising that they form an extensive solid solution. The urania ceria phase diagram has been studied by Markin and Street[32] and by Lorenzelli and Touzelin[33]. Both sets of investigators report that UO_2-CeO_2 form complete solid solutions at elevated temperatures with a lattice parameter which has a very slight negative deviation from Vegard's law. They report that a two phase field does, however, form in this system at low PO_2's. This is an extension into the ternary of the two phase field present in pure CeO_{2-x}.(Figure I.A.6)[32]

NONSTOICHIOMETRY OF URANIA CERIA SOLID SOLUTIONS

The thermodynamics of the deviation from stoichiometry of the ceria-urania system has been studied by several investigators[34,37]. These investigators used

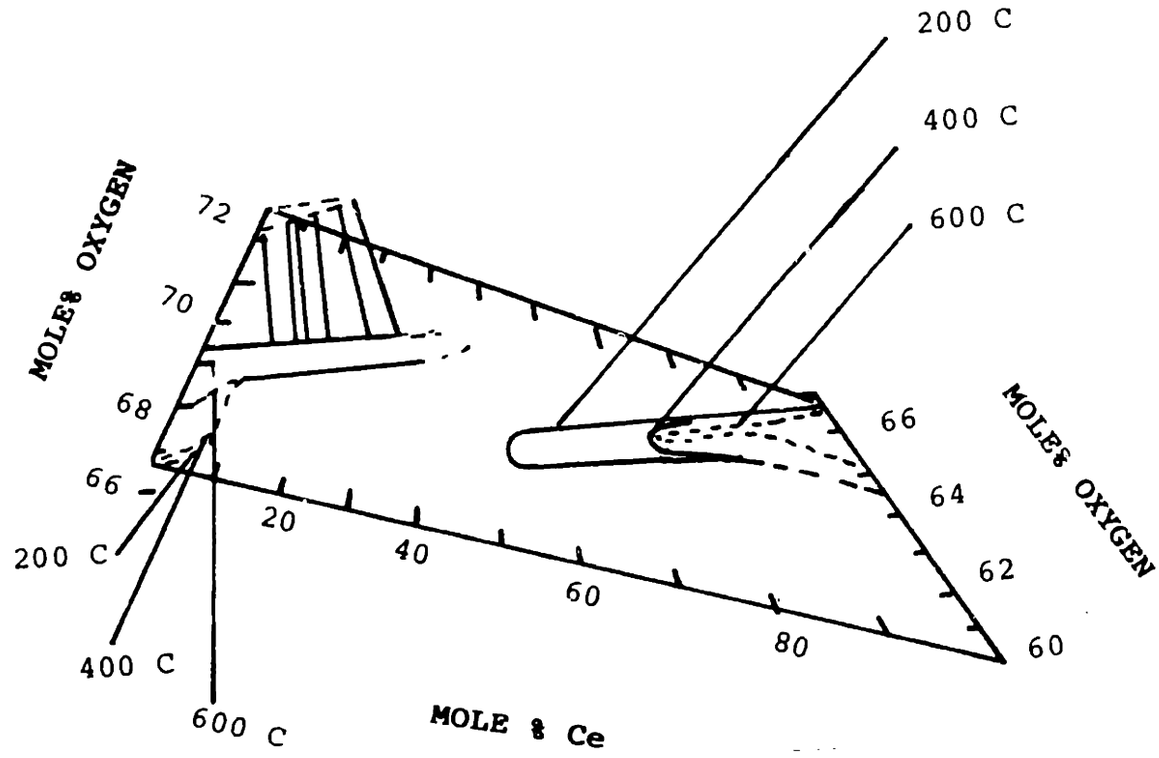

Figure II.A.6 Phase diagram of U-Ce-O system[32].

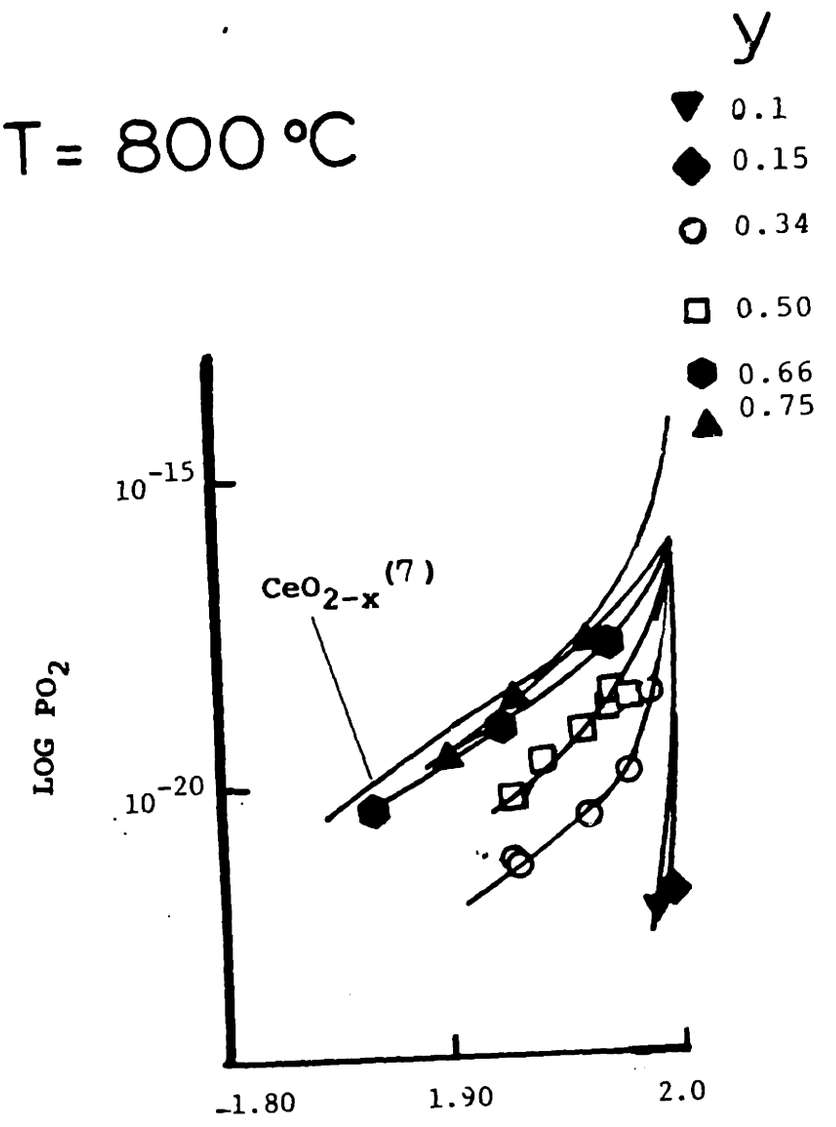

Figure II.A.7 Log PO_2 vs O/M ratio for $Ce_yU_{1-y}O_2$ (35).

either weight gain/loss as a function of PO_2[34,35] or electrochemical titration[36,37] to determine the stoichiometry as a function of PO_2. The results indicate a change of stoichiometry between that of UO_2 and CeO_2 with differences depending on the ratio of Ce to U in the solid solution. The results suggest that as urania is added to ceria rich compositions, they will have a deviation from stoichiometry closer and closer to that of pure urania (see Figure II.A.7)[35].

A signifigant problem with these studies is the identification of the stoichiometric composition. All the studies assume that equilibration of the sample at 800 to 850°C in CO/CO_2 = 1/1 mixtures(PO_2 = $3.7x10^{-19}$ Atm) results in a stoichiometric sample. This value is chosen based on the observation that under these conditions, both ceria and urania exhibit little weight change as a function of PO_2. However, this is clearly an inappropriate reference condition based on Tuller and Nowick's[27] observations that ceria is already oxygen deficient at a PO_2 equal to one atm at 800C. Furthermore, in these materials, and in materials in general, the PO_2 at which stoichiometry occurs is a function of both temperature and composition.

In summary, urania ceria solid solutions are expected to exhibit deviations from stoichiometry somewhere between the end members. The conductivity is expected to be by a small polaron mechanism of either the hole or electron

type. Contributions to the conductivity from ionic carriers are expected to be more important in oxygen deficient rather than in oxygen excess material.

B. ELECTRONIC STRUCTURE

The electronic structure, including electronic band gap, fermi energy, conduction and valence band widths; and the energy of defect species is critical to the understanding of electrical conductivity and nonstoichiometry. Below we review the information available for UO_2 and CeO_2.

A number of techniques have been used to examine the band structure of these materials. They include X-ray Photoelectron Spectroscopy, Bremsstrahlung Isochromat Spectroscopy, and optical absoption and reflectance spectroscopy. Based on the analysis of the data from these techniques, we have determined the relative ionization energy for uranium and cerium in the ceria urania system.

URANIA

A compilation of experimentally determined electronic structures for UO_2 is shown in Figure II.B.1. The diagrams are displayed in arbitrary density units and aligned to the fermi level with diagrams of the same workers to the same scale. The general features of the band structure include an O2p deep valence band, a $U5f^2$ valence band, and conduction band.

Optical absorption measurements made by Ackerman et al.[38], Figure II.B.2b, show a steep rise in the absorption coefficient between 1.8 and 3.1 ev. and were interpreted by Veal and Lam[39] to suggest a band gap of

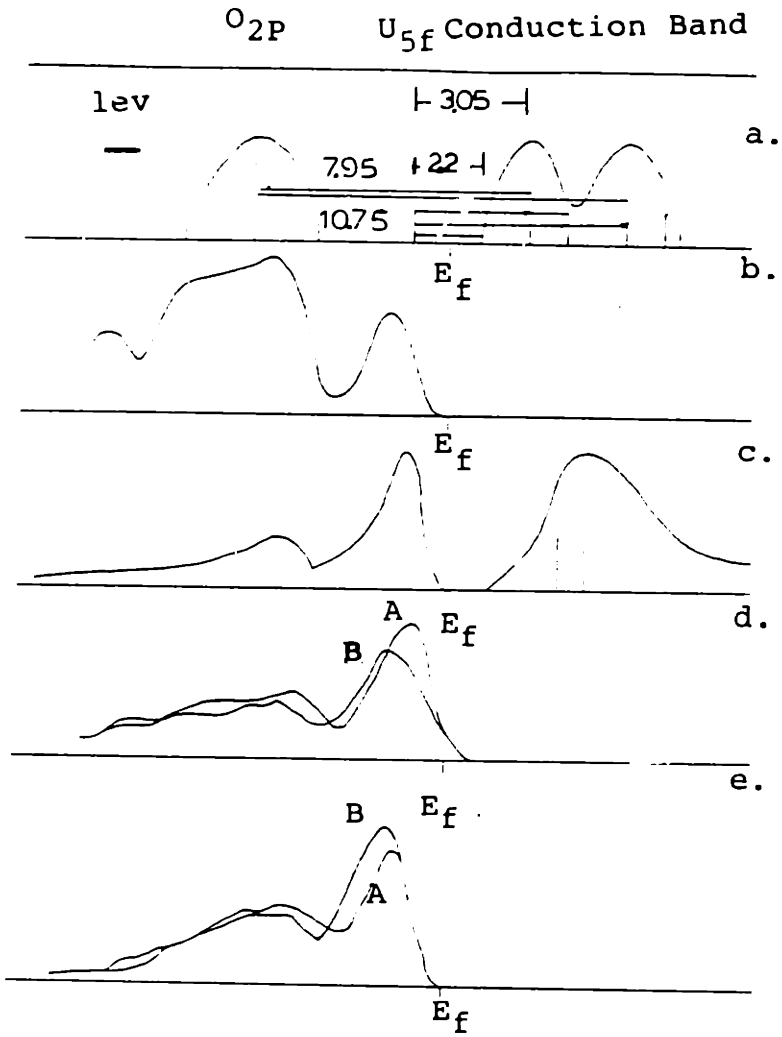

Figure II.B.1 Experimentally determined electronic structures for UO_2.

a. Schoenes[40] Proposed structure based on reflectance measurements.
b. Norton et al.[43] XPS spectra.
c. Baer and Schoenes[42] XPS and BIS Sectra.
d. Veal and Lam[39] XPS spectra A. Oxidized, B. Reduced.
e. Allen et al. XPS spectra A. Oxidized, B. Reduced.

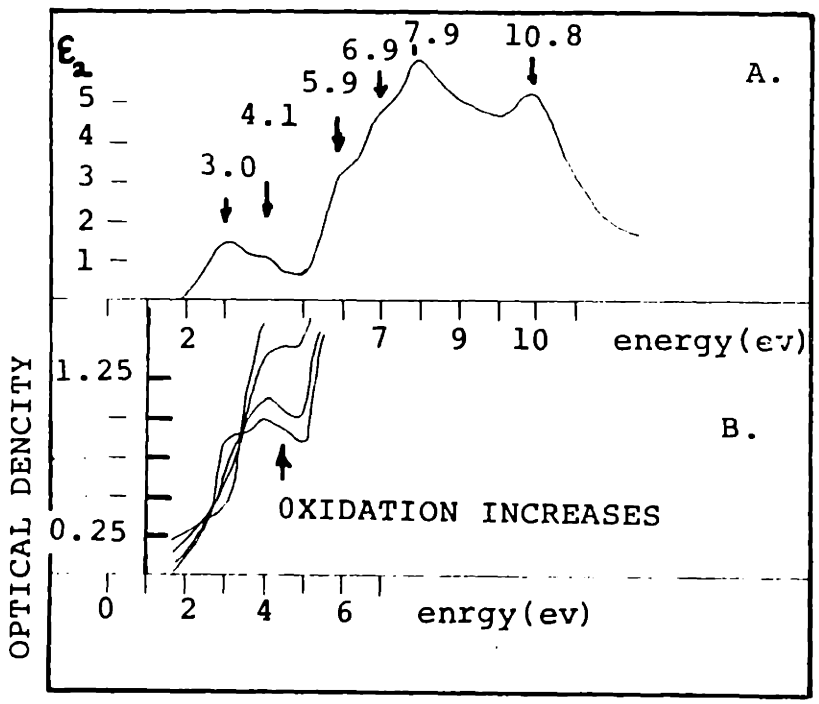

Figure II.B.2 Optical data.
a. Schoenes[40] optical reflectance.
b. Ackerman et al.[38] optical absorption.

about 2.8 ev. Schoenes[40] measured near normal incident reflection of single crystals and made the transition assignments shown in Figure II.B.2a, which are in reasonable agreement with the 3.1ev gap calculated by Wood, Boring and Woodruff[41].

Veal and Lam[39] Figure II.B.2d, Byaer and Schoenes[42] Figure II.B.2c, Norton et.al.[43] Figure II.B.2b, and Allen et.al.[44] Figure II.B.2e used X-ray Photoemission Spectroscopy (XPS) to investigate the valence band structure of UO_2 and place the O2p band peak 3.5 ev below the 5f peak, with the U5f peak at approximately one ev below the fermi level. Byaer and Schoenes also use Bremsstrahlung Isochromat Spectroscopy (BIS) to probe the conduction band. Their results suggest that the high energy tail of the U5f valence band and the low energy tail of the conduction band are only separated by 1.4ev.

Ackerman et al.[38], Veal and Lam[39], and Allen et al.[44] have reported small changes in the electronic structure with changes in oxidation. Veal and Lam reported a decrease of the O2p XPS intensity and a shift of the U5f valence band away from the fermi level with increased reduction produced by sputtering (Figure II.B.2d.), Allen et al.[44] report a corresponding effect. Under stronger oxidizing conditions, the O2p peak 4.7ev below the fermi level increases intensity, and the U5f peak 1.4 ev below the fermi level decreases and shifts closer to the fermi level

by about .1 ev. (Figure II.B.2e). Ackerman et al.[38] report an increased intensity of transition at 300 mu(4.12ev) with oxidation, and a transition at 430mu(2.876ev) that decreases with oxidation (Figure II.B.1b). Transitions at about 3 ev and 4 ev are also seen in the ϵ_2 plot of Schoenes (Figure II.B.1a).

The assignment by Schoenes of the 4 ev transition to a U-U transition is inconsistent with the strong dependence on stoichiometry observed by Ackerman et. al.[38]

Catlow[14] has calculated that the oxidation of UO_2 occurs by the incorporation of doubly ionized oxygen interstitials and suggests that reduction occurs by singly charged oxygen vacancies.

No one model has been suggested which is consistent with all of the above data; however, three properties of the electronic structure of UO_2 are clear. First, the highest filled band is a urania 5f band very close to the fermi level. Second, an energy gap for conduction of about 2ev is present between this band and the lower edge of the conduction band. Third, the oxidation of urania results in an increased electron density about 4ev below the fermi level. This last property suggests that the oxygen interstitials are about 4ev below the fermi level. The simplified band diagram is shown in Figure II.B.3a.

CERIA

There is much less information about the

Figure II.B.3 Simplified band diagrams.
a. $UO_{2\pm x}$.
b. $CeO_{2\pm x}$.
c. Combined.

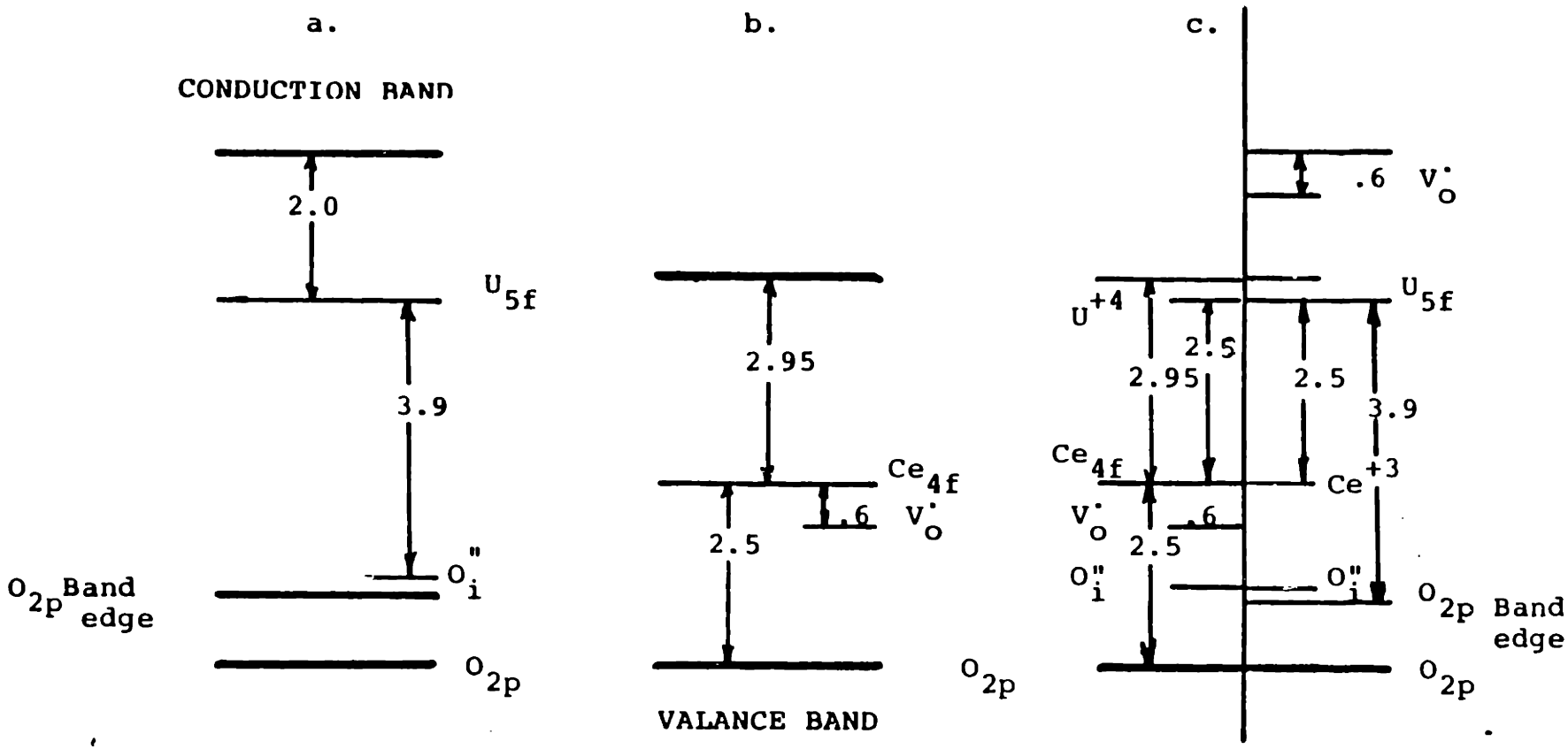

electronic structure of CeO_2. Hass, Ramsey, and Thun[45] measured optical absorption on CeO_2 thin films. Their work was interpreted by Vinokurov et al.[46] to indicate a band gap of 5.2 to 5.5 ev. Andreeva and Gilman[47] report a band gap of 5.5 ev but also report an absorption at 2.95 ev that they attribute to a transition from the Ce^{+3} to the conduction band. This indicates that the band gap which is important for electrical conduction in CeO_2 is about 2.5. Based on the work of Tuller and Nowick the $V_O^{\cdot\cdot}$ defect is approximately .56 ev below the Ce 4f. By combining this with the assumption that the $V_O => V_O^{\cdot\cdot} + e$ has a small energy, the $V_O^{\cdot}$ should occur about0.6 ev below the Ce4f level. The simplified band diagram is shown in Figure II.B.3.4.

SOLID SOLUTIONS OF URANIA-CERIA

Figure II.B.3 combines the information presented above with the energies aligned with the top of the O2p band. The alignment of the bands on the O2p is reasonable and is based on observation that the top of the O2p level is non bonding and thus shifts little during compound formation.[48] The Ce^{3+} lies about 1.5ev below the $U5f^2$ level and about 2.5 ev above the O2p band edge.

The O_i'' level is essentially an oxygen-like state and should occur in CeO_2 at about the same energy with respect to the O_{2p} as it does in UO_2. The uncharged oxygen vacancy is a missing oxygen and two extra electron positioned on the nearest neighbor metal ions. This level takes on the

character of a cation like level. The energy of the ionized oxygen vacancy is that energy needed to remove these electrons to the conduction band. Therefore, while in ceria the $V_O^{\cdot}$ lies .6 ev below the $4f^1$ level, it is expected that in urania it will lie 1.4ev above the $5f^2$ level (0.6ev below the conduction band). The simplified combined band diagram is shown in Figure II.B.3c.

The most important aspect of the above analysis is the relative ionization energies of cerium and uranium, illustrated in Figure II.B.4. The cerium, lying significantly below the uranium, should act as an ionized acceptor at all temperatures in urania-rich solid solutions. Similarly, U^{5+}, lying significantly above the $Ce4f^1$ level, should act as a singly ionized donor at all temperatures in ceria.

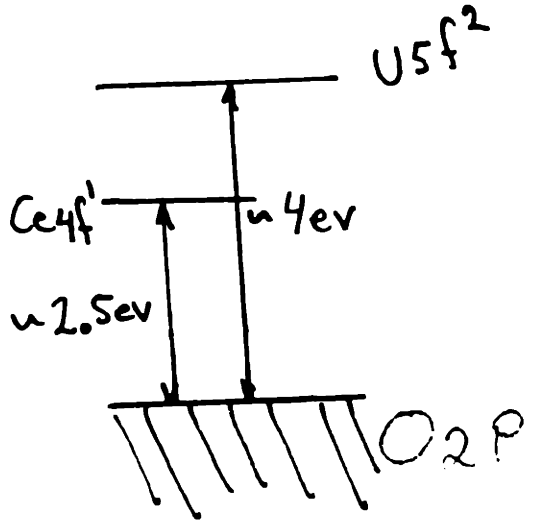

Figure II.B.4
Relative Ionizations of
uranium and cerium in cubic fluorite

III DEFECT AND TRANSPORT THEORY

A. DEFECT MODEL

In this section models of the defect chemistry of U doped CeO_2 and Ce doped UO_2 based on mass action relations of point defects in an ideal solution will be developed. This type of analysis was first applied to solids by Wagner and Schotty[49] and was made significantly more useful by the introduction of what is now called Kroger Vink notation,[50] which will be used in the following analysis. This analysis has been applied to a wide variety of materials[51-54]. The power of this analysis lies in the interrelationships between the defects species. Often the concentration of one defect may be inferred from the concentrations of other defects. Similarly, the PO_2 dependencies, or the changes of the PO_2 dependences of a defect species, provide information about the PO_2 dependence or the concentrations of other defects.

The following assumptions are made. First, the defects are present in low concentrations; e.g., an ideal solution model. The defect activities may then be replaced by concentrations which are related through simple reaction constants. Although this assumption is not valid over the entire range of compositions and experimental conditions to be discussed, it serves as a starting point. Second, all but the most likely defects are ignored. This leaves a system which is both useful and tractable.

A.1 CERIA RICH SOLID SOLUTIONS

The relative ionizations of uranium and cerium determined above suggest that the uranium will remain ionized over the entire range of accessible oxygen partial pressures. Similarly, the oxygen interstitial lies well below the Uranium; therefore, it is expected that as long as uranium and oxygen interstitials are the prevalent ionic defects, the oxygen interstitials will remain fully ionized. It is well known that[6] CeO_2 is an oxygen deficient material while isostructural UO_2 generally has excess oxygen.[3] These two facts suggest that the most important intrinsic ionic defects will be vacancies, V_O, and interstitial oxygen ions, O_i. Uranium dopant ions on ceria sites (U_{Ce}) are assumed to be singly ionized. Electrons (e) and holes (h) will also be considered.

Initially, the following defects will be considered in CeO_2:

$$O_i'' \ , V_O^{\cdot\cdot} \ , \ V_O^{\cdot} \ , \ e' \ , \ h^{\cdot} \ , \ U_{Ce}^{\cdot}$$

The ionization states of uranium and oxygen are chosen based on the above analysis of the electronic structure (Chapter II.B). The ionization for the vacancies was chosen based on previous work of Tuller and Nowick[27]. Given these defects, the following quasichemical defect reactions may be written:

$$O_O^x = O_i'' + V_O^{\cdot\cdot} \quad \text{Frenkel Pair Production (II.A.1.1)}$$

$null = e' + h^{\cdot}$ Electron Hole Pair Production (III.A.1.2)

$O_O^X = V_O^{\cdot\cdot} + 2e' + 1/2O_2\ (g)$ Reduction Reaction (III.A.1.3)

$1/2O_2 g = O_i'' + 2h^{\cdot}$ Oxidation Reaction (III.A.1.4)

$V_O^{\cdot} = V_O^{\cdot\cdot} + e'$ Second Ionization of Oxygen Vacancies (III.A.1.5)

$U_{Ce} = U_{Ce}^{\cdot} + e'$ Ionization of Uranium Ions (III.A.1.6)

Using the above assumptions, the following equilibrium equations may be written:

$[O_i''][V_O^{\cdot\cdot}] = K_1$ (III.A.1.7)

$np = K_2$ (III.A.1.8)

$[V_O^{\cdot\cdot}]n^2 PO_2^{1/2} = K_3$ (III.A.1.9)

$PO_2^{1/2}/([O_i'']p^2 = K_4 = K_3/(K_1K_2^2)$ (III.A.1.10)

$[V_O^{\cdot\cdot}]n/[V_O^{\cdot}] = K_5$ (III.A.1.11)

$[U_{Ce}^{\cdot}]n/[U_{Ce}] = K_6$ (III.A.1.12)

Square brackets indicate concentrations, and the Ks are equilibrium constants and are functions of temperature only. To these equations the electroneutrality and conservation of dopant constraints may be added:

$n + 2[O_i''] = p + 2[V_O^{\cdot\cdot}] + [V_O^{\cdot}] + [U_{Ce}^{\cdot}]$ (III.A.1.13)

$[U_{Ce}^{*}] + [U_{Ce}^{\cdot}] = [U_{Ce}]_{total} = U_T$ (III.A.1.14)

The solution to the above eight simultaneous equations specifies the defect concentration of all defects in terms of the equilibrium constants and PO_2. To ease solution it is possible to solve the equations in a piecewise linear manner by eliminating all but the two defects with the highest concentrations from the electroneutrality equation. This approximation is known as the Brouwer approximation.[55] The solutions to the above equations under the Brouwer approximation are presented in Table III.A.1.1. Each region is specified by the controlling electroneutrality condition and is labeled by number.

The usefulness of these types of relations can be seen, for example, by examining the electron concentration (n). At low oxygen partial pressures, region I, n is proportional to $PO_2^{-1/4}$, whereas in the intermediate region III, n is not dependent on PO_2. Therefore, from the PO_2 dependence, the controlling defect region can generally be identified. Once the region is known, the relation between defects is established. The equations specifying the PO_2 of the boundaries at the corresponding transitions between regions are given in Table III.A.1.2. These are very useful relations because they enable calculations of the reaction constants without concern about mobility dependence of the charge carying species on defect densities.

The previous analysis is significantly simplified by

Table III. A.1.1

Defect concentration for CeO_2 doped with UO_2 $\mathcal{K} = K_6 K_3^{-1/2} K_1^{1/2} PO_2^{1/2}$

Regions	I	II	III	IV	V
controlling electroneutrality equation	$n = [V_O^{\cdot}]$	$2[V_O^{\cdot\cdot}] = n$	$n = [U_{Ce}^{\prime}]$	$2[O_i^{\prime\prime}] = [U_{Ce}^{\prime}]$	$2[O_i^{\prime\prime}] = P$
PO_2 range	low	intermediate	intermediate	intermediate	high
$[V_O^{\cdot\cdot}]$	K_5	$2^{-2/3} K_3^{1/3} PO_2^{-1/6}$	$K_3 \left(\frac{-K_6 + \sqrt{K_6^2 + 4U_T K_6}}{2} \right)^{-2} PO_2^{-1/2}$	$2^{-2} K_1 \left[2 + 2\mathcal{K}^{-1} \pm \sqrt{(-2-2^{-1/2}\mathcal{K}^{-1})^2 - 4} \right]^{-1}$	$2^{2/3} K_3^{1/3} K_1^{2/3} K_2^{-2/3} PO_2^{-1/6}$
$[V_O^{\cdot}]$	$K_3^{1/2} K_5^{-1/2} PO_2^{-1/4}$	$2^{7/3} K_3^{2/3} K_5^{-1} PO_2^{-1/3}$	$K_3 \left(\frac{-K_6 + \sqrt{K_6^2 + 4U_T K_6}}{2} \right)^{-1} PO_2^{-1/2}$	$2^{-1} K_5^{-1} K_3^{1/2} K_1^{1/2} \left[(2+2\mathcal{K}^{-1}) \pm \sqrt{(-2-2^{-1/2}\mathcal{K}^{-1})^2 - 4} \right]^{1/2} PO_2^{1/4}$	$2^{1/3} K_1^{1/3} K_2^{-1/3} PO_2^{-1/3}$
n	$K_3^{1/2} K_5^{-1/2} PO_2^{-1/4}$	$2^{+1/3} K_3^{+1/3} PO_2^{-1/6}$	$\frac{-K_6 + \sqrt{K_6^2 + 4U_T K_6}}{2}$	$2K_1^{1/2} K_3^{-1/2} \left[(2+2\mathcal{K}^{-1}) \pm \sqrt{(-2-2^{-1/2}\mathcal{K}^{-1})^2 - 4} \right] PO_2^{-1/4}$	$K_2^{1/3} 2^{-1/3} K_3^{1/3} K_1^{-1/3} PO_2^{-1/6}$
P	$K_2 K_3^{-1/2} K_5^{1/2} PO_2^{1/4}$	$2^{-1/3} K_3^{-1/3} K_2 PO_2^{1/6}$	$K_2 \left(\frac{-K_6 + \sqrt{K_6^2 + 4U_T K_6}}{2} \right)^{-1}$	$2^{-1} K_2 K_3^{-1/2} \left[(2+2\mathcal{K}^{-1}) \pm \sqrt{(-2-2^{-1/2}\mathcal{K}^{-1})^2 - 4} \right]^{-1/2} PO_2^{1/4}$	$2^{-5/3} K_3^{-1/3} K_1^{1/3} K_2^{2/3} PO_2^{1/6}$
$[O_i^{\prime\prime}]$	$K_1 K_5^{-1}$	$2^{2/3} K_1 K_3^{-1/3} PO_2^{1/6}$	$K_1 K_3^{-1} \left(\frac{-K_6 + \sqrt{K_6^2 + 4U_T K_6}}{2} \right)^2 PO_2^{1/2}$	$2^{-2} \left[(2+2\mathcal{K}^{-1}) \pm \sqrt{(-2-2^{-1/2}\mathcal{K}^{-1})^2 - 4} \right]$	$2^{-2/3} K_3^{-1/3} K_1^{1/3} K_2^{2/3} PO_2^{1/6}$
$U_{Ce}^{\prime}$	$\frac{U_T (K_6 K_3^{-1/2} K_5^{1/2} PO_2^{1/4})}{1 + (K_6 K_3^{-1/2} K_5^{1/2} PO_2^{1/4})}$	$\frac{2^{-1/3} K_3^{-1/3} K_6 PO_2^{1/6} U_T}{1 + (2^{-1/3} K_3^{-1/3} K_6 PO_2^{1/6} U_T)}$	$\frac{-K_6 + \sqrt{K_6^2 + 4U_T K_6}}{2}$	$2^{-1} \left[(2+2\mathcal{K}^{-1}) \pm \sqrt{(-2-2^{-1/2}\mathcal{K}^{-1})^2 - 4} \right]$	$\frac{2^{1/3} K_6 K_2^{-1/3} K_3^{-1/3} K_1^{1/3} PO_2^{1/6}}{1 + 2^{1/3} K_6 K_1^{1/3} K_2^{2/3} PO_2^{1/6}}$

TABLE III.A.1.2

BOUNDARIES FOR REGION DESCRIBED IN TABLE III.A.1.1

REGION	I-II	II-III	III-IVA	IVA-IVB
DEFECTS WHICH ARE EQUAL AT THE BOUNDARY	$[V_O^{\cdot}] = 2[V_O^{\cdot\cdot}]$	$2[V_O^{\cdot\cdot}] = [U_{Ce}^{\cdot\cdot}]$	$U_{Ce}^{\cdot} = 2[O_I^{\prime}]$	$[U_{Ce}] = 1/2 U_{Ce\ total}$
P_{O_2}	$2^{-4} K_3^2 K_5^{-6}$	$2^2 K_3^2 \left(-K_6 + \sqrt{K_6^2 + 4U_T K_6}\ /2\right)^{-6}$	$2^{-2} K_1^{-2} K_3^2 K_6^{-2} U_T^{-4} \left(-K_6 + \sqrt{K_6^2 + 4U_T K_6}\ /2\right)^6$	$2^{10} K_1^{-2} K_2^{-4} K_3^2 U_T^6$

assuming that the urania ions are all singly ionized $U_T = [U_{Ce}]$). This is a reasonable assumption given the uranium lies well above the Ce level. Table III.A.1.3 lists the solutions to the simultaneous equations. The equations specifying the boundaries between regions are listed in Table III.A.1.4. Figure III.A.1.1 shows schematically the defect concentrations for urania doped ceria.

The sharp change of slope at the boundaries between regions in Figure III.A.1.1 is an artifact of the Brower aproximation. Real materials exhibit smooth transitions from one defect regime to another, therefore to determain the PO_2 of the boundary extrapolations of the curves from a PO_2 which is clearly in one region to the intersection must be used. This must be done from both the high and the low PO_2 sides of the boundary. If data from both sides of the boundary is not available then curve fitting techniques may be used to determain the reaction constants. This will be discussed in detail in chapter VI.

The reaction constants defined above are stricktly defined only for one composition. As the composition changes with addition of urania the reaction constants may change. For example the energy to form an oxygen vacancy next to a uranium ion may be higher than the energy needed to form an oxygen vacancy next to a cerium ion. If this is the case then the reaction constant may change with uranium doping. Since pure uranium is known to deviate from stoichiometry to oxygen excess it is expected that

Table III. A.1.3

Defect concentrations for CeO_2 doped with UO_2 - Assuming $U_T=[U'_{ce}]$

Regions	I	II	III	IV	V
electroneutrality equation	$n = [V_O^{\cdot}]$	$2[V_O^{\cdot\cdot}] = n$	$n = [U'_{ce}] = U_T$	$2[O''_i] = [U'_{ce}]$	$2[O''_i] = \rho$
PO_2 range	low	intermediate	intermediate	intermediate	high
$[V_O^{\cdot\cdot}]$	K_5	$2^{-2/3}K_3^{1/3}PO_2^{-1/6}$	$K_3U_T^{-2}PO_2^{-1/2}$	$2K_1U_T^{-1}$	$2^{2/3}K_3^{1/3}K_1^{2/3}K_2^{-2/3}PO_2^{-1/6}$
$[V_O^{\cdot}]$	$K_3^{1/2}K_5^{-1/2}PO_2^{-1/4}$	$2^{7/3}K_3^{2/3}K_5^{-1}PO_2^{-1/3}$	$K_3U_T^{-1}PO_2^{-1/2}$	$2^{1/4}K_5^{-1}K_3^{1/2}K_1^{+1/2}U_T^{-1/2}PO_2^{-1/4}$	$2^{1/3}K_1^{1/3}K_2^{-1/3}PO_2^{-1/3}$
n	$K_3^{1/2}K_5^{-1/2}PO_2^{-1/4}$	$2^{+1/3}K_3^{+1/3}PO_2^{-1/6}$	U_T	$2^{-1/4}K_3^{1/2}K_1^{-1/2}U_T^{1/2}PO_2^{-1/4}$	$K_2^{1/2-1/3}K_3^{1/3}K_1^{-1/3}PO_2^{-1/6}$
ρ	$K_2K_3^{-1/2}K_5^{1/2}PO_2^{1/4}$	$2^{-1/3}K_3^{-1/3}K_2PO_2^{1/6}$	$K_2U_T^{-1}$	$2^{1/4}K_1^{1/2}K_2K_3^{-1/2}U_T^{-1/2}PO_2^{1/4}$	$2^{-5/3}K_3^{-1/3}K_1^{1/3}K_2^{2/3}PO_2^{1/6}$
$[O''_i]$	$K_1K_5^{-1}$	$2^{2/3}K_1K_3^{-1/3}PO_2^{1/6}$	$K_1K_3^{-1}U_T^2PO_2^{1/2}$	$2^{-1}U_T$	$2^{-2/3}K_3^{-1/3}K_1^{1/3}K_2^{2/3}PO_2^{1/6}$
U'_{ce}	U_T	U_T	U_T	U_T	U_T

TABLE III.A.1.4.

Boundaries for Regions Described in TABLE III.A.1.3.

Regions	I-II	II-III	III-IV_B	IV_B-V
Defects equal at boundary	$[V_O^{\cdot}]=2[V_O^{\cdot\cdot}]$	$2[V_O^{\cdot\cdot}]=U_T$	$2[O_i^{''}]=n$	$U_T=P$
PO_2	$2^{-4}K_3^2K_6^{-6}$	$2^2K_3^2U_T^{-6}$	$2^{-2}K_1^{-2}K_3^2U_T^{-2}$	$2^{10}K_1^{-2}K_2^{-4}K_3^2U_T^6$

Figure III.A.1.1 Schematic of defect chemistry model of urania doped ceria.
a. Partially ionized uranium.
b. Fully ionized uranium.

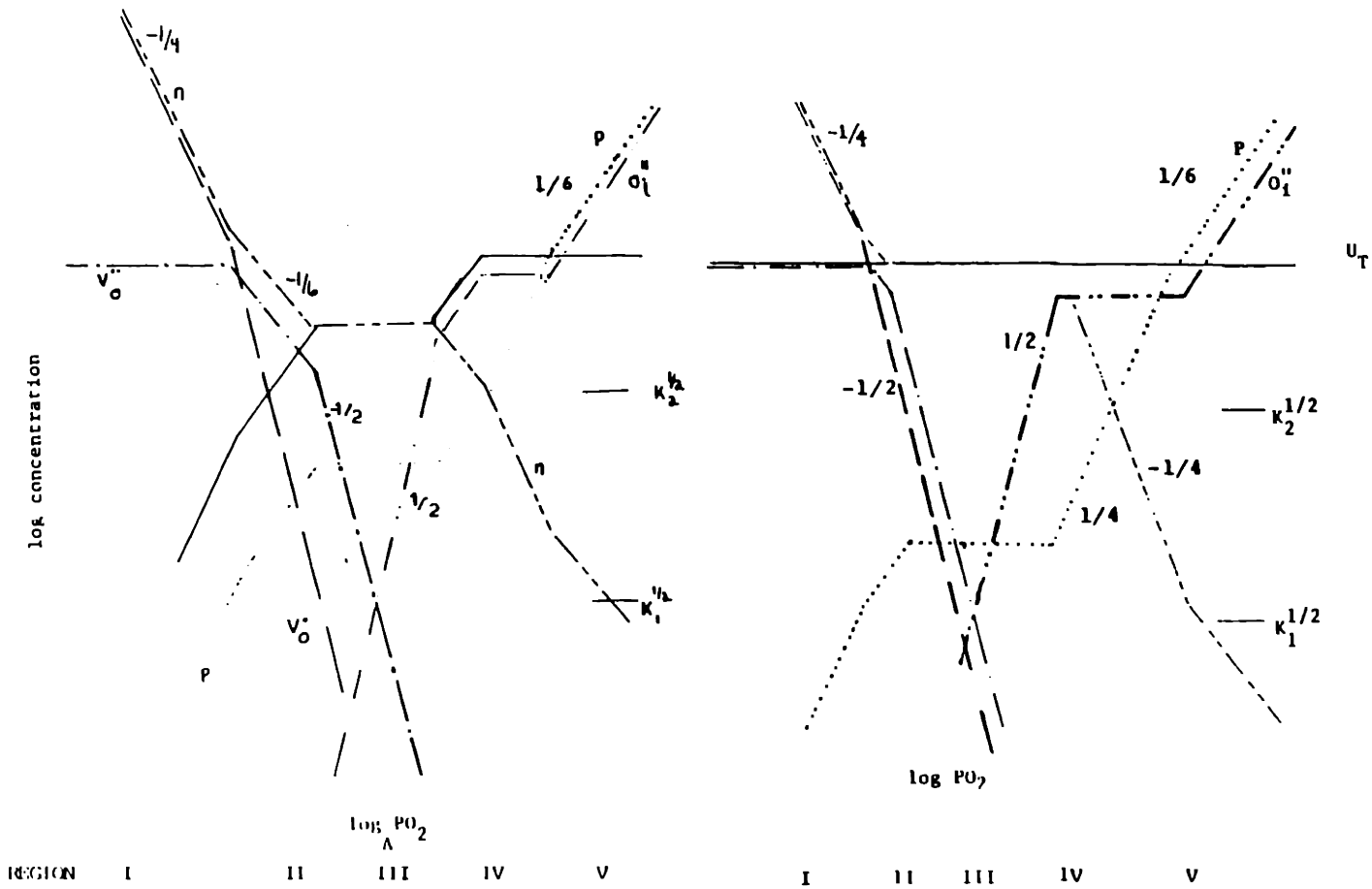

the change in the reaction constants due to the addition of uranium will result in higher concentration of oxygen interstitals.

A.2 URANIA-RICH SOLID SOLUTIONS

The defect chemistry of ceria doped urania is very similar to (almost the mirror image) of the defect chemistry of urania doped ceria presented above. Ceria is known to be either trivalent or quatravalent, and therefore it will be either Ce_U or $Ce_U^{\cdot}$. Ceria and urania both exhibit the flourite crystal structure. Based on this and the band diagram presented earlier the other defects are assumed to be fully ionized and are the same as in CeO_2.

The following defects will be considered in UO_2:

O_i'' , $V_O^{\cdot\cdot}$, e' , $h^{\cdot}$, $Ce_U^{\cdot}$

Given these defects, the following quasichemical defect reactions may be written:

$O_O \rightarrow O_i'' + V_O^{\cdot\cdot}$ Frenkel Pair Production (III.A.2.1)

$null \rightarrow e' + h^{\cdot}$ Electron Hole Pair Production (III.A.2.2)

$O_O \rightarrow V_O^{\cdot\cdot} + 2e' + \frac{1}{2}O_2$ Reduction Reaction (III.A.2.3)

$1/2PO_2 \Rightarrow O_i'' + 2h^{\cdot}$ Oxidation Reaction (III.A.2.4)

$V_O^{\cdot} \rightarrow V_O^{\cdot\cdot} + e'$ Second Ionization of Oxygen Vacancy (III.A.2.5)

$Ce_U \rightarrow Ce_U' + h^{\cdot}$ Ionization of Cerium Ion (III.A.2.6)

Using the above assumptions, the following equilibrium equations may be written:

$$[O_i''][V_O^{\cdot\cdot}] = G_1 \qquad \text{(III.A.2.7)}$$

$$np = G_2 \qquad \text{(III.A.2.8)}$$

$$[V_O^{\cdot\cdot}]n^2 PO_2^{1/2} = G_3 \qquad \text{(III.A.2.9)}$$

$$PO_2^{1/2}/([O_i'']p^2) = G_4 = (G_1 G_2^2)/G_2 \qquad \text{(III.A.2.10)}$$

$$[Ce_U']p/\ [Ce_U] = G_6 \qquad \text{(III.A.2.11)}$$

Again, the square brackets indicate concentrations and the Gs are equilibrium constants, functions of temperature only. The electroneutrality and conservation of dopant constraints may be added to these equations.

$$n + 2[O_i''] + [Ce_U'] = p + 2[V_O^{\cdot\cdot}] \qquad \text{(III.A.2.12)}$$

$$[Ce_U^{*}] + [Ce_U'] = [Ce_U]_{total} = Ce_T \qquad \text{(III.A.2.13)}$$

The solutions to the above equations in the Brouwer approximation are given in Table III.A.2.1. The equations specifying the PO_2 at the boundaries between regions are given in Table III.A.2.2.

A significant simplification can be made to the previous analysis by assuming that the cerium ions are all singly ionized ($Ce_T=[Ce_U']$). This is a reasonable

Table XI.A.2.1

Defect Chemistry of Urania Doped with Ceria

Regions	I	II_A	II_B	III	IV
Controlling electroneutrality equation	$[Ce_u^{\cdot}] = Ce_T$ $2[V_O^{\cdot\cdot}] = n$	$[Ce_u^{\cdot}] \gtrsim Ce_T$ $2[V_O^{\cdot\cdot}]=[Ce_u^{\cdot}]$	$[Ce_u^{\cdot}] \gtrsim Ce_T$ $2[V_O^{\cdot\cdot}]=[Ce_u^{\cdot}]$	$[Ce_T]\gtrsim[Ce_u^{\cdot}]$ $[Ce_u^{\cdot}] = P$	$[Ce_T]\gtrsim[Ce_u^{\cdot}]$ $2[O_i^{\cdot\cdot}] = P$
PO_2 range	low	intermediate	intermediate	intermediate	high
$[V_O^{\cdot\cdot}]$	$(\frac{1}{2}G_3)^{1/3}PO_2^{-1/6}$	$Ce_T/2$	$2^{-2/3}G_3^{1/3}Ce^{2/3}G_6^{2/3}PO_2^{-1/6}$	$G_3G_6Ce_TG_2^{-1}PO_2^{-\frac{1}{2}}$	$2^{2/3}G_3^{1/3}G_1^{2/3}G_2^{2/3}PO_2^{-1/6}$
n	$(2G_3)^{1/3}PO_2^{-1/6}$	$G_3^{\frac{1}{2}}2^{\frac{1}{2}}Ce_T^{-\frac{1}{2}}PO_2^{-\frac{1}{4}}$	$2^{1/3}G_3^{1/3}G_6^{-1/3}Ce_T^{-1/3}PO_2^{-1/6}$	$G_2G_6^{-\frac{1}{2}}Ce_T^{-\frac{1}{2}}$	$2^{-1/3}G_1^{-1/3}G_2^{1/3}G_3^{1/3}PO_2^{-1/6}$
P	$G_2(2G_3)^{-1/3}PO_2^{1/6}$	$\frac{1}{2}G_2G_3^{-1}2^{-\frac{1}{2}}Ce_T^{\frac{1}{2}}PO_2^{\frac{1}{4}}$	$G_2^{-1/3}G_3^{-1/3}G_6Ce_T^{2/3}PO_2^{1/6}$	$G_6^{\frac{1}{2}}G_2^{\frac{1}{2}}Ce_T^{\frac{1}{2}}$	$2^{1/3}G_1^{1/3}G_2^{2/3}G_3^{-1/3}PO_2^{1/6}$
$[O_i^{\cdot\cdot}]$	$G_1(\frac{1}{2}G_3)^{-1/3}PO_2^{1/6}$	$2G_1Ce_T^{-1}$	$G_1^{2/3}G_3^{-1/3}G_6^{1/3}Ce_T^{1/3}PO_2^{1/6}$	$G_1G_2G_3^{-1}G_6^{-1}Ce_T^{-1}PO_2^{\frac{1}{2}}$	$G_1^{1/3}G_2^{1/3}2^{-2/3}G_3^{-1/3}PO_2^{1/6}$
$Ce_u^{\cdot}$	$G^{-1}Ce_T(2G_3)^{-1/3}PO_2^{1/6}$	$2^{-\frac{1}{2}}Ce_T^{3/2}G_3^{-\frac{1}{2}}G_6^{-1}PO^{\frac{1}{2}}$			
$[Ce_u^{\cdot}]$	Ce_T	Ce_T	$2[V_O^{\cdot\cdot}]$	P	$2^{-1/3}G_1^{-1/3}G_2^{1/3}G_3^{1/3}G_6Ce_TPO_2^{-1/6}$

TABLE III.A.2.2.

Boundaries for Regions Described in Table III.A.2.1.

Regions	I-II_a	II_a-II_b	II_b-III	III-IV
Defects equal at boundaries	$n=[Ce'_v]$	$[Ce'_u]=\frac{1}{2}Ce_T$	$2[V_O^{\cdot\cdot}]=P$	$[Ce'_v]=2[O_i'']$
PO_2	$2^{-4}G_3^2Ce_T^{-6}$	$2^8G_3^2G_6^4Ce_T^{-2}$	$2^2G_2^{-3}G_3^2G_6Ce_T$	$2^{-2}G_1^{-2}G_2^1G_3^2G_6^3Ce_T^3$

assumption based on the relative ionizations for cerium and uranium presented previously. Ce lies well below the uranium level. Therefore, to deionize cerium, uranium would first have to substantially deionize. The solutions to the simultaneous equations are listed in Table III.A.2.3. The equations specifying the PO_2 at the boundaries are listed in Table III.A.2.4. Figure III.A.2.1 shows schematically the expected defect concentrations for ceria doped urania, assuming full ionization of the cerium.

As discussed in section IIA, the previous work[11,14,1] of Willis, Catlow, and Dudney has shown that at high PO_2 the above assumption of unassociated defects does not apply. This changes the details of the defect chemistry at high PO_2. Consider the (2:1:2) Willis cluster (Figure II.A.5). The proper Kroger Vink notation for this cluster is $[2O''_{i111}\ 1O''_{i110}\ 2V^{\cdot\cdot}_{O}]''$ where the subscripts denote the direction along which the interstitial is displaced. The net excess oxygen and net charge of this defect make it equivalent to a single O''_i. If the details of the defect reactions are worked out this defect has the same PO_2 dependence as an O''_i but the defect is also more likely to trap a hole[14]. The net charge of this defect is minus one. This defect $[2O''_{i111}\ 1O''_{i110}\ 2V^{\cdot\cdot}_{O}\ h^{\cdot}]'$ would have a PO_2 dependence like that of O'_i. The result of this

TABLE III.A.2.3.

Defect Concentration for UO_2 Doped with CeO_2 Assuming Full Ionization

Regions	I	II	III	IV
Limiting electroneutrality equation	$2[V_O^{\cdot\cdot}]=n$	$2[V_O^{\cdot\cdot}]=[Ce_u']$	$P=[Ce_u']$	$2[O_I'']=P$
PO_2 range	Low	Intermediate	Intermediate	High
$[V_O^{\cdot\cdot}]$	$2^{2/3}G_3^{1/3}PO_2^{-1/6}$	$2^{-1}Ce_T$	$G_2^{-2}G_3Ce_T^2PO_2^{-1/2}$	$2^{2/3}G_3^{1/3}G_1^{2/3}G_2^{-2/3}PO_2^{-1/6}$
n	$2^{1/3}G_3^{1/3}PO_2^{-1/6}$	$2^{1/2}G_3^{1/2}Ce_T^{-1/2}PO_2^{-1/4}$	$G_2Ce_T^{-1}$	$2^{-1/3}G_1^{-1/3}G_2^{1/3}G_3^{1/3}PO_2^{-1/6}$
P	$2^{-1/3}G_2G_3^{-1/3}PO_2^{-1/6}$	$2^{-1/2}G_2G_3^{-1}Ce_T^{1/2}PO_2^{1/4}$	Ce_T	$2^{-1/3}G_1^{1/3}G_2^{2/3}G_3^{-1/3}PO_2^{1/6}$
$[O_I'']$	$2^{2/3}G_1G_3^{-1/3}PO_2^{1/6}$	$2\,G_1Ce_T^{-1}$	$G_1G_2^2G_3^{-1}Ce_T^{-2}PO_2^{1/2}$	$G_1^{1/3}G_2^{1/3}{}_2{}^{-2/3}G_3^{-1/3}PO_2^{1/6}$

TABLE III.A.2.4.

Boundaries for Regions Described in Table III.A.2.3.

Regions	I-II	II-III	III-IV
Defects equal at boundaries	$2[V_o^{\cdot\cdot}]=Ce_T$	$P=Ce_T$	$Ce_T=2[O_i'']$
PO_2	$2^{-4}G_3^2Ce_T^{-6}$	$2^2G_2^{-4}G_3^4Ce_T^2$	$G_1^{-2}G_2^{-4}G_3^2Ce_T^6$

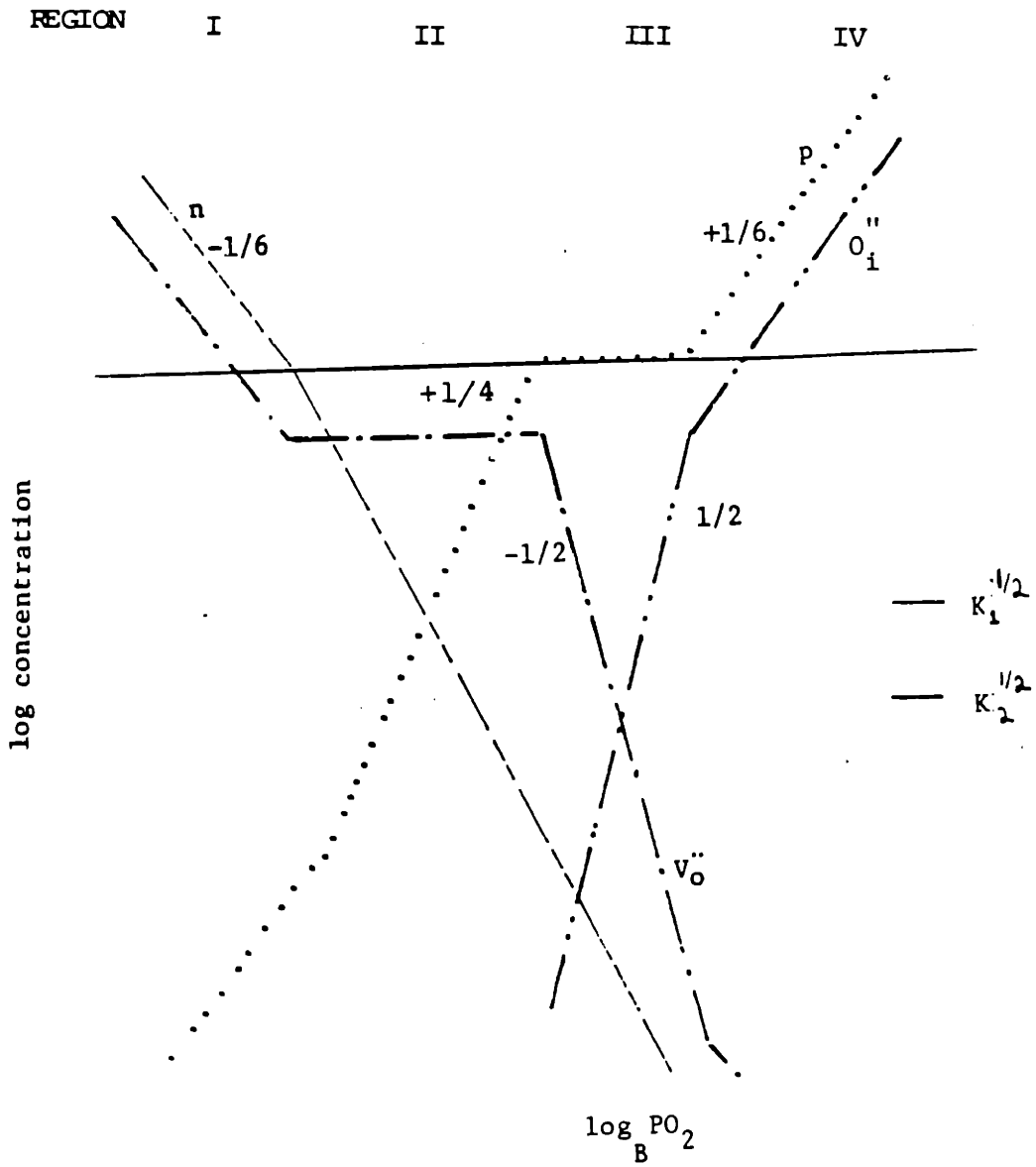

Figure III.A.2.1 Scematic of defect chemistry model of ceria doped urania assuming full ionization.

singly charged cluster is a steeper PO_2 dependence of defect species at high PO_2 than would be seen for fully ionized isolated defects. The smaller the ratio of effective charge of the defect to effective excess oxygen of the defect, the steeper the PO_2 dependence. For example, at high PO_2, the concentration of O_i'' is proportional to $PO_2^{1/6}$; however, if the controlling defect is O_i', the proportionality is $PO_2^{1/4}$. If by some partially ionized defect cluster the effective charge to excess oxygen ratio is 1/2, the proportionality would be $PO_2^{1/3}$.

In subsequent analysis of our data, defect clustering will be used to provide a picture consistent with the data when the simple unassociated defect reactions fail to account for the data.

B.1 CONDUCTIVITY

Measurement of the electrical conductivity (σ)of a material provides a simple, reliable means of obtaining information about the concentration of carriers. The conductivity can be written as the sum of the conductivities of each of the charge carrying species

$$\sigma_{total} = \sigma_1 + \sigma_2 + \sigma_3 + \ldots \qquad \text{(III.B.1.1)}$$

The conductivity of a particular species is the product of the charge of the carrier (q_i) the number of carriers per unit volume (n_i) and the mobility of the species (μ_i).

$$\sigma_i = q_i \, n_i \, \mu_i \qquad \text{(III.B.1.2)}$$

The mobility term is dependent on the specific conduction mechanism. In a broad band semiconductor with a nearly empty conduction band, the mobility is dominated by impurity and phonon scattering.[56] The result is a mobility which is a weak function of temperature. The mobility for hopping type conduction, on the other hand, may be written as[29]

$$\mu_{polaron} = (\mu_o/T) \exp(-E_m/(k_B T)) \qquad \text{(III.B.1.3)}$$

where E_m is the activation energy for the jump process, T is the temperature in K , and k_B is the boltzman constant. μ_o may be written[29] as

$$\mu_o = (P e \bar{c} q a^2 \nu)/k \qquad \text{(III.B.1.4)}$$

where P is the probability that a jump will occur during any given lattice vibration. If P = 1 the polaron is called adiabatic, $\bar{c}$ is the concentration of available sites to which a carrier may jump, e is the charge of an electron, ν is the jump attempt frequency (usually taken as the longitudinal vibration frequency for the material), and a is the jump distance. For fluorite crystals with carriers on the cation sublattice this value is related to the lattice parameter (a_o) by $a_o/1.414$.

For certain cases it is possible to obtain direct correlation between the concentration of a dopant and the conductivity. For example, consider the case of CeO_2 doped with UO_2 in region III of Table III.A.1.1. Let y be the mole fraction
U in $Ce_{1-y}U_yO_2$.

Then

$$n = y(4/a_o) \quad . \qquad \text{(III.B.1.5)}$$

and

$$\bar{c} = A - Bx \qquad \text{(III.B.1.6)}$$

where A is the number of electrons per Ce site in the conduction band, $1 < A < 2$, and B is a constant equal to two if the U_{Ce} sites are unavailable as carrier sites and one if they are available. According to the band diagram presented earlier, U_{Ce} will be at an energy sufficiently

above the Ce_{Ce} that they will be unavailable for jumps. Therefore, the conductivity in terms of dopant concentration is

$$\sigma = q\, y(4/a_o)((P\ (A-By)\ q\ a^2\ \nu\ )/k/T)\ \exp(-E_m/(k_BT)). \qquad \text{(III.B.1.1)}$$

This formula is often expressed in the simple form c(1-c) where c is the concentration of carries . In this form it is clear the conductivity wil go through a maximum at c=.5. There may be additional effects of the dopant implicitly contained in the lattice parameter.

The mobility for ionic conduction takes a form similar to that for small polaron hopping. It is also possible to relate the ionic mobility to the ionic diffusion, via the Nernst Einstein equation:

$$\mu_{ion} = (fD_{ion}n_{ion}q_{ion}^2)/(k_BT) \qquad \text{(III.B.1.8)}$$

f is a function of the crystal structure related to the number of equivalent sites for the diffusing ion, and D_{ion} is the diffusion coefficient for the ion or defect, which is actually the charge carrying species. For example, if charge carrying species is a vacancy, then

$$D_{ion} = D_V\ D_{lattice}^{tracer} / n_{vacancy}$$

In materials for which the mobility and the charge are not functions of stoichiometry and where one species dominates the conduction process, it is possible to use the conductivity to measure the concentration of that species, assuming that the charge and mobility are known. More importantly, even if the charge and mobility are not known, by assuming that the mobilities are not a function of PO_2, it is possible to use the PO_2 dependence of the conductivity or the boundaries between the changes of the PO_2 dependence of the conductivity to determine the defects controlling the defect chemistry and the reaction constants for the defect reactions.

B.2 THERMOELECTRIC POWER

The conductivity as described above provides information about the mobility concentration product for charge carriers. To separate these quantities, the thermoelectric power (TEP) is useful. The TEP, the slope dV/dT at zero current, and virtually zero temperature gradient for a material with a single charge carrier is

$$\Theta_i = (1/q_i)(Q_i^*/T + \bar{S}_i) \qquad \text{(III.B.2.1)}$$

where q_i is the charge of the carrier, Q_i^* is the heat of transport for the charge carrier, and $\bar{S}$ is the partial molar entropy of the charge carriers.

For ionic charge carriers, Q^* can be related to the carrier formation energy and to a geometrical parameter describing the size of the region of lattice deformation due to the carrier.[57] Sugisaki, Sato, and Furuya have made estimates of Q^*, and their values will be used in the discussion. $\bar{S}$ for ionic carriers is composed of two parts:

$$\bar{S}_i = S_{config} + S_{vib} \qquad \text{(III.B.2.2)}$$

The S_{config} is the configurational entropy due to the presence of the carriers and can be written as

$$\bar{S}_{config} = -(k_b)\ln[(1-\rho)/\rho), \qquad \text{(III.B.2.3)}$$

the Heikes' formula, where ρ is the mole fraction of

sites filled. The second contribution to the entropy is the vibrational term which results from a change of the vibrational states of the material as a result of the presence of the carriers and is $S_{vib} \sim -1\ k_b$ [58] for a Frenkel mechanism. This will make a small contribution to the total TEP.

There is disagreement about the value of q^* for polarons. It has been calculated to range from 0 [59] to equal to the polaron hopping energy [60]. After reviewing the different models, Hodge concluded that a knowledge of the details of transport are needed to say more than " the heat of transport will be equal to some fraction of the activation energy for hopping."[61] In the following analysis, Q^* will be assumed to be equal to zero. The implication of this assumption is that both the currently occupied polaron site and the target site have the same energy at the moment when the jump actually occurs.

The entropy for polarons has both a cofigurational and a vibrational component. Austin and Mott [62] have estimated the magnitude of $\Delta\ S_v/k_b$ to be about 0.1 to 0.2. The configurational entropy for localized carriers has been worked out by Chaikin and Beni[63] for the one dimensional case with no polaron interaction, on-site repulsion, and extended polaron-polaron repulsion. If the polaron interaction energy is small, two polarons of opposite spin

may occupy the same site. The entropy for this case is

$$S_{config} = k_b \ln[(2-\rho)/\rho] \qquad \text{(III.B.2.4)}$$

If the polaron interaction is repulsive, then two polarons occupying the same site is unlikely no matter what their spins. For electrons the entropy in this case is

$$S_{config} = k_b \ln[2(1-\rho)/\rho] \; . \qquad \text{(III.B.2.5)}$$

As the polaron-polaron repulsive interaction increases, more and more sites will be excluded from the sites available for polaron occupancy. If B is the number of sites to which the repulsion effectively excludes polarons, then the entropy for electrons is

$$S_{config} = k_b \ln[2(1-B\rho-\rho)^{B+1})/(\rho(1-B\rho)^{B})]. \qquad \text{(III.B.2.6)}$$

This formula also applies to on site repulsion if B=0. The entropy for hole polarons with strong repulsion is

$$S_{config} = k_b \ln[2(1-\rho)(1-B(1-\rho))^{B})/((\rho-1)B+\rho)^{B+1})]. \qquad \text{(III.B.2.7)}$$

The equations for the electrons and holes are not symmetric because the entropy for holes depends not on the number of holes but on the number of electrons.

Q^* for a broad band semiconductor is[61]

$$Q^* = rk_bT \qquad \text{(III.B.2.8)}$$

where r is dependent on the particular scattering mechanism

and should be on the order of -1/2 to 3/2[64]. The entropy of carriers in a semiconductor is given by[61]

$$\bar{S} = k_b(\ln N_c/n) + 5k_b/2 \qquad \text{(III.B.2.9)}$$

where N_c is the density of states in the conduction band and n is the number of carriers per unit volume. For materials with multiple carriers

$$\theta_{total} = \frac{\sum_i \theta_i \sigma_i}{\sum_i \sigma_i} \qquad \text{(III.B.2.10)}$$

Carriers which contribute little to the conduction process also contribute little to the TEP.

C. TEP and CONDUCTIVITY AT LARGE CARRIER CONCENTRATIONS

Jonker[65] has detailed the information which is available from a plot of the log conductivity vs. TEP for the case of low carrier concentration. Jonker's analysis does not apply for high carrier concentration, and it is instructive to examine what some simple models for conduction predict at high carrier concentrations. For the simple case, we will assume a single polaron mechanism and examine the results when the concentration of carriers is in the range of .1 to .5 mole fraction. If we let = n/Na and $\bar{c}$ = 1- and combine equations III.B.1.2, III.B.1.3 and III.B.1.4 we have

$$\sigma = \rho\ (1-\rho\ )K_a, \qquad \text{(III.C.1)}$$

where K_a is a constant which contains all quantities not explicitly dependent on carrier concentration. Similarly, for the TEP setting $Q^*_{polaron}$ and S_{vib} equal to zero 0 and combining equations III.B.2.1, III.B.2.2 and III.2.3

$$= K_c \ln((1-\rho\ )/\rho\ ), \qquad \text{(III.C.2)}$$

where K_c is a constant which contains all terms which do not explicitly depend on the carrier concentration. This equation ignores both electron spin degeneracy and on site repulsion. Figure III.C.1 is a plot of $\ln(\sigma\ )$ vs (θ) in arbitrary units in the region of ρ = 0.5. For this case

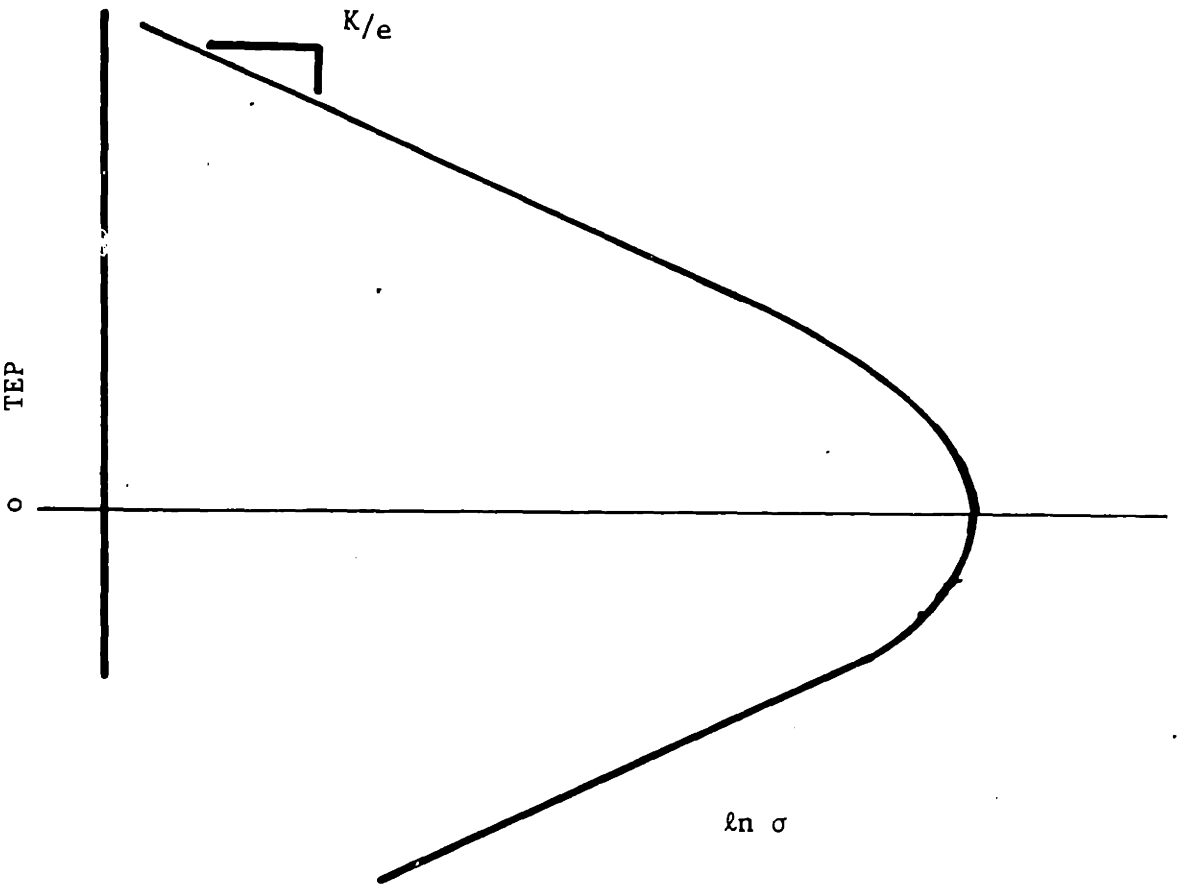

Figure III.C.1 Theoretical ln(σ) vs TEP for simple hopping conduction.

$dTEP/d\ln = k/e$ at $\rho = 0$.

If both the electron spin degeneracy and on site repulsion are included in the expressions for conductivity and TEP, then

$$\sigma = \rho (1 - \rho) K_A \qquad \text{(III.C.3)}$$

$$\theta = K_C \ln (2(1-\rho)/\rho) \qquad \text{(III.C.4)}$$

Figure III.C.2A plots these equations. The difference between these equations is a displacement of the nose from $\theta = 0$ by a factor of $K_C \ln 2$ If further neighbor interactions are included, then the nose of the curve tends to flatten out (Figure III.C.2B). The curves are not symmetric about $\theta = 0$ as noted in section III.B.2 above.

In the above analysis, K_A and K_C are assumed to be independent of ρ ; however, it is reasonable that the parameter associated with a polaron jump might change as ro is increased. Specifically, the activation energy for a jump may differ for holes ($\rho > .5$), and for electrons ($\rho < .5$). In this case the nose will display a further lack of symmetry depicted in Figure III.C.3, where the conduction process with the lower activation energy will have a relatively higher conductivity.

As the concentration of carriers is decreased, the curves tend towards the shape and slopes of the Jonker Pear. It is possible to splice together these two types of

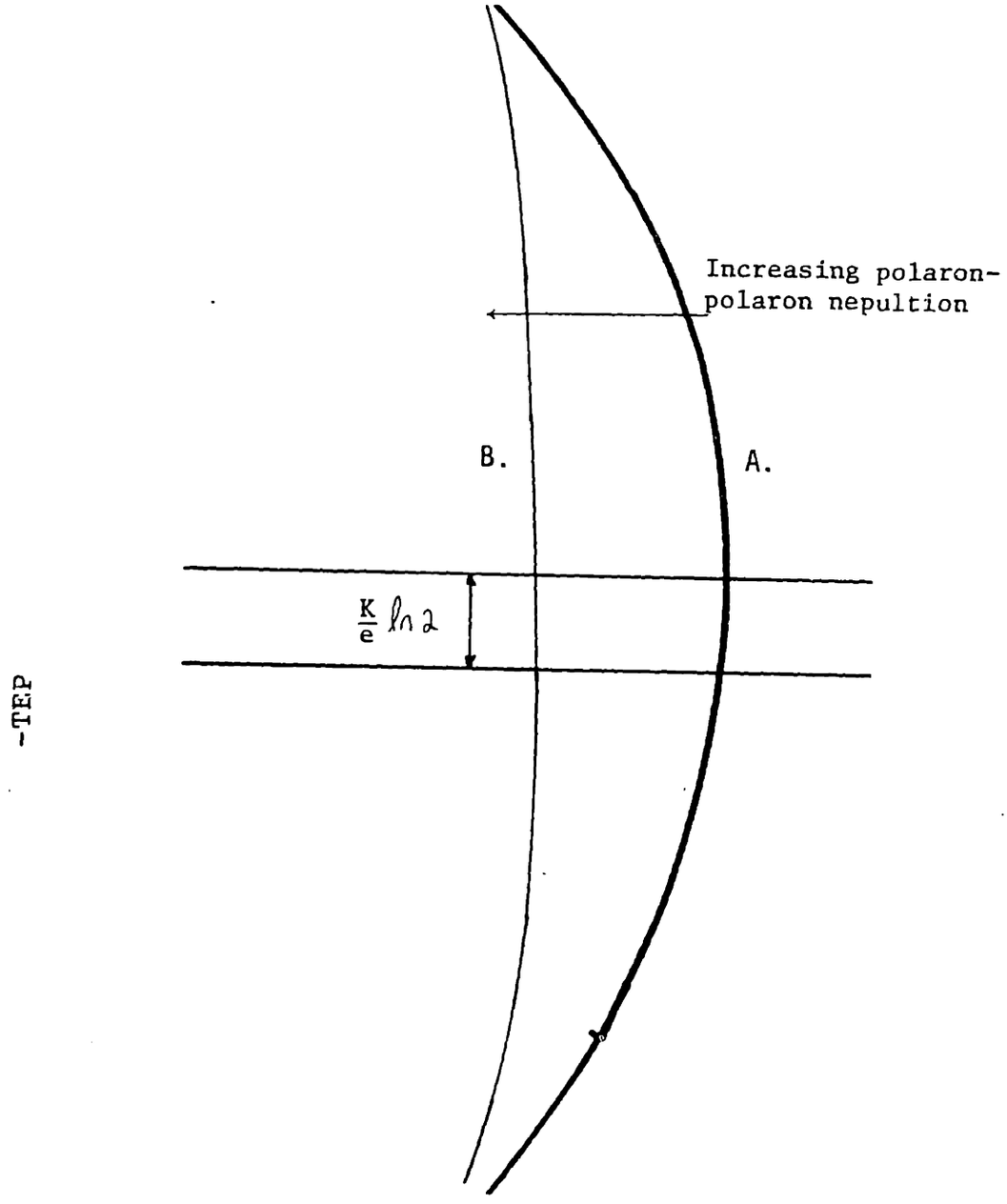

Figure III.C.2 Theoretical ln(σ) vs TEP near $\rho = 0.5$.

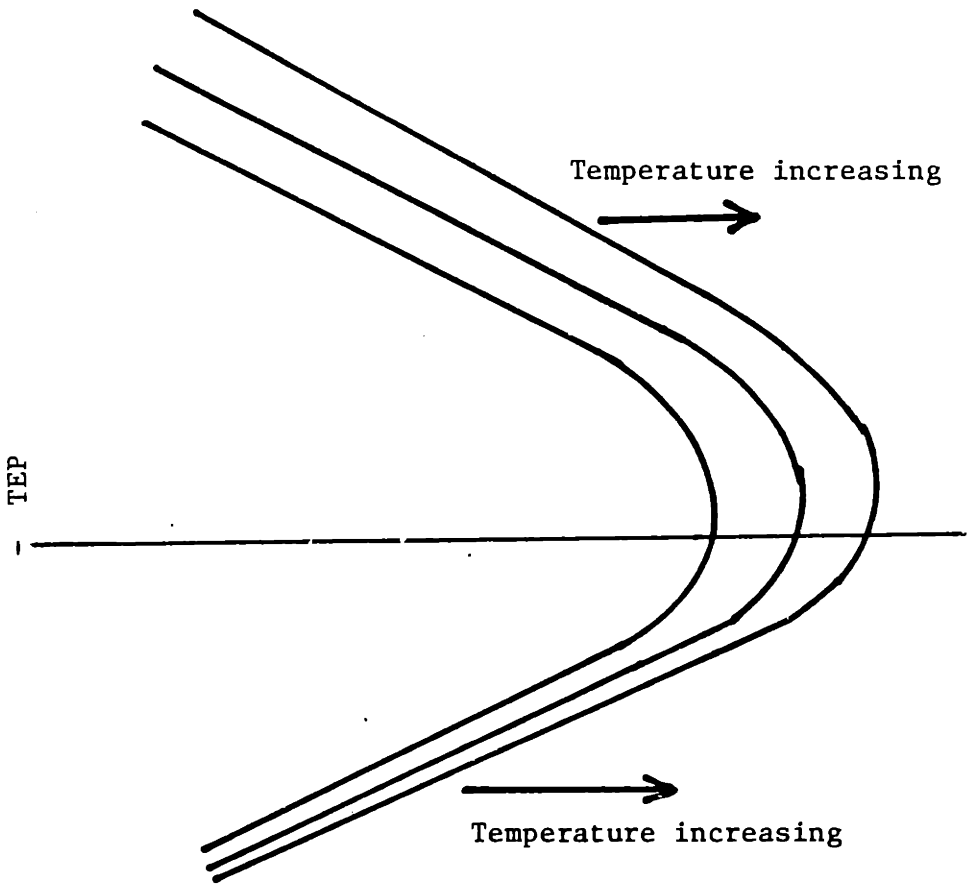

Figure III.C.3 ln(σ) vs TEP plots at several emperatures with different activation energies for hole and electron hopping.

analysis; however, the result wiil not except in very special conditions be a closed curve. For the case in which ρ equals approximately zero, a few electron polarons in an otherwise empty band, the band gap which is of importance is the difference between the energy of the band in which the polarons occur and the valance band below. On the other hand, when ρ aproaches 1, a few holes in an otherwise full band, the band gap which is of importance is the energy difference between the band in which the polarons occur (the same as that for the electrons) and the band above. Figure III.C.4 illustrates the situation.

For a material which has a very large range of stoichiometry, the shape of the ln σ vs TEP plot will be a triangular spiral, Figure III.C.5, in which the curve may or may not cross itself.

This section has shown that near the nose of the TEP-ln σ curve there are two types of assymetry which may occur one related to the mobility as discussed previously by Jonker and the other related to the difference of the entropies of holes and electrons. This analysis is applicable to small polaron conduction, but it should be remembered that is is only strictly valid for onsite repulsion or no site repulsion because it was developed using statistics fora one dimensional system.

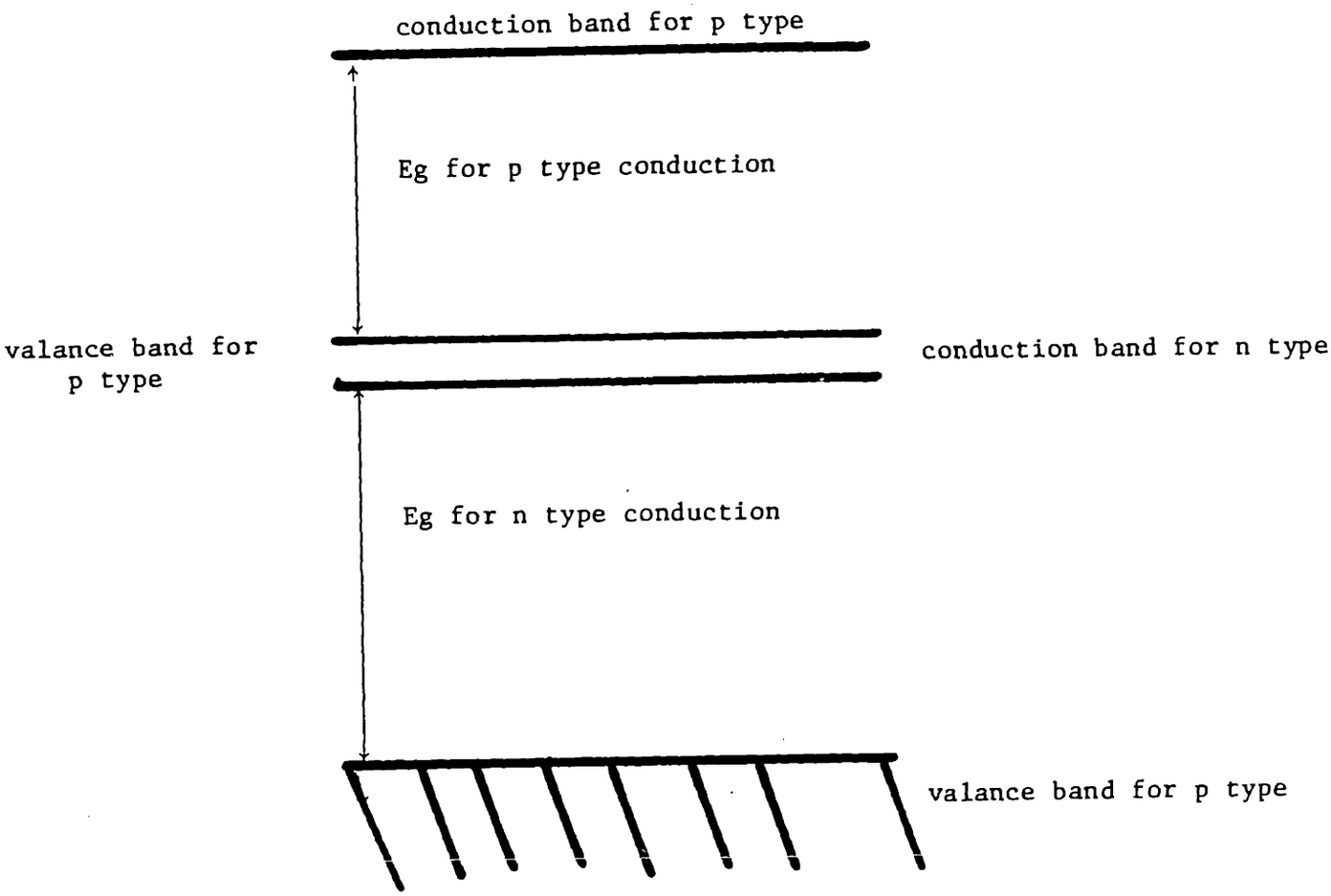

Figure III.C.4 Schematic of band gap change with filling of conduction Band.

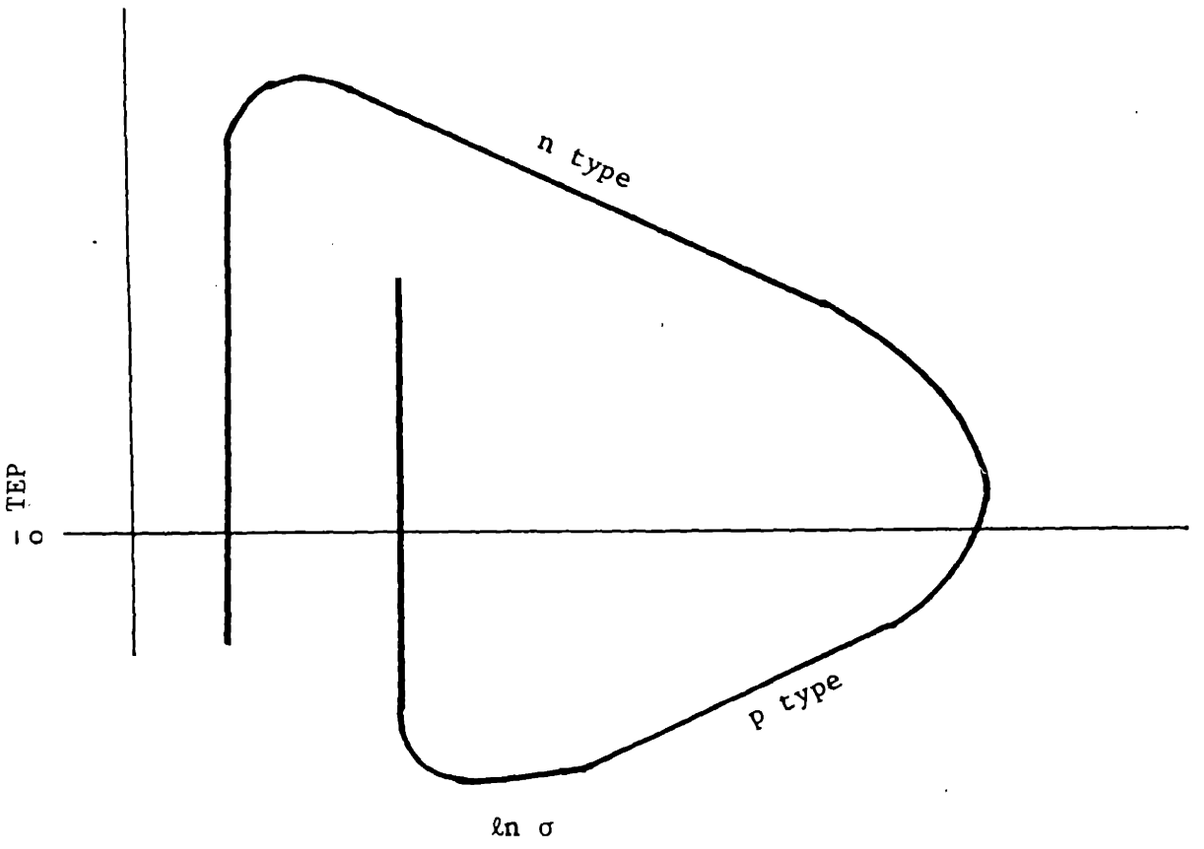

Figure III.C.5 Schematic of TEP vs ln( ) for a highly nonstoichiometric material.

D. TEP AND CONDUCTIVITY FOR MID RANGE SOLID SOLUTIONS

Based on the results of previous investigators Tuller[27], Dudney[24], and Naik[28], at concentration greater than 10m/o dopant the mobility of charge carriers is a function of dopant concentrations. Therefore the conductivity does not reflect simple defect relations. The most important tool for this speculation is the band diagram developed in section II.E. For the stoichiometric material, as the composition of the material is changed by adding more U to CeO_2, one or two electrons are added to the Ce 4f band, one if the uranium is $U_{Ce}^{\cdot}$ and two if the uranium is $U_{Ce}^{\cdot\cdot}$. The simple model for conductivity in small polaron materials, section III.B.1, predicts that the conductivity is proportional to $c\bar{c}$ where c is the concentration of electrons (i*U) where i= 1 or 2, depending on the relative charge of the urainium; and $\bar{c}$ is the concentration of available sites to which an electron can jump. For the simple model $\bar{c}$=1-2c. For $Ce_{.60}U_{.40}$ and U_{total} = $U_{Ce}^{\cdot}$ c is 0.4, and $\bar{c}$ is 0.6. At stoichiometry there are more electrons than sites to wnich the electrons can jump. This is then effectively a p type conductor with the empty sites behaving as holes. As the stoichiometry of the material is changed to excess oxygen, the electrons from the $Ce^{\cdot}$ compensate for the $O_i^{''}$. As c decreases to 0.375, the conductivity goes through a maximum and becomes n type decreasing with increasing $O_i^{''}$, Figure III.D.1.

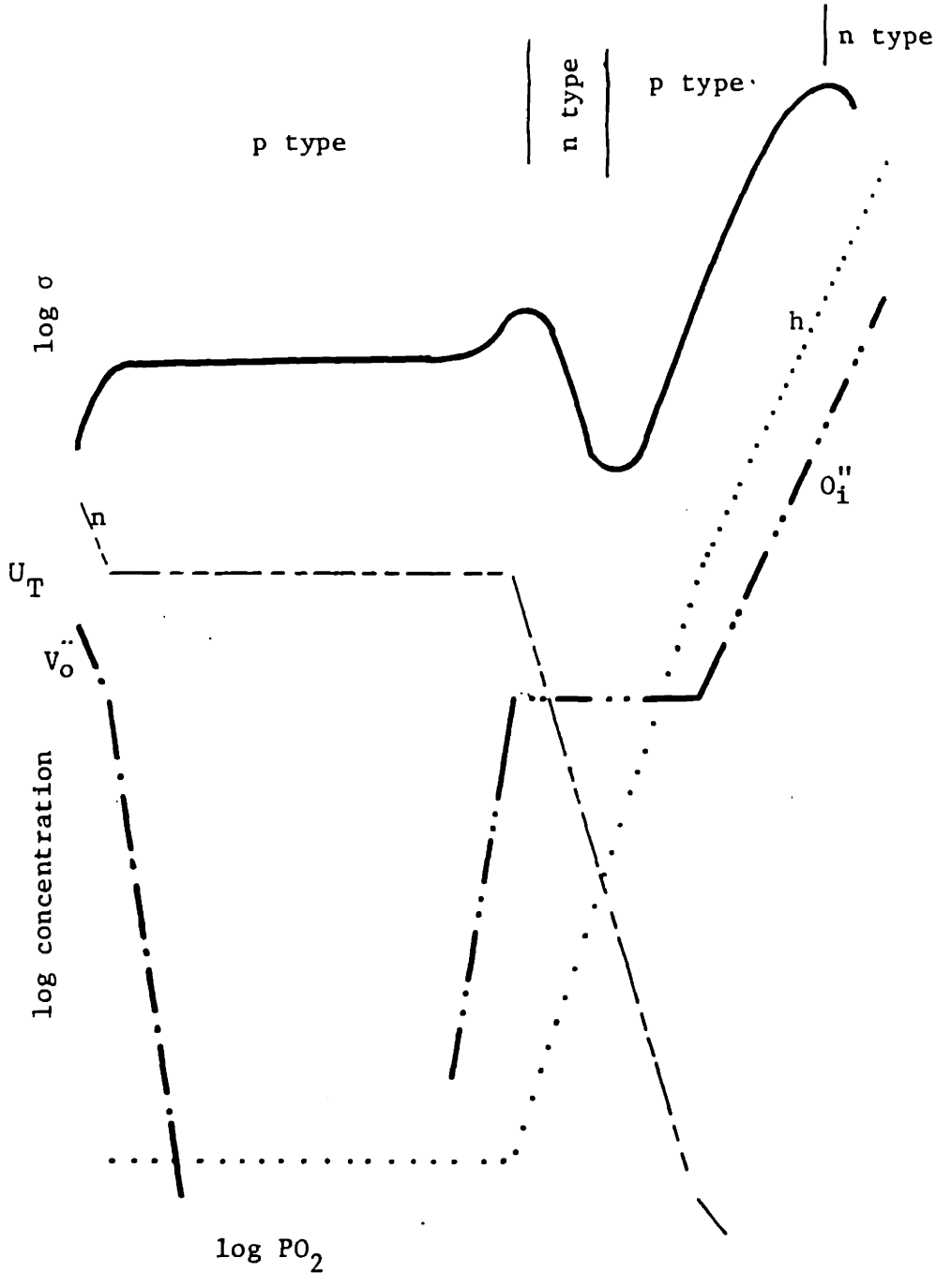

Figure III.D.1 Schematic diagram of expected defect concentrations and conductivity for $Ce_{.6}U_{.4}O_{2\pm x}$.

For the $U_{.75}Ce_{.25}O_2$, at stoichiometry the $U^{\bullet}$ concentration is only .25, so the conductivity should be p type. As the O_i'' concentration is increased, the U 5f band is depopulated past the halfway point, and the conductivity goes through a maximum and changes to n type. Conductivity decreases with increasing O_i' , (Figure III.D.1).

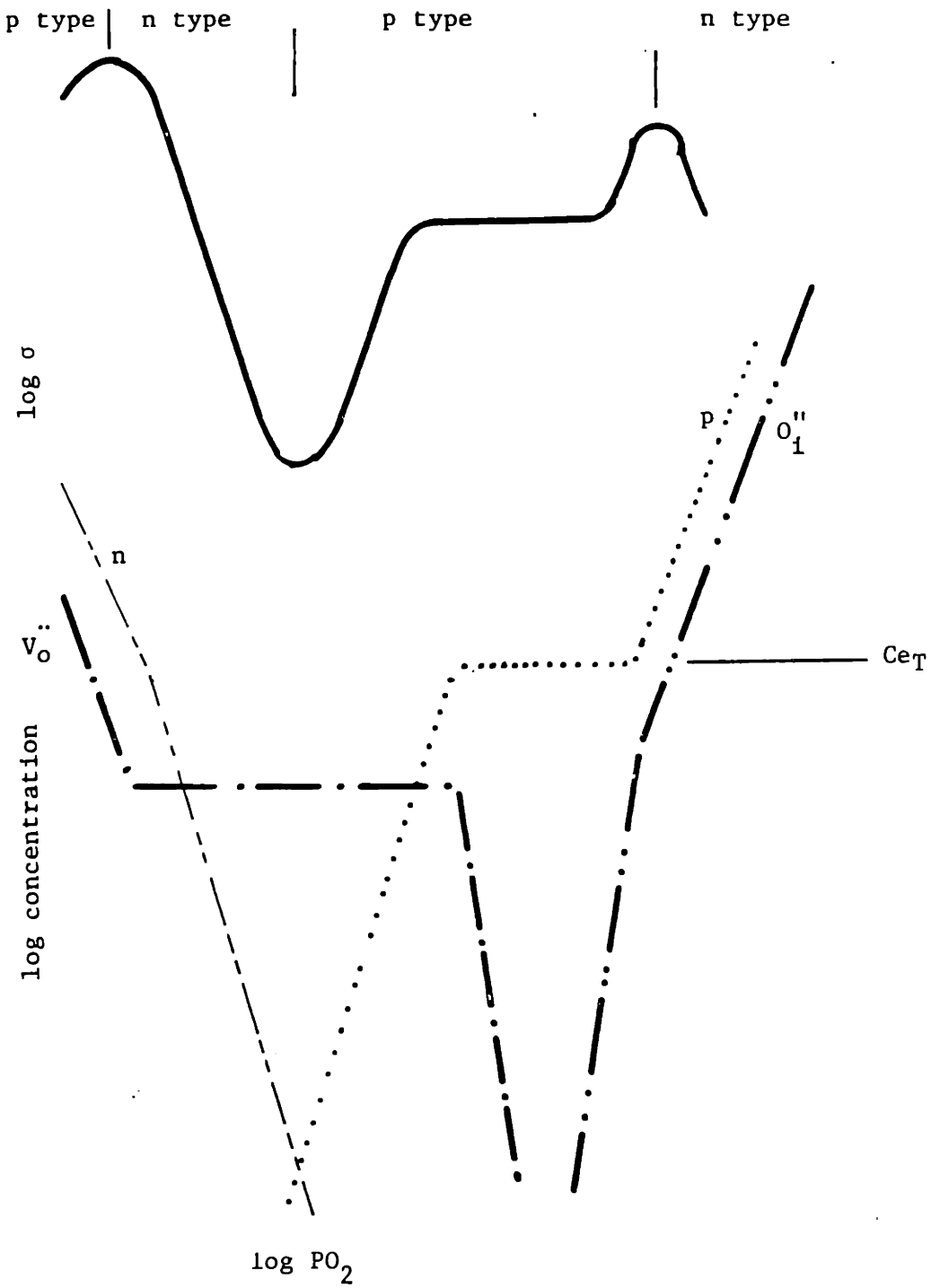

Figure III.D.2 Schematic diagram of expected defect concentrations and conductivity for $Ce_{.25}U_{.75}O_{2\pm x}$.

IV EXPERIMENTAL PROCEDURE

A SAMPLE PREPARATION

Powder for the various compositions was obtained from one of two sources. Compositions of $Ce_{.75}U_{.25}O_2$ and $Ce_{.031}U_{.969}O_2$ were provided by O. Toft Sorenson of Riso Labs, Denmark, and were mechanical mixtures of reduced UO_2 and CeO_2 powders. The remainder of the powders were prepared by coprecipitation. The steps were as follows:

1 Ceric ammoniumnitrate $(NH_4)_2Ce(NO_3)_6$(Alfa products lot #100z83) and UO_2 obtained from Battel NW Laboratories (see Table IV.A.1[65] for chemical analysis) were dissolved in nitric acid (70% Mallinckrodt). For high UO_2 compositions this required vigorous stirring overnight.

2 NH_4(58% Mallinckrodt) was added dropwise to the well-stirred solution until the pH rose to 8.9-9.0.

3 The precipitate was washed and collected in a Buchner funnel. The wash consisted of three rinses each in deionized water, acetone , toluene, and acetone.

4 The resulting cakes could easily be broken up into fine, fluffy powder. For the $Ce_{.25}U_{.75}O_2$ composition a piece of the cake was left intact for reduction and firing. For the other compositions, the cakes were broken up by light grinding.

TABLE IV A.1.

ISOTOPIC CONTENT OF THE URANIA AND CHEMICAL ANALYSIS OF URANIA POWDER

	P.P.M. by Weight
U^{235}	.231(1)
U^{236}	.0046(1)
U^{238}	99.763(1)
Ag	<0.01
Al	<5.
B	<0.1
C	100.
Ca	<5.
Cd	<0.2
Cl	5.
Cr	10.
Cu	0.5
F	<10.
Fe	40.
Mg	2.
Mn	2.
Mo	1.
N	10.
Ni	70.
Pb	<1.
Si	50.
Sn	<1.

(1) weight %

5. The powder or cake was then placed in an alumina boat and reduced to a CeO_2-UO_2 solid solution in flowing hydrogen at 800 C for one hour.*

The powders were then pressed. Die pressing was done in 0.75 inch dies at 18,750 psi. Isostatic pressing was done at at 40,000 psi. The powder from composition $Ce_{.75}U_{.25}O_2$ was isostatically pressed directy into .25 inch diameter rods. The pellets or rods were placed in an alumina boat on pure powder of the major component and fired in a reducing atmosphere of either CO/CO_2 or H_2 for 48 hours. See Table IV.A.2 for details of pressing, sintering and measured density.

Conductivity samples were either cut from the pellets or from the rods. The cutting was done on a Buehler Isomet low speed wafering saw with a diamond blade using Isomet cutting fluid.

The samples were mounted for four probe conductivity and TEP measurements as shown in Figure IV.A.1. Each sample was contacted with 4 10 mil Pt leads and two Pt/Rh 10%

---

*The nominal composition was $Ce_{.1}U_{.9}O_2$, but x-ray analysis showed that the lattice parameter was consistent with $Ce_{.031}U_{.969}O_2$

Table IV.A.2 Details of sample preperation.

COMPOSITION: .999Ce
POWDER PREPARATION METHOD: Coprecipitation, reduced at 840C
PRESSING
DIE PRESSED: 3000 psi, oleic acid lubricant
ISOSTATIC PRESSING: 40000 psi
Reground , Repressed, Reground, Die pressed only
FIRING
ATMOSPHERE: CO/CO_2 1/10
TEMPERATURE: 1515 C
TIME: 48 hours
CUTTING: yes
DENSITY
ACTUAL: 6.2827 gm/cc
PER CENT THEORETICAL:85.48
COMMENTS:

COMPOSITION: .99 Ce
POWDER PREPARATION METHOD: Coprecipitation, reduced at 840C for 1 hour
PRESSING
DIE PRESSED: 3000 psi
ISOSTATIC PRESSING: 40000 psi
FIRING:
ATMOSPHERE: CO/CO_2
TEMPERATURE: 1515 C
TIME: 48 hours
CUTTING: yes
DENSITY
ACTUAL: 6.7679 gm/cc
PER CENT THEORETICAL: 91.6
COMMENTS:

COMPOSITION: .95 Ce
POWDER PREPARATION METHOD: Coprecipitation, reduced at 840C for 1 hour
PRESSING
DIE PRESSED: 3000 psi
ISOSTATIC PRESSING: no
FIRING:
ATMOSPHERE: CO/CO_2 1/10
TEMPERATURE: 1515 C
TIME: 48 hours
CUTTING: yes
DENSITY
ACTUAL: 6.006 gm/cc
PER CENT THEORETICAL: 79.67
COMMENTS:

Table IV.A.2

COMPOSITION: .75 Ce
POWDER PREPARATION METHOD: Supplied by T. Sorenson
PRESSING
    DIE PRESSED: no
    ISOSTATIC PRESSING: 40000 psi
FIRING:
    ATMOSPHERE: CO/Co_2 1/10
    TEMPERATURE: 1525
    TIME: 48 hours
CUTTING: no
DENSITY
    ACTUAL: 6.984
    PER CENT THEORETICAL: 84.13
COMMENTS: Pressed directly into rods

COMPOSITION: .4 Ce
POWDER PREPARATION METHOD: Coprecipitated, reduced H_2 at 800 C for 1 hour
PRESSING
    DIE PRESSED: 39500 psi ,oleic asid lubricant
    ISOSTATIC PRESSING: 40000
FIRING:
    ATMOSPHERE: H_2
    TEMPERATURE: 1525 C
    TIME: 48 hours
CUTTING:yes
DENSITY
    ACTUAL: 8.754 gm/cc
    PER CENT THEORETICAL: 91.15
COMMENTS:

Table IV.A.2

COMPOSITION: .25 Ce
POWDER PREPERATION METHOD: Coprecipitated, cast, reduced in H_2 at 800 C for 1 hour
PRESSING
    DIE PRESSED:no
    ISOSTATIC PRESSING:no
FIRING:
    ATMOSPHERE:H_2
    TEMPERATURE:1525
    TIME:48 hours
CUTTING: no
DENSITY
    ACTUAL:8.362 gm/cc
    PRE CENT THEORETICAL: 82.91
COMMENTS: cast pellet no pressing used

COMPOSITION: .05 Ce
POWDER PREPARATION METHOD: Coprecipitated, reduced in H_2, at 820 C for 1 hour
PRESSING
    DIE PRESSED: 3000 psi
    ISOSTATIC PRESSING: 40000 psi
FIRING:
    ATMOSPHERE: H_2
    TEMPERATURE:1525 C
    TIME: 48 hours
CUTTING: yes
DENSITY
    ACTUAL:9.992
    PER CENT THEORETICAL: 91.2
COMMENTS:

COMPOSITION:.031 Ce
POWDER PREPERATION METHOD: Supplied by T.Sorenson
PRESSING
    DIE PRESSED: 3000
    ISOSTATIC PRESSING:no
FIRING:
    ATMOSPHERE: H_2
    TEMPERATURE: 1525 C
    TIME: 48 hours
CUTTING:yes
DENSITY
    ACTUAL:10.46 gm/cc
    PER CENT THEORETICAL: 97.9
COMMENTS: Nominal composition was .1Ce

Table IV.A.2

COMPOSITION: .015 Ce
POWDER PREPERATION METHOD: Coprecipitated, reduced in H_2 at 800 C for 1 hour
PRESSING
    DIE PRESSED: 3000
    ISOSTATIC PRESSING: 40000
FIRING:
    ATMOSPHERE: H_2
    TEMPERATURE: 1525 C
    TIME: 48 hours
CUTTING:yes
DENSITY
    ACTUAL:10.75 gm/cc
    PER CENT THEORETICAL: 97.84
COMMENTS:

leads, one at each end of the sample. Thermocouples often have a slight systematic error due to small variations of the composition from the nominal value. Since thermoelectric power determination requires accurate temperature difference measurement but is not extremely sensitive to small differences of the absolute temperature, care was taken to insure that the wire used for both thermocouples of one sample were from the same lot of wire. Unfluxed Pt paste (Engelhard #6926) fired at 1000°C was used to ensure good electrical contact to the samples.

Due to the radioactive nature of the samples no detailed microstructural charaterization was performed.

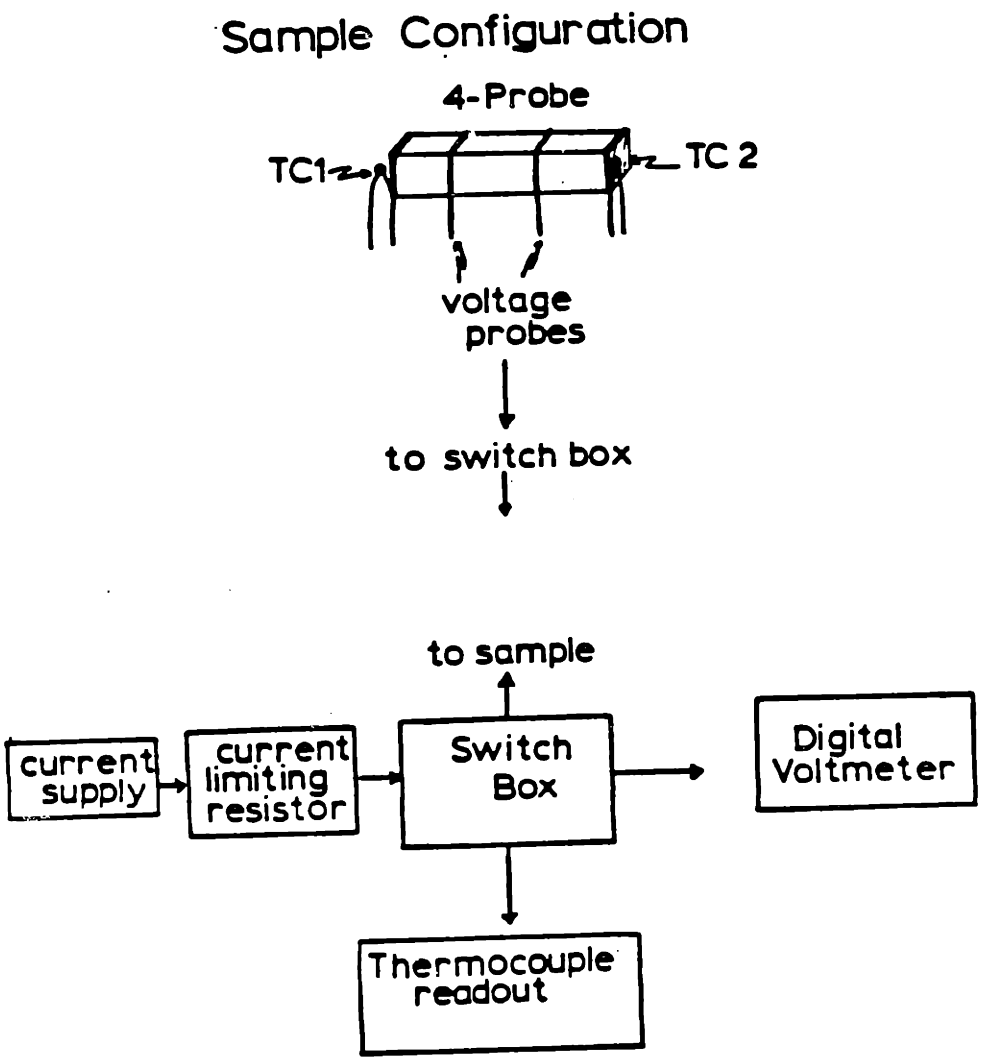

Figure IV.A.1 4 Probe Sample Configuration and Schematic of Conductivity Measuring System

B APPARATUS AND MEASUREMENT TECHNIQUE

Conductivity measurements were made using a standard four probe conductivity technique. A DC power supply was used to provide current which flowed through a ballast resistor and through the outer electrodes of the sample. A voltmeter, HP model #3465B digital multimeter with an input impedance of $>10^{10}$ ohms, placed across the ballast resistor, and measured the voltage from which the current could be calculated. The same voltmeter was placed across the inner leads to determine the voltage drop between them. The conductivity was calculated from the current, the voltage, and the geometry of the sample. This measurement was made at three different currents and in both polarities to ensure ohmic behavior. All reported conductivities have been corrected for porosity (p) using the equation

$$\sigma_{sample} = (1+(p/(1+p^{2/3}))) \sigma_{measured} \quad (67)$$

AC measurements were made using a Wayne Kerr auto balance universal impedance bridge, model #B634, or a GenRad precision capacitance model #1616 in conjunction with a General Radio oscillator model #1210c and a PAR lock-in amplifier, model #5204, to insure that the 4-probe DC technique measured bulk conductivity. These measurements were only made as spot checks and yielded conductivities in excellent agreement, typically better than 1%, with the DC values. There was no measurable capacitance contribution to

the impedance. This is good evidence that grain boundary and surface effects were not interfering with the measurement of bulk conductivity.

The TEP of the samples was measured using the thermocouples, one at either end of the sample. An auxiliary heater produced a temperature gradient across the sample. Measurements of the temperature at each end of the sample and the voltage across the sample were made for several values of auxiliary heater power. A least squares fit was used to determine the value of the TEP. The maximum temperature gradient across the sample was 10C, and was usually less than 3°C. Samples were often equilibrated in a small (<3°C) temperature gradient. The auxiliary heater was used to produce both positive and negative temperature gradients.

Two electrical resistance furnaces were used for electrical conductivity measurements. One was wound with a platinum rhodium alloy and controlled with a Leeds and Northrop electromax controller and a Serensen model SRL60-35 dc power supply. The other furnace was wound with Kanthal-A alloy wire and was controlled with a Eurotherm 919 controller and 931 power supply. Temperature stability was better than ± 2 K.

The oxygen partial pressure was varied by mixed gases of either O_2/Ar, CO/CO_2, or by use of an oxygen pump. Bevan and Kordis[7] have shown that in the CeO_2system establishment of the oxygen partial pressure by either both

CO/CO_2 and H_2/H_2O buffer systems results in the same deviation from stoichiometry. The urania ceria solid solution system should behave in a similar manner. The pump consisted of a yttria stabilized zirconia tube, with platinum electrodes on both the interior and the exterior, inserted into a small Kanthal wound furnace. Control of the potential across the electrodes allowed for control of the PO_2 of the gas flowing through the tube. (See Figure IV.B.1. The mixtures were either purchased from Matheson or mixed in an electronically controlled gas mixing system; a Hastings automatic flow controller with model NALL-500p,NALL-100p, NALL-5p flow meters and model MV-33 electromechanical needle valve. This mixing system produced ratios of 1000/1 to 1/1000 CO/CO_2.

The oxygen partial pressure was measured by a zirconia galvanic cell. The cell was usually located downstream from the sample furnace, although at times it was installed upstream to check for leaks in the sample furnace. The cell was operated in the temperature range of 700°C to 1050°C. Outside of this range it demonstrated significantly nonideal emfs. The cell, Figure IV.B.2 was constructed from a yttria stabilized zirconia closed end tube (Zircoa composition #1372). The electrodes were unfluxed Pt paste (Engalhard#6926) and the leads were cp grade Pt wire. A Pt/Pt10%Rh thermocouple was used to determine the cell temperature.

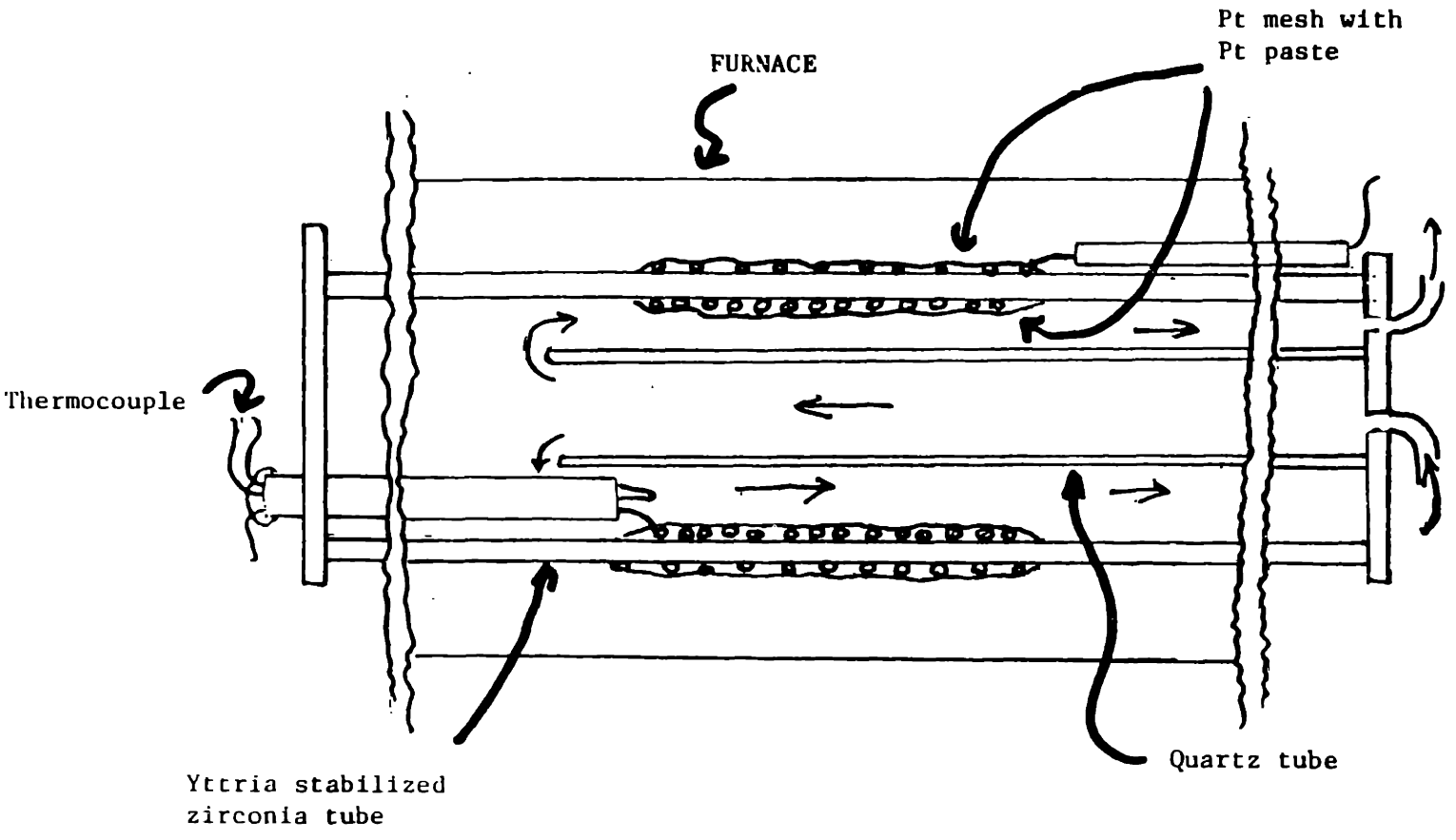

Figure IV.B.1 Schematic diagram of oxygen pump.

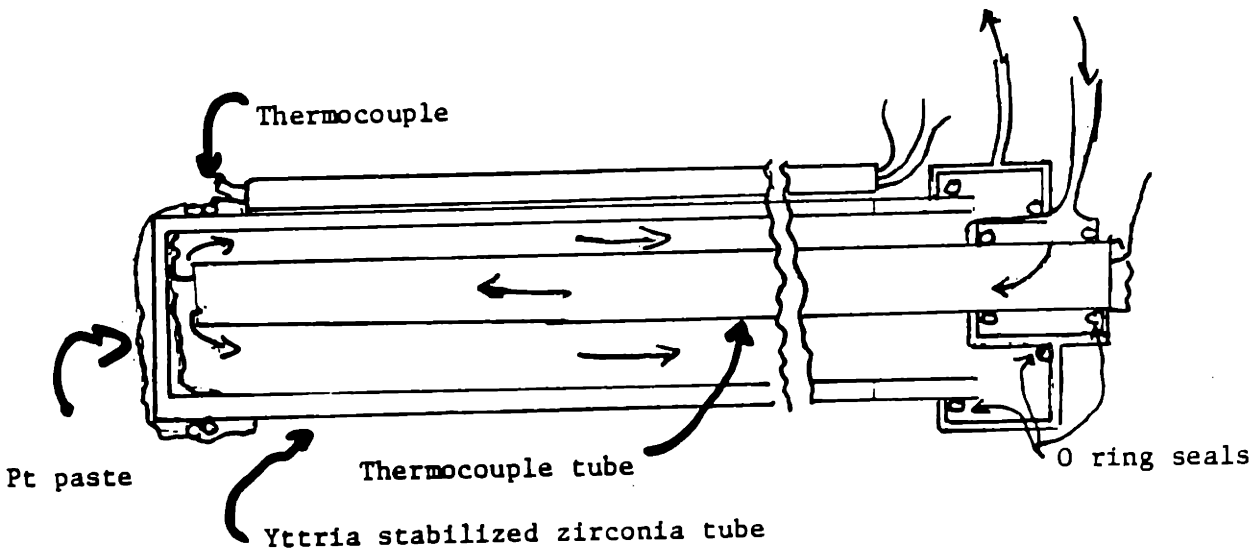

Figure IV.B.2 Schematic diagram of oxygen partial partial pressure sensor.

X-ray powder diffraction patterns of all compositions were taken using Cu K_α peak with a Ni filter . Figure IV.B.3 shows a typical diffraction pattern. The patterns showed no second phase; however, a x-ray pattern taken from the surface of a $U_{.6}Ce_{.4}O_2$ pellet did show evidence of $CeAlO_3$ attributed to contact between the edge of the pellet and the edge of the alumina crucible in which the pellet was fired. Conductivity samples were never cut from a part of the pellet which had been in contact with the alumina boat.The lattice parameters determined from a PhiTanPhi analysis (an algorithym which corrects for systematic errors in the measured difraction angle) of the high angle peaks are given in Figure IV.B.4 along with the value expected from the data of Lorenzelli and Touzelin.[33] This data shows good agreement indicating that the nominal compositions are close to the actual value except for the nominally $Ce_{.1}U_{.9}O_2$ specimen. Assuming that the lattice parameter for compositions $Ce_{.05}U_{.95}O_2$, $Ce_{.15}U_{.985}O_2$, and $Ce_{.1}U_{.9}O_2$(nominal) are all correct and that the nominal composition of $Ce_{.15}U_{.985}O_2$ is correct, then by linear interpolation a composition of $Ce_{.031}U_{.969}O_2$ was determined for the nominally $Ce_{.1}U_{.9}O_2$ composition. This is the composition which will be used for the purpose of data analysis.

An attempt was made to have the samples analyzed by atomic absorption for Ce/U ratio; however, during the

Figure IV.B.3 Typical diffraction pattern $Ce_{.015}U_{.985}O_{2\pm x}$.

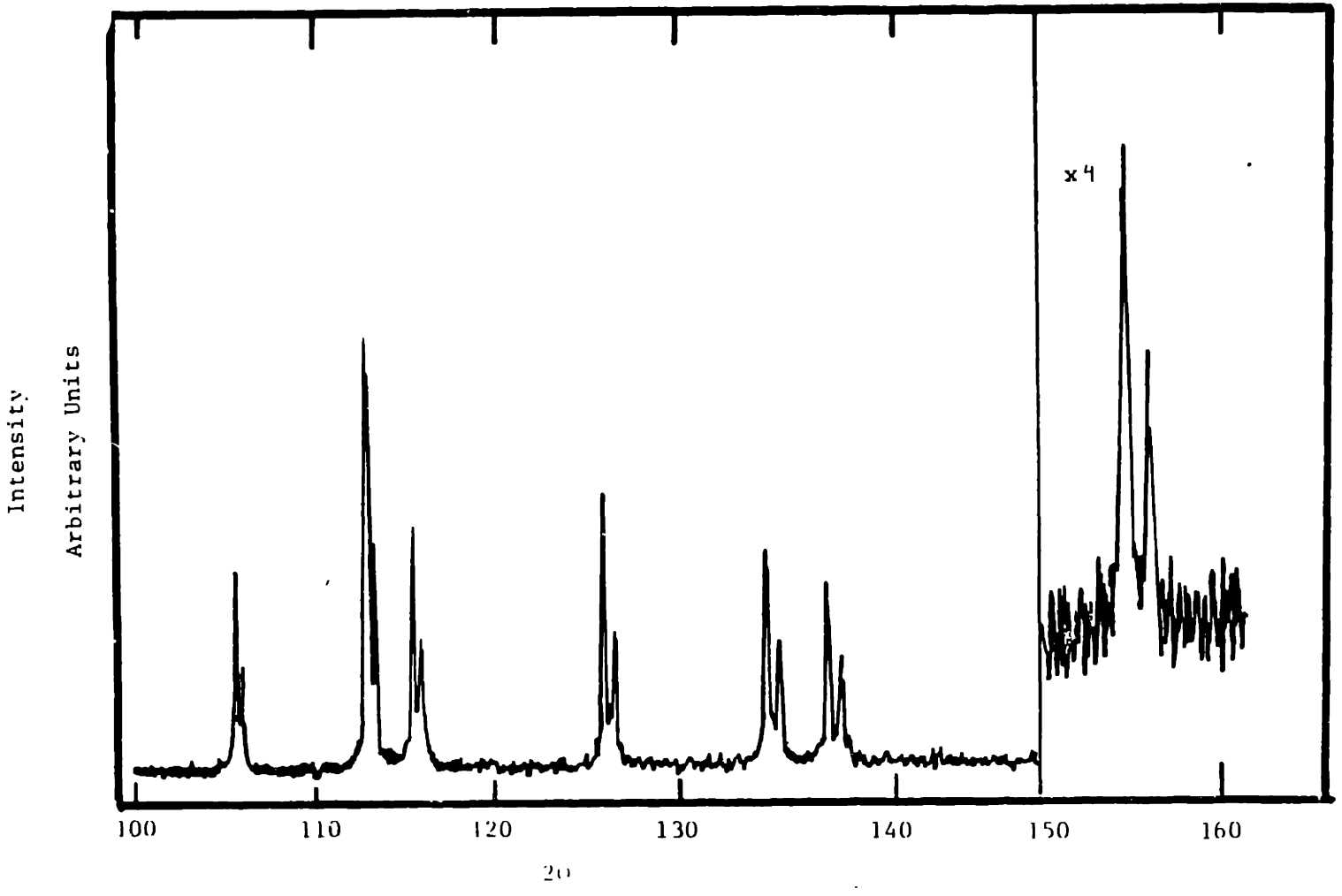

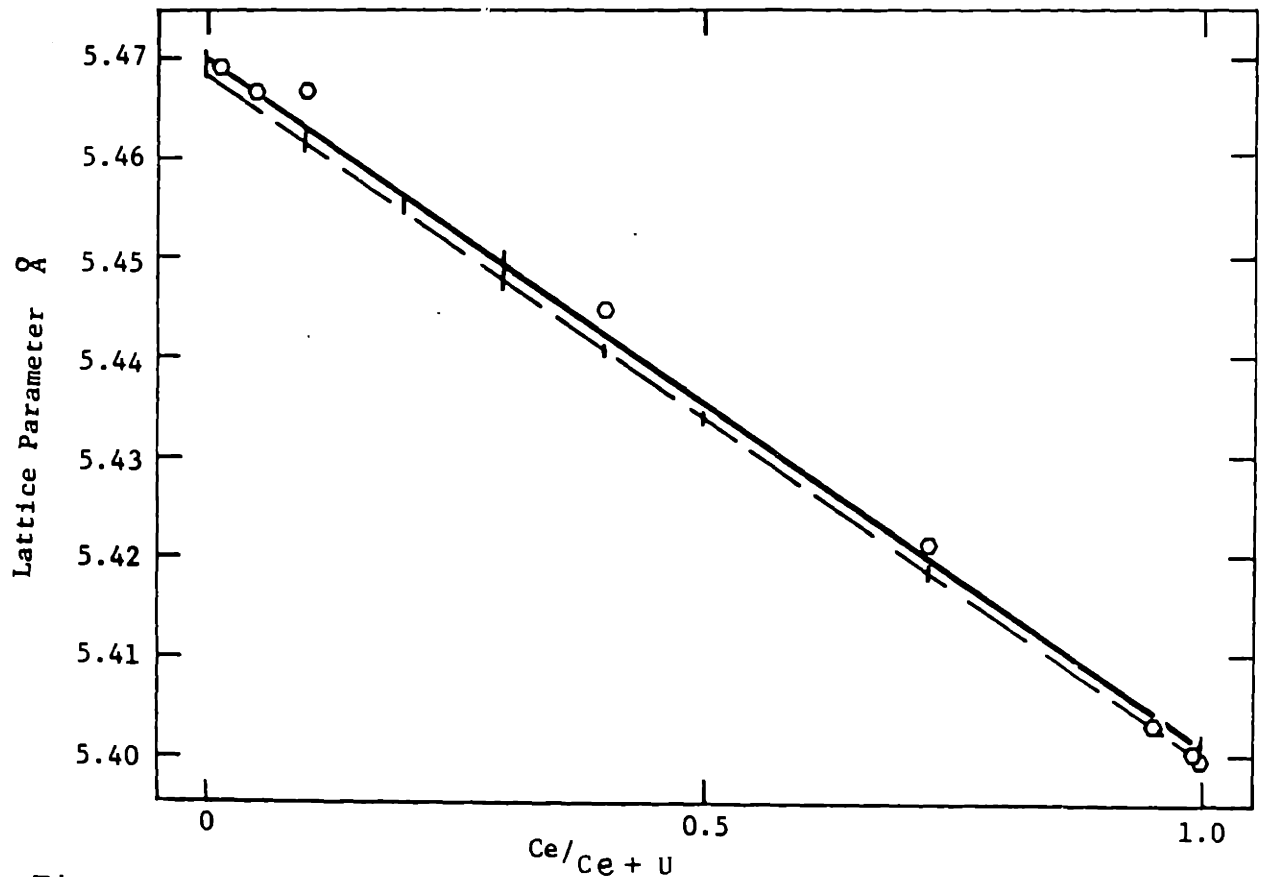

Figure IV.B.4 Lattice parameter vs nominal composition.

preparation of a solution for analysis, a compound (presumably a high CeO_2 compound) precipitated. The white powder could not be redissolved. Therefore no accurate ratio was obtained. Assuming that the powder was CeO_2, extensive tests were made on pure CeO_2 to attempt to dissolve it. No successful method was found.

V RESULTS

The electrical conductivity of urania ceria solid solutions was measured over a range of compositions from 1.5,3.1,5,25,40,75,95,99,99.9 m/o ceria over a temperature range from 1290°C to 465°C and over a range of oxygen partial pressures from one atm. to 10^{-28} atm. The TEP was also measured although over a more limited temperature and PO_2 range.

The electrical conductivity of all specimens was measured using standard 4 probe dc conductivity techniques. The measurements were made as a function of PO_2 at constant temperature. Samples were equilibrated at each PO_2 for between 1 hour at the highest temperature, and 48 hours at the lowest temperature. The DC measurements were checked with four probe AC single frequency technique to insure that grain boundaries and polarization effects were negligible. Simultaneous measurements of the TEP were made using thermocouples at each end of the sample and an auxiliary heater to induce small changes in the temperature gradient across the samples. These results will be used to establish the defect chemistry and electrical properties of ceria urania solid solutions.

A Ceria Rich Solid Solutions

The conductivity as a function of PO_2 for the compositions $Ce_{.999}U_{.001}O_2$, $Ce_{.99}U_{.01}O_2$, and $Ce_{.95}U_{.05}O_2$ is plotted in Figure V.A.1. Each curve is divided into

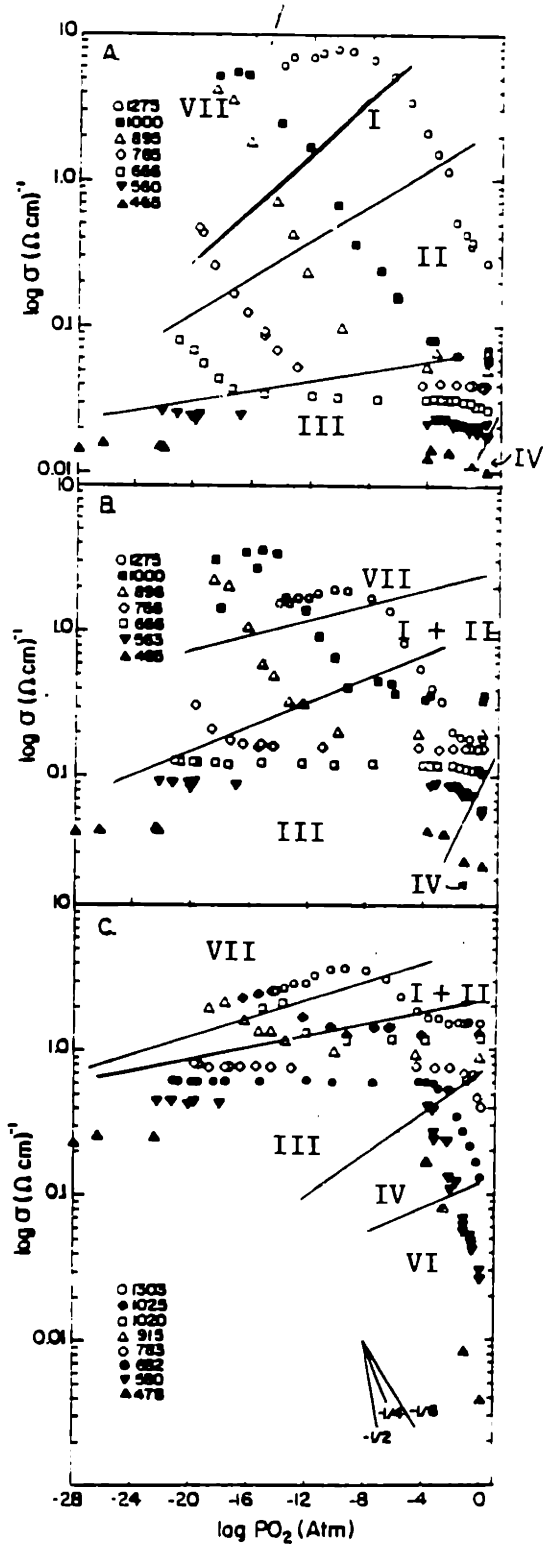

Figure V.A.1 Conductivity of ceria rich solid solutions.

A. $Ce_{.999}U_{.001}O_{2\pm x}$.

B. $Ce_{.99}U_{.01}O_{2\pm x}$.

C. $Ce_{.95}U_{.05}O_{2\pm x}$.

regions labeled I through IV which correspond to regions of defect chemistry described in Table III.A.1.3; and regions VI and VII, which do not correspond to any of the regions described by Table III.A.1.3. Examining the curves for $Ce_{.999}U_{.001}$, it is clear that region III predominates over a wide range of oxygen partial pressure at low temperature. This region is defined by the electroneutrality condition $n = [U_{Ce}^{\cdot}]$; and the material is oxygen deficient at low PO_2s within this range, stoichiometric in the middle of this range, and oxygen excess at the high PO_2 end of this region. Region III is bounded at higher PO_2 by a barely detectable PO_2 dependent region, IV, which, according to the theory, should have a dependence of $\sigma \propto PO_2^{-1/4}$. The 1/4 law dependence is not clearly demonstrated at this composition in this range of experimental conditions. The electroneutrality condition for this region is $[U_{Ce}^{\cdot}] = 2[O_i^{''}]$.

At lower oxygen partial pressure the PO_2 independent conductivity region is bounded by a region of conductivity proportional to $P_2^{-1/6}$. This corresponds to region II of Table III.A.1.3 with an electroneutrality condition controlled by electrons compensating for doubly ionized oxygen vacancies. With increasing temperature this region moves to higher oxygen partial pressures until at 1275°C there is no observable PO_2 independent region.

At still lower oxygen partial pressures and higher temperatures a region corresponding to region I of Table

A.1.3 ($\sigma \propto PO_2^{-1/4}$)is observed as a region of steeper conductivity dependence on PO_2.

Region VII appears at low oxygen partial pressures at the highest temperatures used in this study. This region is characterized by a decreasing dependence of the conductivity on PO_2 coupled with an obvious maximum in the conductivity at 1275°C. This, we later show corresponds to a strong dependence of mobility on carrier concentration.

The same general description can be applied to the conductivity of the $Ce_{.99}U_{.01}$ composition. One again finds the PO_2 independent region, III, bounded above and below by PO_2 dependent regions. For this composition Region IV is much better defined. However, the predicted power law is still not clear from the data given the regions' limited size. With increasing uranium concentration, the clear division between region I and II is not observed. Again, at high temperature a region is observable in which the conductivity goes through a maximum.

For the composition $Ce_{.95}U_{.05}O_2$ region III, a PO_2 independent conductivity region is clearly observed bounded by region IV, a PO_2 dependent region at high oxygen partial pressure; and by a PO_2, dependent region at low oxygen partial pressure. At this high concentration of uranium there are some important differences from the previously described compositions. First the PO_2 dependence of region IV is clearly visible as $PO_2^{-1/4}$ consistent with predictions. Second, an additional region becomes

observable at high PO_2 and low T that we label VI, which has a PO_2 dependence steeper than that of region IV. This region is not predicted by the model developed earlier and will be subsequently discussed in terms of defect association. Third, although there is still a clear transition from a PO_2independent to a PO_2 dependent region at the low oxygen partial pressure end of region III, the transition between region II and region I has completely disappeared.

In summary, Figure V.A.1 displays data consistent with the model of Table III.A.1.3. This data clearly shows that the material is oxygen excess in certain temperature oxygen partial pressure regions and is oxygen deficient in others. There are clear boundaries between the regions controlled by different electroneutrality conditions and these boundaries will be used to calculate specific defect equilibria constants.

Figure V.A.2 is a plot of $\ln(\sigma T)$ vs inverse temperature for region III. Such plots are important for determining the activation energy of different mechanisms. This figure clearly shows that for all three ceria rich solid solutions there is a constant activation energy of about 0.31ev in this region. This region is of particular interest because here the electron concentration is believed to be fixed by the uranium concentration and thus allows the activation energy of mobility to be assessed.

Figure V.A.3 is a similar plot for atmospheres corresponding to other defect regimes. Few of these curves

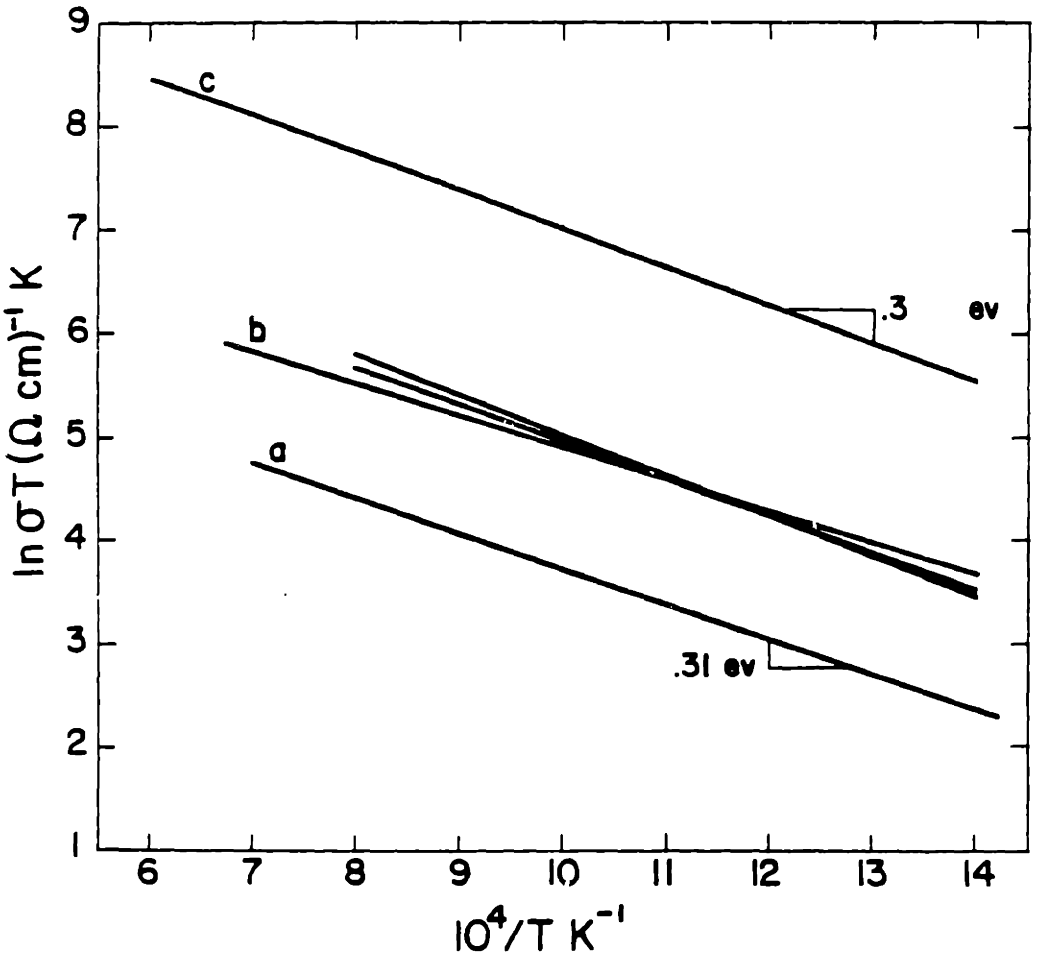

Figure V.A.2 ln(σ T) vs 1/T for ceria rich solid solutions.

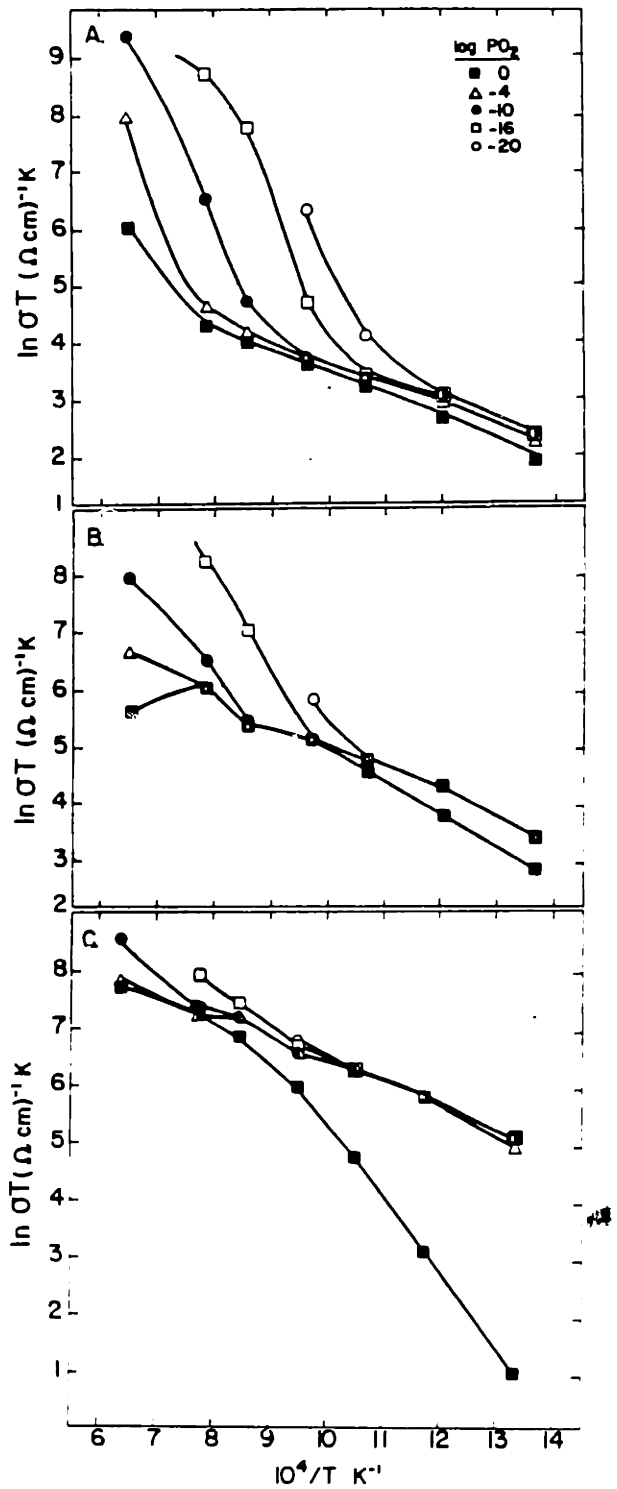

Figure V.A.3 ln(σ T) vs 1/T for several PO_2s.

A. $Ce_{.999}U_{.001}O_{2\pm x}$.

B. $Ce_{.99}U_{.01}O_{2\pm x}$.

C. $Ce_{.95}U_{.05}O_{2\pm x}$.

are Arrhenius over any signifigant temperature range. This is a result of the change in defect regimes with temperature at fixed PO_2 as is readily observed in Figure V.A.1. For example, composition $Ce_{.999}U_{.001}O_{2\pm x}$ at log PO_2=-4 is in region III at low temperatures and in region II at high temperatures. Some of the segments of the curves which do show a linear dependence of log (σ T) on 1/T will be used in the discussion section to determine activation energies related to mechanisms important in specific defect regions.

The conductivity of ceria rich solid solutions in region III is plotted as a function of uranium concentration in Figure V.A.4. The conductivity is not strictly linear, with uranium concentration displaying a slightly depressed conductivity with increasing uranium concentration. This deviation from the simple conduction model will be discussed later.

The thermoelectric power (TEP) vs ln (σ) is plotted in Figure V.A.5. The data for composition $Ce_{.999}U_{.001}O_{2\pm x}$ forms a well defined nose corresponding to the peak in the conductivity in region VII of Figure V.A.1. The data at the higher uranium concentrations each form a less extensive nose as the concentration of the uranium is increased. Although there is significant scatter in the data one important feature remains clear. Consistent with expectations from theory, the nose of the curve occurs not at TEP = 0 but at between -200 to -300 μ V/K below zero.

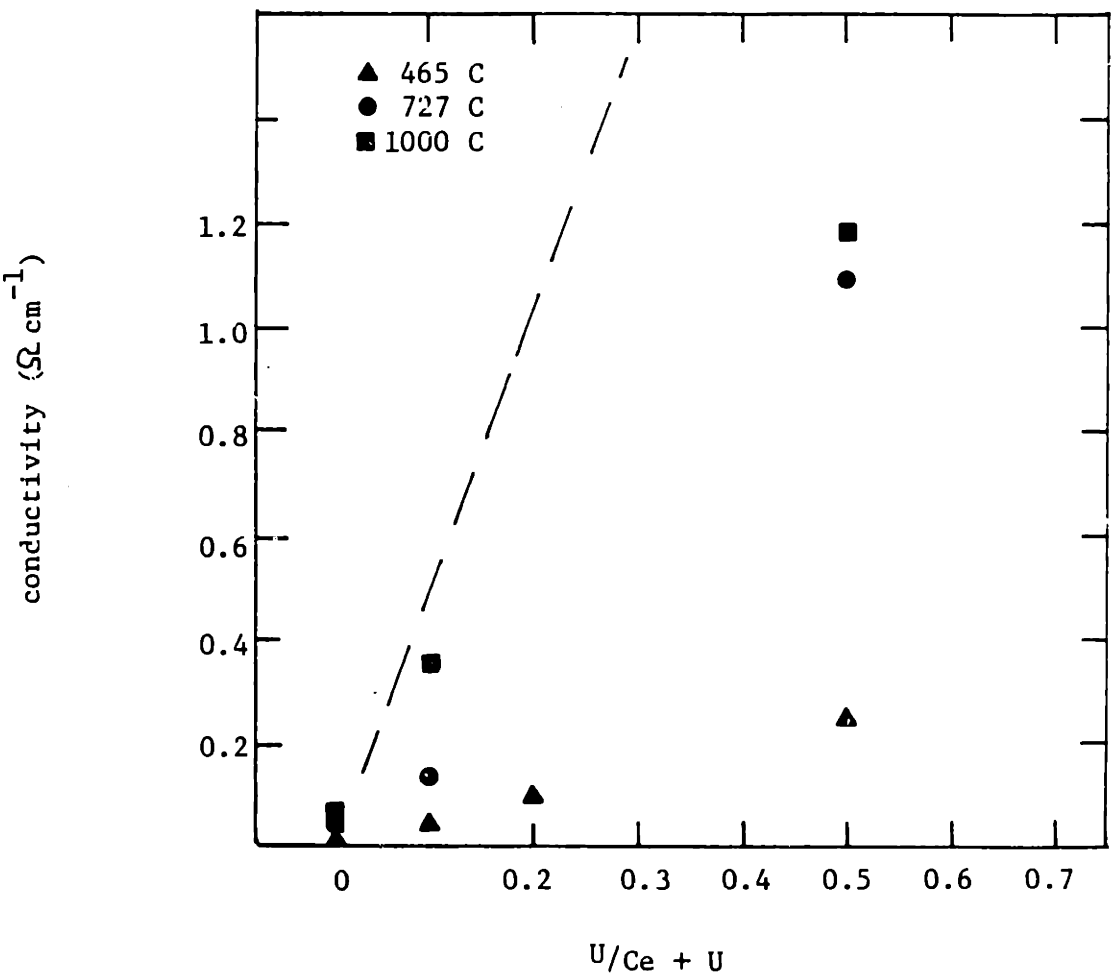

Figure V.A.4 PO_2 independent conductivity vs composition for ceria rich solid solutions.

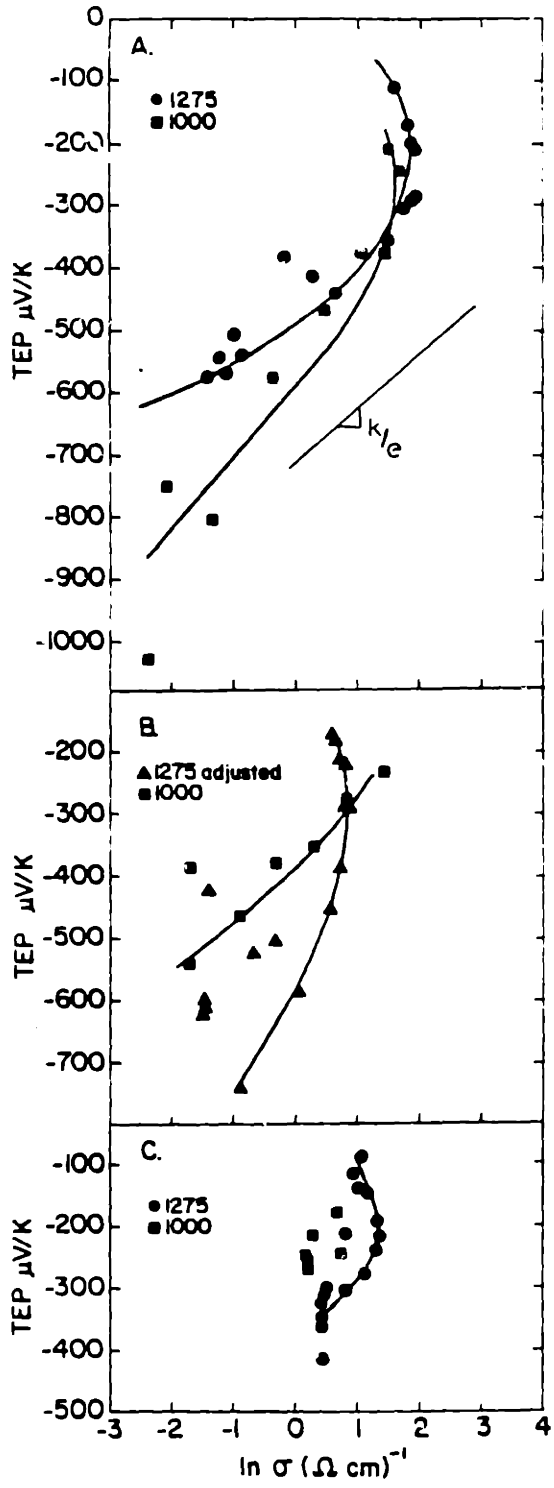

Figure V.A.5 TEP vs ln(σ).

A. $Ce_{.999}U_{.001}O_{2\pm x}$.

B. $Ce_{.99}U_{.01}O_{2\pm x}$.

C. $Ce_{.95}U_{.05}O_{2\pm x}$.

As discussed in the theory section, this is related to the difference of the entropy of electrons and holes. This also will be discussed in more detail in a later section.

B. URANIA RICH SOLID SOLUTIONS

From the models developed in the theory section it is clear that significant information can be obtained from the PO_2 dependence of the concentration of a defect. With the assumption that the conductivity is directly related to the dominant current carrier (holes in this case), this same information may be obtained from the PO_2 dependence of the conductivity. Therefore, the conductivity is plotted as a function of PO_2 for the UO_2 rich compositions in Figure V.B.1. There are 3 prominent features in these figures: a nearly PO_2 independent region and two PO_2 dependent regions. The nearly PO_2 independent conductivity region is most clear at the composition of $Ce_{.015}U_{.985}O_2$. In this region the electroneutrality condition is dominated by $p=[Ce_U^{\cdot}]$ (See table III.A.2.1.). It is in this region that the material is predicted to change from oxygen excess at high PO_2 to oxygen deficiency at lower PO_2. This region is very narrow in ceria dope urania and the width decreases significantly with increasing concentrations of cerium. The region is not truly PO_2 independent at high uranium concentrations due to overlap of this region with the regions above and below it.

Bounding the region of nearly PO_2 independent conductivity are two regions of PO_2 dependent conductivity. At lower oxygen partial pressure corresponding to oxygen deficient material, there is a clear change to a region in which $\sigma \propto PO_2^{1/4}$. This corresponds to region II of Table

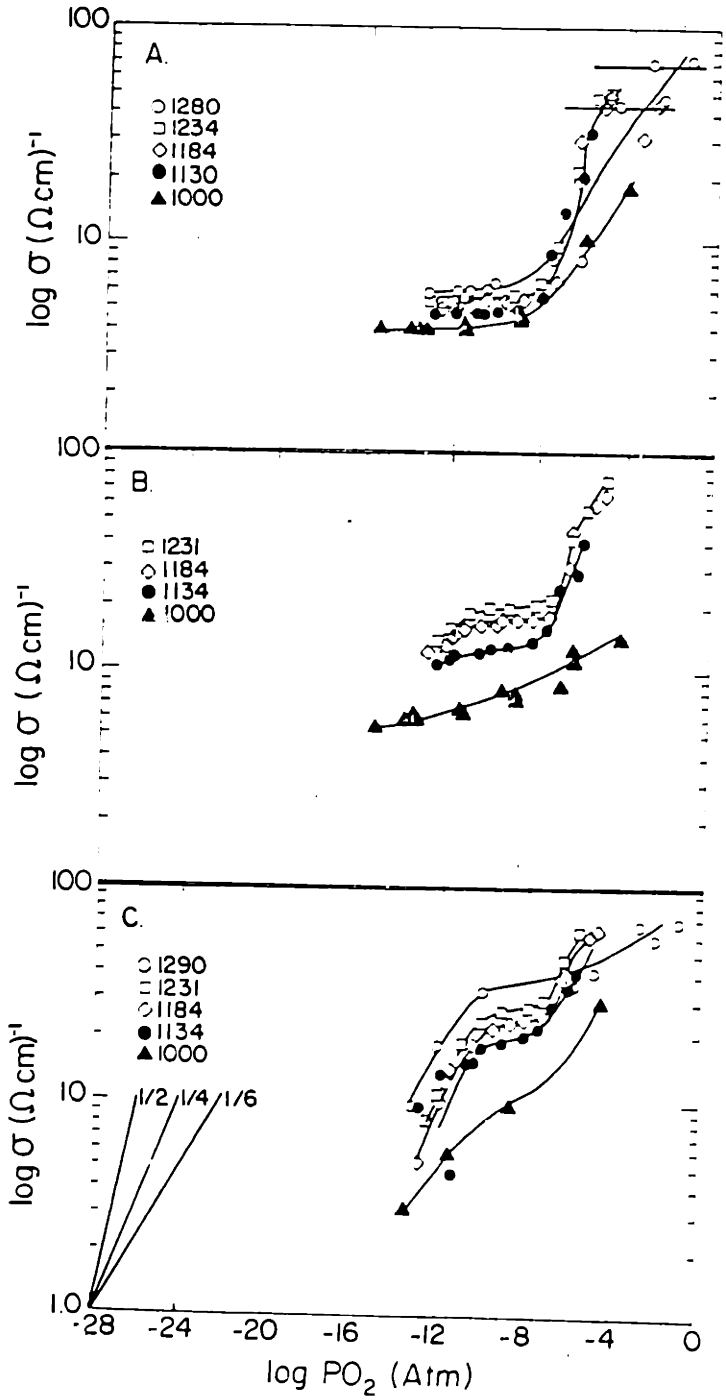

Figure V.B.1 Conductivity of urania rich solid solutions.

A. $Ce_{.015}U_{.985}O_{2\pm x}$.

B. $Ce_{.031}U_{.969}O_{2\pm x}$.

C. $Ce_{.05}U_{.95}O_{2\pm x}$.

III.A.2.3 in which the electroneutrality condition is dominated by $2[V_O^{\bullet\bullet}] = Ce_T$. On the other hand, at high oxygen partial pressures corresponding to excess oxygen, a strongly PO_2 dependent conductivity is observed. This finding, consistent with previous observations[24], is, however, not predicted by the simple models developed in the theory section. The stong PO_2 dependence is consistent instead with certain defect clustering, as will be discussed later.

In general, the data at 1000°C does not show the features as crisply as the data at higher temperatures. This is probably related to the difficulty of equilibrating the samples, which has been discussed by previous investigators[24] and also observed in these investigations.

Figure V.B.1 corresponds to conductivity variations resulting from nonstoichiometry change from oxygen deficiency to oxygen excess. Later sections will examine how readily defect parameters may be extracted from this data.

Because activation energies for various mechanisms can be derived from plots of log(σ T) vs 1/T, we present such data obtained for several PO_2s in Figure V.B.2. The situation here is similar to that observed in CeO_2 in that the curves exhibit significantly non-Arrhenius behavior as a result of changing defect regimes with temperature at constant PO_2. Again, portions of these curves may be used

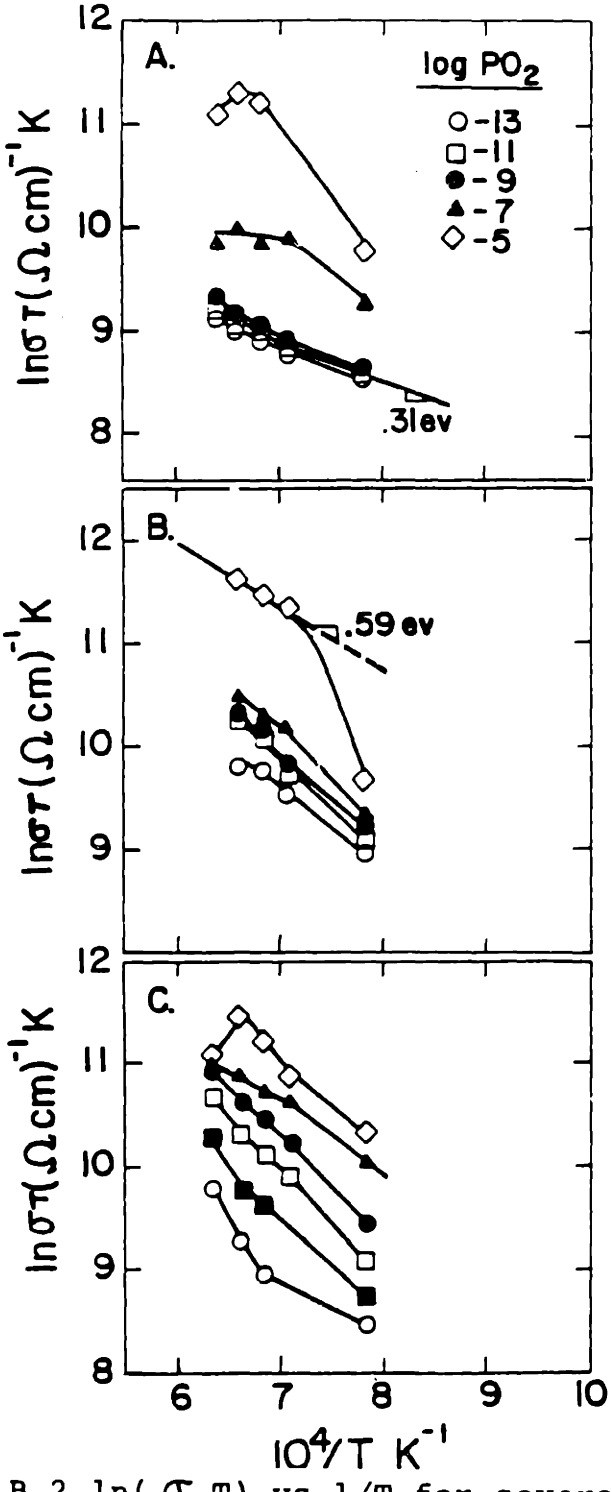

Figure V.B.2 ln(σ T) vs 1/T for several PO_2's.

A. $Ce_{.015}U_{.985}O_{2\pm x}$.

B. $Ce_{.031}U_{.969}O_{2\pm x}$.

C. $Ce_{.05}U_{.95}O_{2\pm x}$.

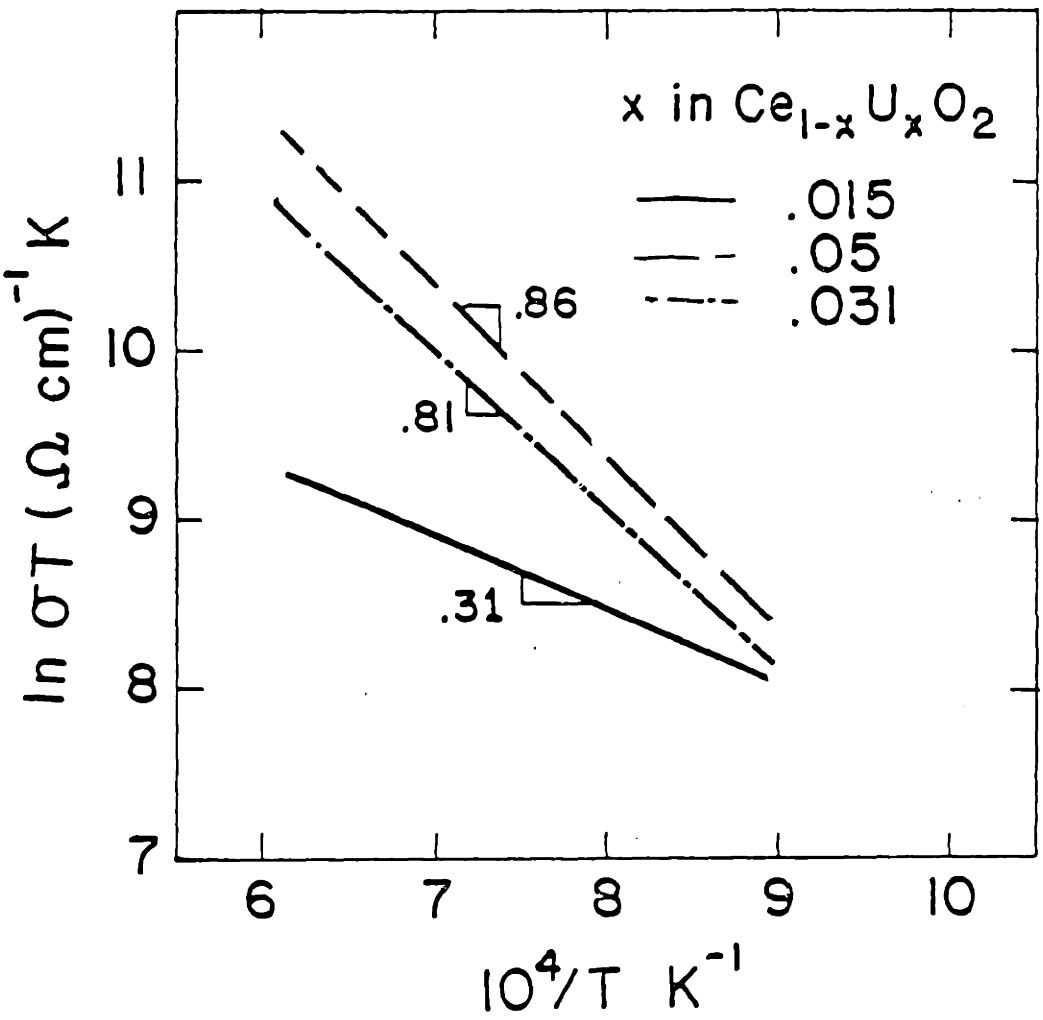

Figure V.B.3 ln(σ T) vs 1/T for the PO_2 independent region urania rich solid solutions.

to determine activation energies in regions of interest. For example, Figure V.B.3 is a plot of $\log(\sigma T)$ vs $1/T$ in the nearly PO_2 independent region. The data for the composition $Ce_{.015}U_{.985}O_{2\pm x}$, which exhibits an activation energy of 0.31 ev, corresponds to a truly PO_2independent region. The concentration of carriers is therefore fixed and this energy is the activation energy for the mobility of carriers. On the other hand, the activation energy of both compositions with higher cerium concentrations are determined in a region in which there is some PO_2 dependence of the conductivity, indicating some overlap of the regions which result in activation energies which are significantly higher and do not represent a single defect mechanism.

From these two figures it is apparent that the activation for mobility is 0.3lev, while other mechanisms are contributing to the carrier concentration in the nearly PO_2 independent regions for compositions with higher cerium concentration.

In previous studies the conductivity has been shown to be stongly dependent on the concentration of dopant[24]. To examine this issue, the conductivity is plotted vs composition at 1184°C in Figure V.B.4. Also included is the data of Dudney[24] for comparison. It is evident that the decreasing dependence of conductivity on dopant levels above 1m/o observed by Dudney is not observed in this study. This result and its implication for the transport mechanism in urania will be discussed later.

In Figure V.B.5 we plot the TEP vs $\ln \sigma$. The results for the composition $Ce_{.015}U_{.985}O_{2\pm x}$ follows a nearly straight line with a slope close to k/e (86 μ V/K). This correlates well with the simple theory for polaron conduction in the region far from saturation of the band (Figure III.C.1). At higher cerium concentrations, a significant deviation from this behavior is observed. The data at high conductivity is still approximately the same. However, at lower conductivity the TEP flattens out and becomes nearly independent of conductivity. This is not consistent with any of the simple models describing the TEP conductivity relations unless additional contributions to the TEP from other mechanisms are included. A discussion of one plausible mechanism will later be examined.

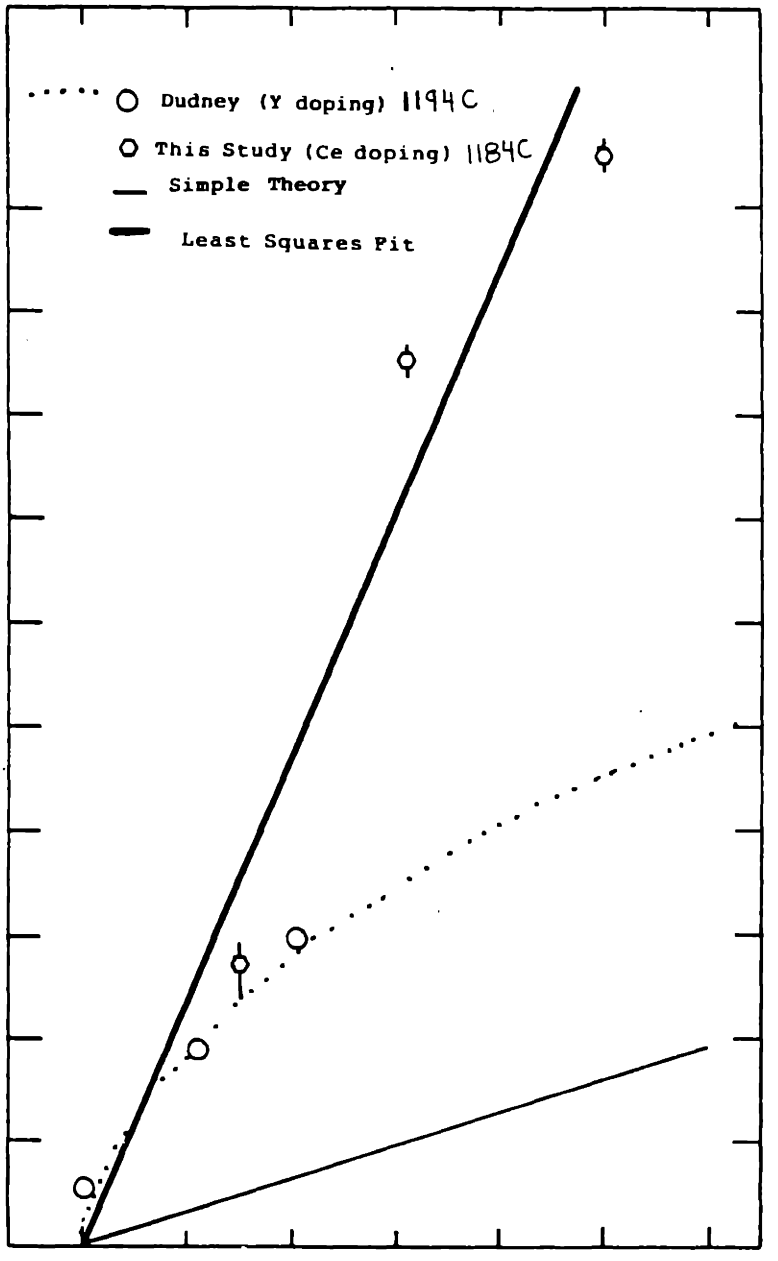

Figure V.B.4 Conductivity vs composition for urania rich solid solutions.

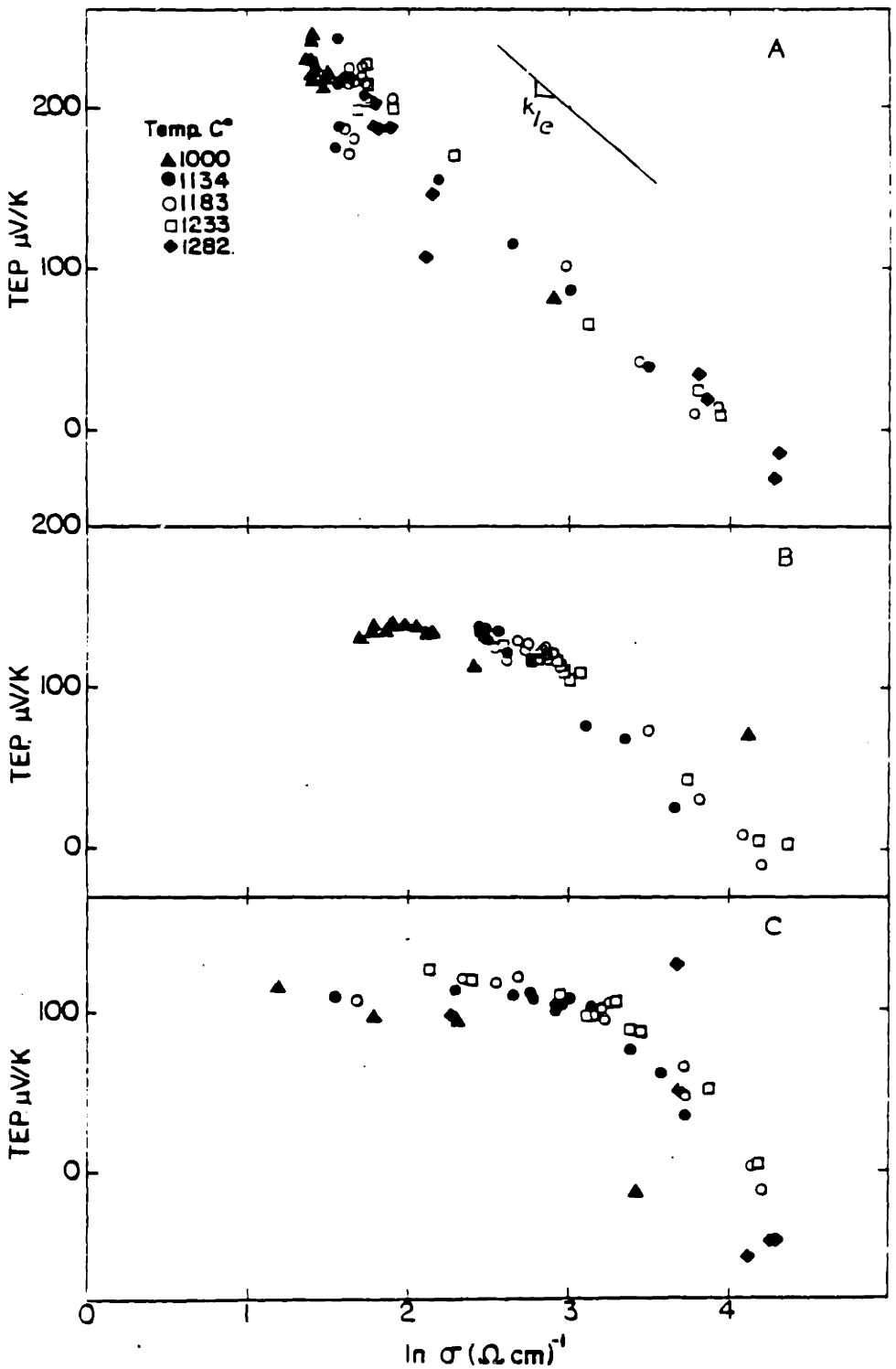

Figure V.B.5 TEP vs ln(σ).

A. $Ce_{.015}U_{.985}O_{2\pm x}$.

B. $Ce_{.031}U_{.969}O_{2\pm x}$.

C. $Ce_{.05}U_{.95}O_{2\pm x}$.

VI.A DISCUSSION OF THE DEFECT CHEMISTRY

The primary purpose of this work is to understand the defect structure of ceria urania solid solutions. Of critical importance to this understanding is the nature of the intrinsic ionic disorder in these materials as reflected in the Frenkel product, K_1. The square root of this value is the concentration of oxygen vacancies and oxygen interstitials at stoichiometry. Because these materials pass through stoichiometry in the PO_2 independent region we focus our attention there. The defect chemistry for this region will be briefly reviewed and the data used to determine K_1 and other equilibria constants for the ceria rich solid solutions.

CERIA RICH SOLID SOLUTIONS

The defect concentrations in the regions near stoichiometry are replotted schematically in Figure VI.A.1. This schematic shows that stoichiometry occurs in the center of the PO_2 independent regime. For a given concentration of U_T

$$K_1^{1/2} = [O_i'']_{intrinsic} = [V_O^{\cdot\cdot}]_{intrinsic}$$

can be readily calulated from the $PO_2^{\pm 1/2}$ dependences of the oxygen interstitials and vacancies which are extrapolated from the boundaries at which $2[V_O^{\cdot\cdot}] = U_T$ and $2[O_i''] = U_T$ at the low and high PO_2 boundaries respectively. Therefore, tc calculate K_1 one need only know the locations

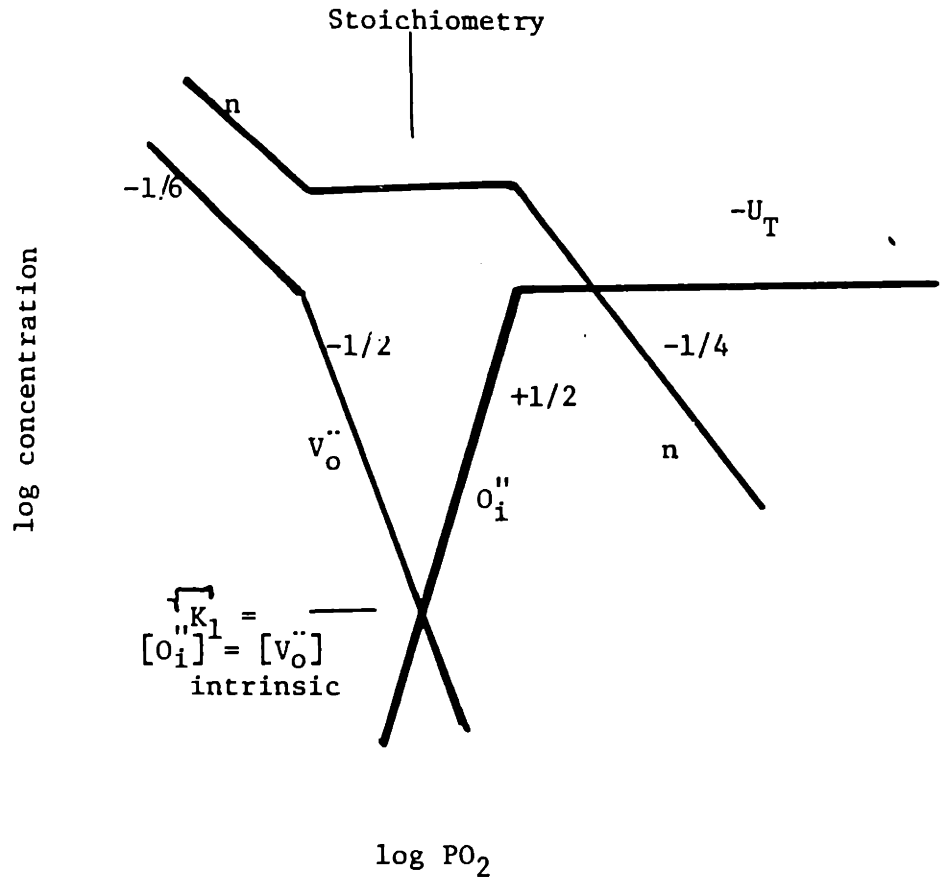

Figure VI.A.1 Schematic diagram of defect regions near stoichiometry.

of the boundaries of the PO_2 independent region and the total concentration of dopant.

However, to use the Brouwer approximation to determine the reaction equilibria it is necessary to have data well away from the boundaries between regions in order to determine them accuratly. Figure V.A.1 shows that for most compositions and temperatures there is data on one side of the boundary but not on both sides. To determine reaction constants from data which does not extend well beyond the boundary it is necessary to solve the set of simultaneous equations, III.A.1.7 to III.A.1.12, with an additional charge species in the electroneutrality constraint. For example, in the vacinity of the boundary between regions II and III the electroneutrality condition is

$$n = 2[V_O^{\cdot\cdot}] + U_T. \qquad \text{(VI.A.1)}$$

Using this and substituting into equation III.A.1.8 one may write

$$K_3^{-1}\, n^3 - U_T\, K_3^{-1}\, n^2 = 2PO_2^{-1/2} \qquad \text{(VI.A.2)}$$

Conductivity is the experimentally measured quantity, therefore it is appropriate to transform the above equation using equation III.B.1.2. One may then write

$$K_3^{-1}\, (e\mu)^{-3}\sigma - U_T\, K_3^{-1}\, (e\mu)^{-2} = 2PO_2^{-1/2}\, \sigma^{-2} \qquad \text{(VI.A.3)}$$

Now let $A_3 = K_3^{-1} (e\mu)^{-3}$ (VI.A.4)

and $A_2 = K_3^{-1} (e\mu)^{-2}$ (VI.A.5)

then solving for K_3

$$K_3 = -A_3^2 A_2^{-3} U_T^3 \qquad \text{(VI.A.6)}$$

Linear regression annalysis with an equation of the form of equation VI.A.3 has been used on the data in the vacinity of the boundary between regions II and III and coefficients A_3 and A_2 have been determined. Using this K_3 has been calculated.

In the vacinity of the boundary between regions III and IV the electroneutrality constaint is $n + 2[O_i''] = U_T$. The resulting equation used in the linear regression is

$$B_2 \sigma^{-1} + B_1 = 2 \sigma P O_2^{1/2} \qquad \text{(VI.A.7)}$$

then

$$K_1 = B_1^{-2} B_2 K_3 U_T^{-1} . \qquad \text{(VI.A.8)}$$

Linear regression analysis has been applied to the data from the vacinity of the boundary between regions III and IV, using an equation of the form of VI.A.7. Therby B_1 and B_2 have been determined and K_1 calculated using previously determined values for K_3.

Using the above linear regression analysis, a value of K_1 for each composition has been derived. These values are plotted in Figure VI.A.2. The lines represent linear least squares fit to the determined values of K_1 at each temperature excluding data at 465°C. At the highest uranium

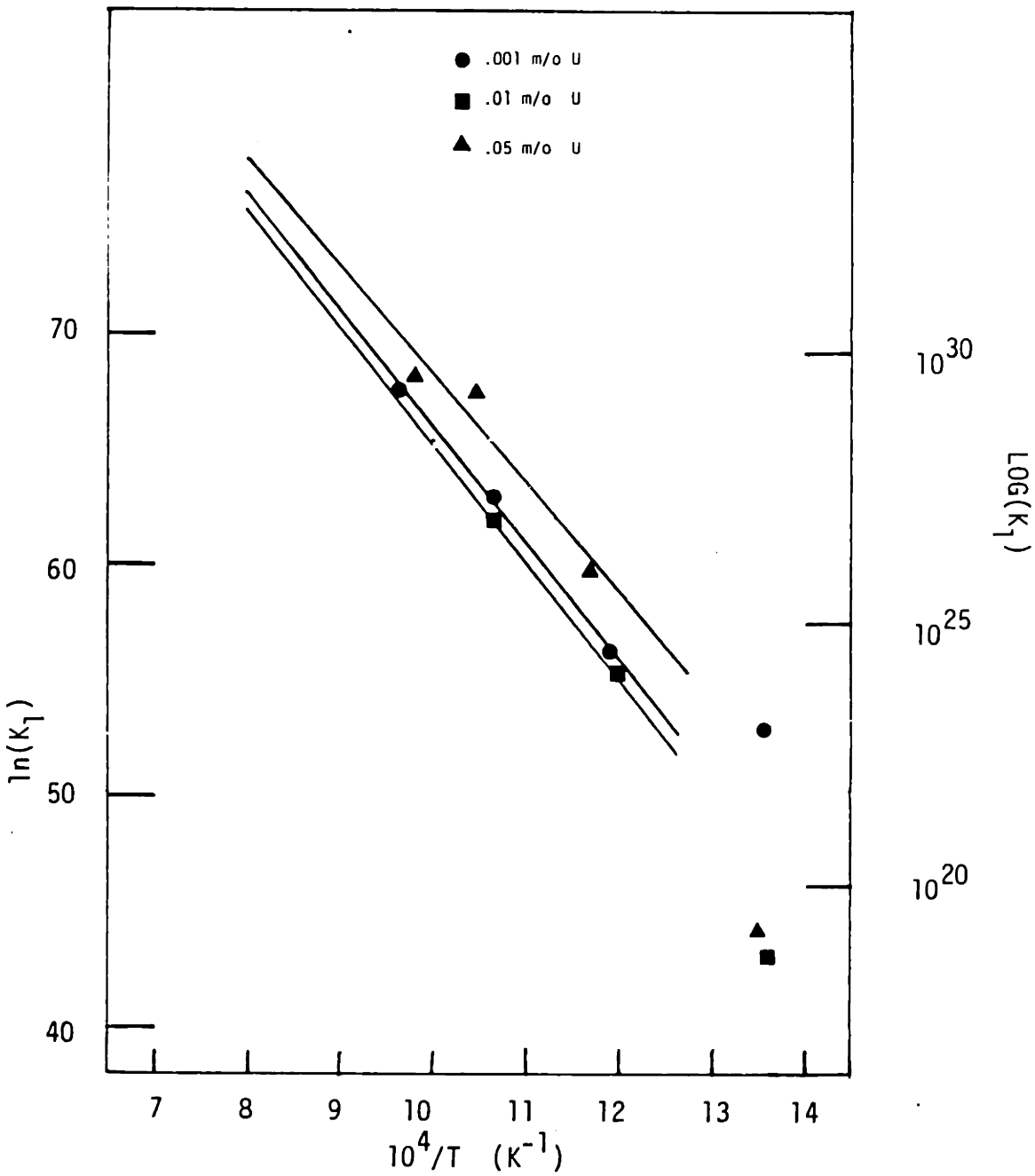

Figure VI.A.2 ln K_1 vs 1/T.

concentration and temperature of 465°C the PO_2 dependence of the conductivity was closer to a -1/2 slope than a -1/4 slope. Therefore, the data at that temperature will not fit the previously described detailed defect model and the values of K_1 for those temperatures are suspect.

Note the high intrinsic disorder in these compositions; e.g., $10^{33}cm^{-6}$ at 977°C. This is consistent with the large deviation from stoichiometry. As Anderson[68] pointed out, materials with large intrinsic disorder will tend to have large deviations from stoichiometry.

Values for K_1 for each doping level calculated from the above figure are as follows.

$$K_{1(.999)} = 3.2x10^{50}x10^{\pm 1.5} \exp(-4.34\pm.5ev/kT) \quad \text{(VI.A.9)}$$

$$K_{1(.99)} = 2.3x10^{50}x10^{\pm 1.5} \exp(-4.37\pm.5\ ev/(k_bT)) \quad \text{(VI.A.10)}$$

$$K_{1(.95)} = 6.4x10^{49}x10^{\pm 1.5} \exp(-4.01\pm.5\ ev/(K_bT)) \quad \text{(VI.A.11)}$$

The valuse diplay some scatter but all are equal within the uncertainty of the data.

To test whether the assumptions made in the above analysis are self consistent, we compare the above values with those from theory. The preexponential term in K_1 should be the product of the number of O_o sites times the maximum number of interstitial sites. For the fluorite structure there are four O_o per unit cell. There are four interstitial sites equivalent to 1/2,1/2,1/2 per unit cell. Using these values $K_{1\ o}$ is 1.27E45. Additional

contributions to the preexponential arise from two sources. First there is an additional entropy contribution due to vibrational terms not considered above. This is ussually less than 10 and may be less than one for Frenkel disorder.[58]. The second source is the temperature coefficient of the activation. This term arises in part due to the thermal expansion of the crystal which changes the defect formation energy. This term is expected to contribute a factor of 10 - 100 to the preexponential term. If we take the high value the the theoretical $K_{1\ o}$ is $1x10^{47}$. This is still about two orders of magnitude below the experimentally determined value. This additional discrepancy may be due to errors in the determined activation energy. For example an activation energy of 3.64ev and preexponential of 10^{47} yields approximatly the same value of K_1 in the range of temperatures for which data is available. The data used to calculate the K_1's included data at 565°C. This data may also have some small contribution from the association reaction discussed earlier, therefore lowering the appearent value of K_1 at low temperature and increasing the activation energy and the preexponential slightly.

The activation energy will now be compared to some calculations which have been done using computational point defect simulations. The measured activation energy is lower than the value of 5.52ev, recently calculated by Shiun

Ling[69] for CeO_2. Shiun Ling's value, however, is quite close to that which Catlow[14] calculated for UO_2. The similarity of these calculated values is reasonable given the similarity of the structure of the two materials; however, it is well known that these types of calculation methods are sensitive to the details of the apriori assumptions, and the relative energies between defects are much more certain than the absolute magnitude of the energy[14].

In this section it has been shown that both oxygen excess and deficient ceria has been produced by judicious choice of dopant, control of the oxygen partial pressure, and control of temperature. The intrinsic Frenkel product for ceria has been determined and shown to be weakly dependent on the doping concentration. The preexponential values have been shown to be in reasonable agreement with theory. Further, these results have cast doubt on the Frenkel energy determined by computational point defect simulations.

Defect reactions which occur further from stoichiometry will now be considered. Values of K_3 were determined by the fitting procedure described above. These values are plotted in Figure VI.A.3. The lines represent linear least squares fit to the determined values of K_3 at each temperature. Also plotted is the value of K_3 reported by Tuller and Nowick[27] for pure CeO_2. Besides the value of K_3 this figure shows two important results.

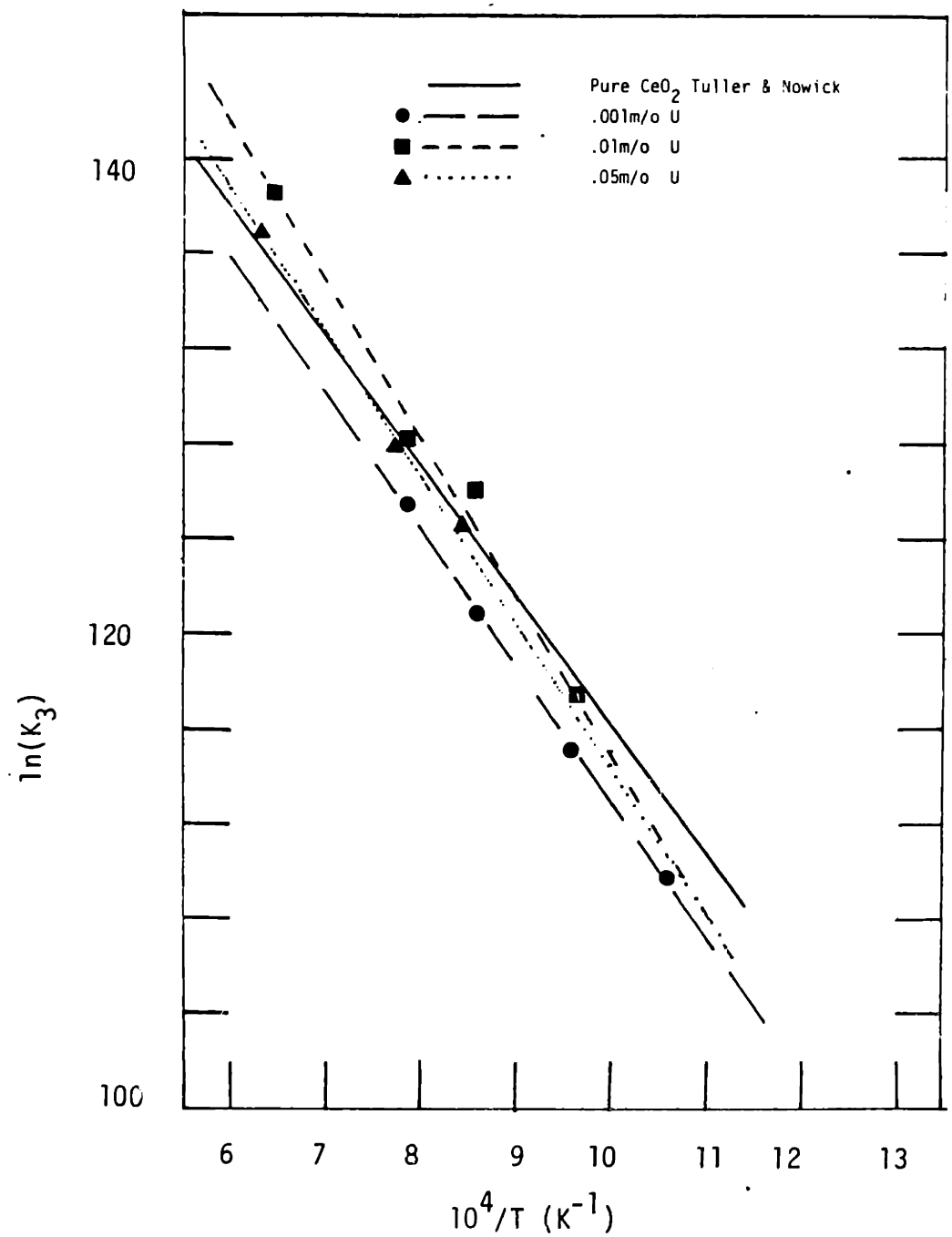

Figure VI.A.3 ln K_3 vs 1/T.

First the K_3 determined for .999 Ce is about 1/20 of the value of Tuller and Nowick with very close to the same activation energy. If this is due to a difference of the measured value of oxygen partial pressure it represents a diffrence of about two orders of magnitude of partial pressure. It should be noted that a rough "by eye fit" of the data of this study to a slope of 1/6 and PO_2 independent conductivity resulted in much better agreement between the two studies. Second, There is no trend of the value of the preexponential or the activation energy with uranium concentration. The numerical values for K_3 are

$$K_{3\,(.999)} = 1.1\times10^{74}\times10^{\pm1.5}\ \exp(-4.96\pm.5\ \text{ev}/(kT))\ \ \text{cm}^{-9}\text{Atm}^{1/2} \qquad \text{(IV.A.12)}$$

$$K_{3\,(.99)} = 4.8\times10^{78}\times10^{\pm1.5}\ \exp(-5.95\pm.5\ \text{ev}/(kT))\ \ \text{cm}^{-9}\text{Atm}^{1/2} \qquad \text{(IV.A.13)}$$

$$K_{3\,(.95)} = 9.5\times10^{75}\times10^{\pm1.5}\ \exp(-5.20\pm.5\ \text{ev}/(kT))\ \ \text{cm}^{-9}\text{Atm}^{1/2} \qquad \text{(IV.A.14)}$$

So far, the model of Table III.A.3 has been used to determine the equilibria constants. This model assumes fully ionized urania and doubly ionized oxygen interstitials and singly or doubly ionized oxygen vacancies. Using this model and the band diagrams presented earlier, three more equilibria constants will now be determined. The intrinsic electron-hole pair production equilibrium constant, K_2, is determined by the energy of the band gap and the density of states in both the

conduction and valence band. The band diagram suggests that the energy for the intrinsic electron-hole pair production is about 2.5 ev. Assuming a localized electron model in which only one electron may reside on each cerium and each cerium is available as a site for an electron, one obtains a density of states in the conduction band of about $2.5x10^{22}$. Similarly, assuming that each oxygen contributes two electrons to the valence band, the density of states in the valence band is $1x10^{23}$. Combining these two approximations with the band gap results in the following value for K_2:

$$K_2 = 2.53E45\exp(-2.5ev/(K_bT)) \qquad \text{(VI.A.15)}$$

This estimate can then be combined with K_1 and K_3 derived earlier to determine the equilibrium constant for oxidation of the material, K_4. The relation between these constants was given in equation II.A.1.10. From this relation the following values of the oxidation equilibrium constant are determined:

$$K_{4(.999)} = 5.22x10^{-67}x10^{\pm 1.5} \exp(4.38\pm.5ev/(k_bT)) \qquad \text{(VI.A.16)}$$

$$K_{4(.99)} = 3.31x10^{-63}x10^{\pm 1.5} \exp(3.42\pm.5ev/(k_bT)) \qquad \text{(VI.A.17)}$$

$$K_{4(.95)} = 2.4x10^{-65}x10^{\pm 1.5} \exp(3.81\pm.5ev/(k_bT)). \qquad \text{(VI.A.18)}$$

And finally the set of equilibrium constants is completed

by determination of K_5, the equilibrium constant for the ionization of the oxygen vacancy from singly ionized to doubly ionized. To determine this constant, the PO_2 of the boundary between region I and II is plotted as a function of 1/T in Figure VI.A.4. Only the data for the composition $Ce_{.999}U_{.001}O_{2-x}$ is plotted because at the higher doping levels both regions narrow so that no boundary is readily discernible. The data can be fit to the equation:

$$PO_{2(I-II)(.999)} = 5.93E29 \exp(-9.88 \text{ ev}/(k_b T)) \quad \text{(VI.A.19)}$$

Combining this with the value of K_3 in the equation for this boundary from Table III.A.1.2 results in the following value for $K_{5(.999)}$

$$K_{5(.999)} = 1.7x10^{19} \exp(-.007 \pm .5 \text{ ev}/(k_b T)). \quad \text{(VI.A.20)}$$

This result has a significantly smaller activation energy than the results of Tuller and Nowick.[27] However both of these numbers are derived from the difference of two large numbers and are therefore subject to error.

With the determination of this last equilibrium constant, the model becomes complete (Table VI.A.1). The system is now specified for the entire temperature range and oxygen partial pressure range over which the model of Table III.A.1.1 is valid.

This study has been able to determine all important defect equilibria constants for the ceria system doped with urania. This was accomplished by measurements of electronic

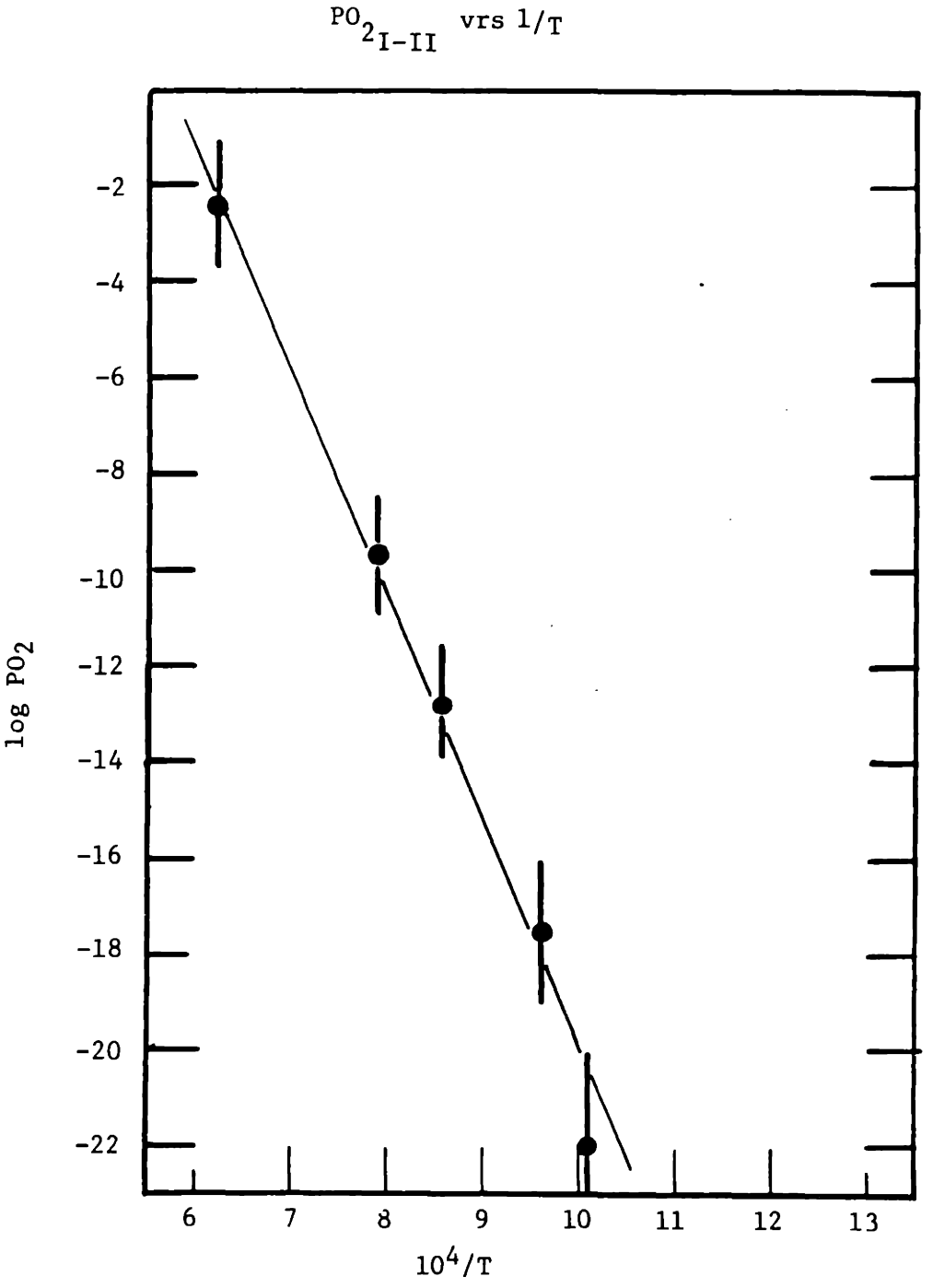

Figure VI.A.4 log PO_2 of boundary between regions I and II.

TABLE VI.A.1 COMPLETE SET OF EQUILIBRIA CONSTANTS FOR THE URANIA DOPED CERIA SYSTEM

$K_{1(.999)} = 3.2\times10^{50}\times10^{\pm1.5}\ \exp(-4.34\pm.5\text{ev}/(k_bT))$ (cm^{-6})

$K_{1(.99)} = 2.3\times10^{50}\times10^{\pm1.5}\ \exp(-4.37\pm.5\ \text{ev}/(k_bT))$ (cm^{-6})

$K_{1(.95)} = 6.4\times10^{49}\times10^{\pm1.5}\ \exp(-4.01\pm.5\ \text{ev}/(K_bT))$ (cm^{-6})

$K_2 = 2.53E45\exp(-2.5\text{ev}/(K_bT))$ (cm^{-6})

$K_{3(.999)} = 1.1\times10^{74}\times10^{\pm1.5}\ \exp(-4.96\pm.5\ \text{ev}/(k_bT))$ $(cm^{-9}Atm^{1/2})$

$K_{3(.99)} = 4.8\times10^{78}\times10^{\pm1.5}\ \exp(-5.95\pm.5\ \text{ev}/(k_bT))$ $(cm^{-9}Atm^{1/2})$

$K_{3(.95)} = 9.5\times10^{75}\times10^{\pm1.5}\ \exp(-5.20\pm.5\ \text{ev}/(k_bT))$ $(cm^{-9}Atm^{1/2})$

$K_{4(.999)} = 5.22\times10^{-67}\times10^{\pm1.5}\ \exp(4.38\pm.5\text{ev}/(k_bT))$ $(cm^{9}Atm^{1/2})$

$K_{4(.99)} = 3.31\times10^{-63}\times10^{\pm1.5}\ \exp(3.42\pm.5\text{ev}/(k_bT))$ $(cm^{9}Atm^{1/2})$

$K_{4(.95)} = 2.53\times10^{-64}\times10^{\pm1.5}\ \exp(3.81\pm.5\text{ev}/(k_bT))$. $(cm^{9}Atm^{1/2})$

$K_{5(.999)} = 7.7\times10^{19}\times10^{\pm1.5}\ \exp(-.007\pm.5\ \text{ev}/(k_bT))$. (cm^{-3})

parameters and correlation of these measurements with the defect model for the system. A complete list of defect reaction equilibrium constants is given in Table VI.A.1.

The above analysis uses linear least squares fits to determine th reaction constants. For this type of analysis the paramater R^2 (the coefficient of determination) is a measure of the goodness of the fit. The value of R^2 for the determination of values of K for a specific composition and temperature range from 0.999 to 0.55 with most values above 0.9. These fits correspond to at least 5 and as many as 24 data points each. For the fit to the 1/T plots from which the activation energy and preexponential were derived the fits are all better than 0.93. These fits representing from 2 to 5 points each. Another way to consider the certainty of the data is to consider how much the actual value of the reaction constant will change for a given change of the PO_2 of the boundary between two regions. For example if the boundary between regions III and IV changes by two orders of magnitude the derived value of K_1 will only change by 1/2 order of magnitude. For the boundary between regions II and III if the PO_2 of the boundary changes by 1 order of magnitude the value of K_3 derived from that boundary will change by 1/2 of an order of magnitude. Based on these considerations the uncertainty of the activation energies is about 0.5 ev and the uncetainty of the preexponential (which is related to the uncertainty of the activation energy), is about $\pm x20$.

The analysis above has made use of data over a wide temperature range. At the lowest temperatures the gas phase may not be in equilibrium, resulting in an oxygen partial pressure which is not fixed by the buffer reaction. For example, if some reaction besides the CO/Co_2 reaction was fixing the oxygen partial pressure at 465°C, the conductivity at low oxygen partial pressures would not be a PO_2 independent conductivity but would be a single conductivity at a single PO_2. However, certain aspects of this study suggest that this did not effect the analysis. First, the samples were electroded with platinum paste to improve electrical contact; however, it is well known that platinum catalyzes gas phase reactions on its surface. Therefore, the sample, at least near the electrodes, is likely to have been in a PO_2 established by the thermodynamic equilibrium. Second, the data shows distinct PO_2 dependent oehavior at temperatures as low as 666°C; therefore, above that temperature the equilibrium should be well established. Third extrapolations of the PO_2 independent to pO_2 dependent transition from higher temperature indicates that no PO_2 dependence is expected at low temperatures in the low oxygen partial pressure region. Finally, the conductivity measured in the PO_2 independent region at low temperatures is consistent with the expected conductivity based on extapolations from higher temperatures where gas phase equilibrium is assured.

The region at high partial pressure and low

temperature, where the defect model used above does not apply, will now be examined. As was mentioned in the results section, the conductivity for the composition $Ce_{.95}U_{.05}O_{2+x}$ measured at 465°C and near one atmosphere of oxygen partial pressure (region VI), deviates from the expected 1/4 power law dependence on PO_2. The dependence is very close to conductivity proportional to $PO_2^{-1/2}$. Therefore, the simple model must be revised. The deviation from the simple model occurs at low temperature where defect-defect association reactions are known to occur. The region of conductivity proportional to $PO_2^{-1/2}$ at high PO_2 could be explained by the existence of singly charged oxygen interstitials; however, given the band diagram Figure II.B.3 it is unlikely that O_i'' will deionize as long as $U_{Ce}^{\bullet}$ controls the electroneutrality. Also, Catlow[14] has calculated that in UO_2 the singly charged oxygen interstitial is energetically less favorable than the doubly charged interstitial. However, in another calculation, Catlow[14] has shown that $(O_i'' \; h^{\bullet})'$ is stable relative to its constituents if the hole is localized on the second nearest neighbor. This indicates that such defect associations may also occur in CeO_2 even though the nature of the hole in CeO_2 is fundamentally different than that of a hole in UO_2. (In CeO_2 the holes are in the O_{2P} band while in UO_2 the holes are essentially $U_U^{\bullet}$). A defect model for urania doped ceria involving such an associated

pair is detailed in Tables VI.A.2and VI.A.3. This model assumes that the important defect association is

$$O_i'' + h^{\cdot} \Rightarrow (O_i'' h_{2NN}^{\cdot})' \qquad [(O_i'' h_{2NN}^{\cdot})']/[O_i'']p = K_8 \qquad \text{(VI.A.21)}$$

and correctly predicts the PO_2 dependence of the conductivity. Other defect associations which may intuitivelyseem more likely, such as $U_{Ce}^{\cdot}$ associating with an oxygen interstitial, do not predict the observed PO_2 dependence. Because of the limited data represented in this region and the uncertainty about the exact nature of the defects involved, no calculations of defect equilibria for this region are attempted.

Table VI.A.2 Defect concentrations for urania doped ceria including O_i'' $h^{\cdot}$ association.

Region	II	III	IV_{a1} may not be present	IV_{a2}
Limiting electroneutrality equation	$n=2[V_o^{\cdot\cdot}]$	$[U_{Ce}^{\cdot}]=U_T=n$	$[U_{Ce}^{\cdot}]=U_T=2[O_i'']$	$[U_{Ce}^{\cdot}]=U_T=[O_i''h_{2NN}^{\cdot}]$
PO_2 range	Low	Intermediate	Intermediate	High
$[V_o^{\cdot\cdot}]$	$2^{-2/3}K_3^{1/3}PO_2^{-1/6}$	$K_3U_T^{-2}PO_2^{-1/2}$	$[V_o^{\cdot\cdot}]=2K_1U_T^{-1}$	$K_1^2K_2^2K_3^{-1}U_T^{-2}PO_2^{1/2}$
$[O_i'']$	$2^{2/3}K_1K_3^{-1/3}PO_2^{1/6}$	$K_1K_3^{-1}U_T^2PO_2^{1/2}$	$2^{-1}U_T$	$K_1^{-1}K_2^{-2}K_3U_T^2PO_2^{-1/2}$
n	$2^{1/3}K_3^{1/3}PO_2^{-1/6}$	U_T	$2^{-1/2}K_1^{-1/2}K_3^{1/2}U_T^{1/2}PO_2^{-1/4}$	$K_1^{-1}K_2^{-2}K_3K_8U_TPO_2^{-1/2}$
p	$2^{-1/3}K_2K_3^{-1/3}PO_2^{1/6}$	$K_2U_T^{-1}$	$2^{1/2}K_1^{1/2}K_2K_3^{-1/2}U_T^{-1/2}PO_2^{1/4}$	$K_1K_2^2K_3^{-1}K_8^{-1}U_T^{-1}PO_2^{1/2}$
$[O_i''h_{2NN}]'$	$2^{1/3}K_1K_2K_3^{-2/3}K_8PO_2^{1/3}$	$K_1K_2K_3^{-1}K_8U_TPO_2^{1/2}$	$2^{-1/2}K_1^{1/2}K_2K_3^{-1/2}K_8U_T^{1/2}PO_2^{1/4}$	U_T

Table VI.A.3 Boundaries of defect regions described in Table VI.A.2.

	$III\text{-}IV_{a1}$	$III\text{-}IV_{a2}$	$IV_{A1}\text{-}IV_{A2}$
PO_2	$2^{-2}U_T^{-2}K_1^{-2}K_3^2$	$K_1^2K_2^2K_3^2K_8^{-2}$	$2^2K_1^{-2}K_2^{-4}K_3^2K_8^{-4}U_T^2$
K_8		$K_1^{-1}K_2^{-1}K_3PO_{2\,II\text{-}III_A}^{1/2}$	$2^{1/2}K_1^{-1/2}K_2K_3^{1/2}U_T^{1/2}PO_{2\,III\text{-}III_A}^{-1/4}$

URANIA RICH SOLID SOLUTIONS

A complete set of equilibria constants were derived for the ceria rich solid solutions. In principle the same type of analysis should provide similar information for the urania rich solid solutions. The defect relations near stoichiometry for the urania rich system are replotted in Figure VI.A.5. The relations are the mirror image of those for ceria. There is a PO_2 independent region bounded by PO_2 dependent regions at both higher and lower oxygen partial pressures. It is in this PO_2 independent region that the material passes through stoichiometry. The data illustrated in Figure V.B.1 is qualitatively consistent with this model. Clearly, by 5m/o ceria the material achieves both oxygen excess and oxygen deficiency at the limits of the PO_2 examined. Compared to the CeO_2 case, however, the PO_2 independent range is significantly narrower and gets visibly narrower with increasing cerium concentration. If the reaction constant for frenkel equilibria G_1 is calculated by the simple model, a strong dependence on ceria concentration is found. Another difference from the simple model is the very steep PO_2 dependence of the conductivity on oxygen partial pressure at high PO_2s. Therefore, the situation in ceria doped urania is more complicated than in urania doped ceria. However, it is

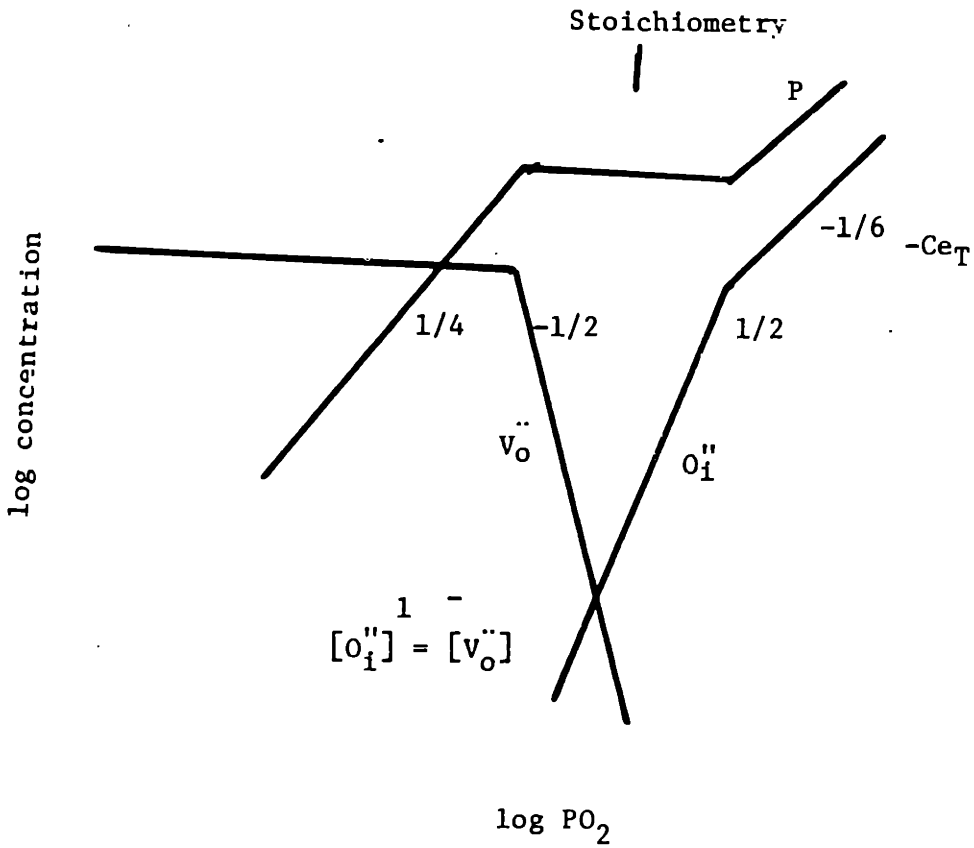

Figure VI.A.5 Schematic of defect concentrations near stoichiometry.

clear that ceria drives the solid solution far enough towards oxygen deficiency so that both oxygen deficient and oxygen excess material are observed.

A defect model will now be proposed in an attempt to derive some important defect parameters of the system. The defect chemistry for ceria doped urania detailed in the theory section (Table III.A.2.3) must be modified to be consistent with the data. This model predicted that the boundary between regions IV_A and III, $PO_{2IVA-III}$, would be proportional to Ce^4. It also predicted that the boundary between regions III and II_A, $PO_{2IIA-III}$, would be proportional to Ce^2. As can be seen in Figure VI.A.6, $PO_{2IVA-III}$ is proportional to $Ce^{1.5}$ and $PO_{2IIA-III}$ is proportional to Ce^x where x is between six and eight. The Ce dependence of $PO_{2IVA-III}$ is the inverse of the dependence of the hole concentration in region IV. Therefore, a model in which p is proportional to 2/3 in region IVA would fit the data better. As discussed in section III.A.2, the PO_2 dependence of the hole concentrations in this region is related to the ratio of net oxygen excess to net charge of the defect compensating for the holes. As discussed in section II.A, Catlow[14] and others have suggested that the (432) Willis clusters are an important defect in highly oxygen rich UO_2. Of the various charge states of this cluster, the $(432)'''$ cluster has the correct charge to oxygen excess ratio to result in a hole

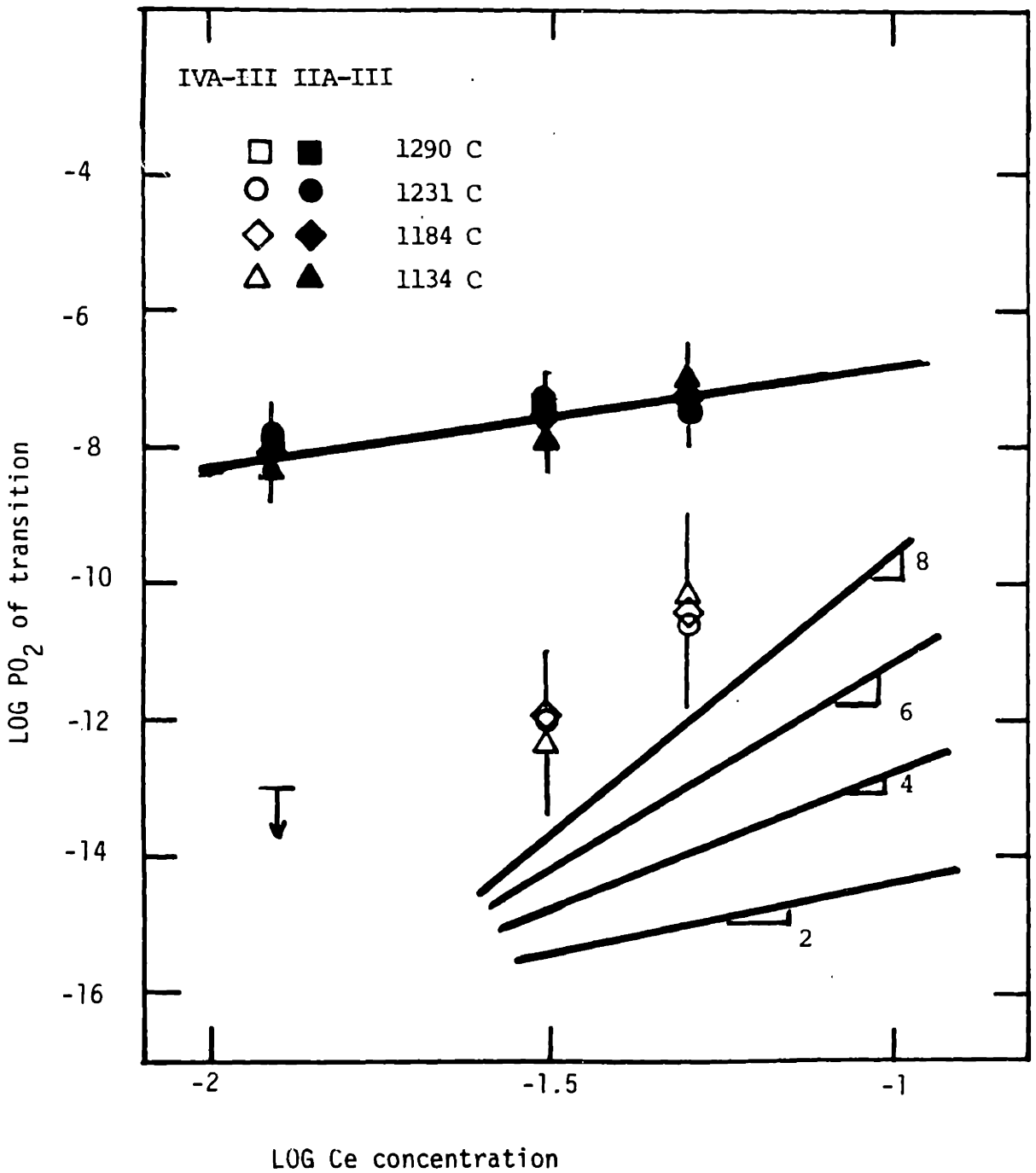

Figure VI.A.6 Log PO_2 of the boundary between regions IIA or IVA1 and region III vs ln Ce concentration.

concentration proportional to 5/8, which is very close to the value of 2/3 needed to fit the Ce dependence of the data. The details of the defect chemistry at high PO_2, assuming that at high PO_2 the electroneutrality is controlled by $3(432)''' = p$ and including the following defect association reaction

$$7O_i'' + 2V_O^{\cdot\cdot} + 7h \Rightarrow (432)''' \quad , G_8$$

is detailed in Table VI.A.4 for the higher oxygen partial pressure regions.

The Ce dependence of $PO_{2IIA-III}$ in a defect model is related to the number of Ce_U in the defect which compensates for the Ce_U' in region IIA. To account for $PO_{2IIA-III}$ proportional to Ce^6, it is necessary to postulate a defect which includes two Ce_U' for each $V_O^{\cdot\cdot}$. For example, a $(2Ce_U'V_O^{\cdot\cdot})$ defect would result in $PO_{2IIA-III}$ proportional to Ce^6. However, such a defect results in a hole concentration proportional to only $PO_2^{1/8}$. Another explanation of the strong relation between the concentration of ceria and $PO_{2IIA-III}$ is that one of the equilibrium constants in the expression for PO_2 is a function of ceria concentration. For example, assume that the activation energy of G_3 is a linear function of ceria concentration

$$G_3 = G_{3o}\exp(-(A+BCe_T)/(k_bT)).$$

Then the derivative of $\log(PO_{2IIA-III})$ from Table

Table VI.A.4 Defect chemistry of Ceria Doped Urania Assuming $[432]''' = p$ at High PO_2 $[Ce'_U] = Ce_T$.

Region	III	IV A
Controlling electroneutality equation	$Ce_T=P$	$[432]''' = 3P$
PO_2 range	Intermediate	High
$[V_o^{\cdot\cdot}]$	$Ce_T G_2^{-1} G_3 PO_2^{-1/2}$	$3^{-1/20} G_1^{-7/5} G_2^{12/5} G_3^{3/2} PO_2^{-3/4}$
$[O_i'']$	$Ce_T^{-1} G_1 G_2 G_3^{-1} PO_2^{1/2}$	$3^{1/2} G_1^{12/5} G_2^{-12/5} G_3^{-3/2} PO_2^{3/4}$
n	$Ce_T^{-1} G_2$	$3^{7/4} G_1^{-7/4} G_2^{6/4} G_3^{5/4} G_8^{5/4} PO_2^{-5/8}$
p	Ce_T	$3^{-7/4} G_1^{7/4} G_2^{-1/2} G_3^{-5/4} G_8^{-5/4} PO_2^{5/8}$
$[432]'''$	$Ce_T^2 G_1^7 G_2^5 G_3^{-5} G_8 PO_2^{5/2}$	$3^{-7/4} G_1^{7/4} G_2^{-1/2} G_3^{-5/4} G_8^{-5/4} PO_2^{5/8}$

III.A.2.6 with respect to log Ce_T is

$$2 - (2B\ Ce_T)/(k_bT).$$

From the data (Figure VI.A.6) this should have a value of about six. The value of the parameter B at a temperature of 1134C for Ce_T=.05 equals -4.85ev/mole . The data (Figure VI.A.7) confirms that this value is not unreasonably large. Unfortunately, the uncertainty of determining the PO_2 is large, and there are only two compositions for which data is available.

Equilibrium constants have not been determined because of uncertainty in determining $PO_{2IIA-III}$ and the possible effect of ceria on the equilibrium constants. However, Figure VI.A.8 and VI.A.9 show expected concentrations of the majority defects in the PO_2 range of the experiment.

The defect chemistry of both ceria rich and urania rich solid solution has been discussed. The results for ceria rich solid solutions are consitent with weekly interacting defects, allowing the determination of a complete set of defect reaction equilibrium constants. The urania system, on the other hand, deviates from the simple predictions. A cluster model was suggested which is consistent with the data, but due to the limited data available no unique solution was obtained.

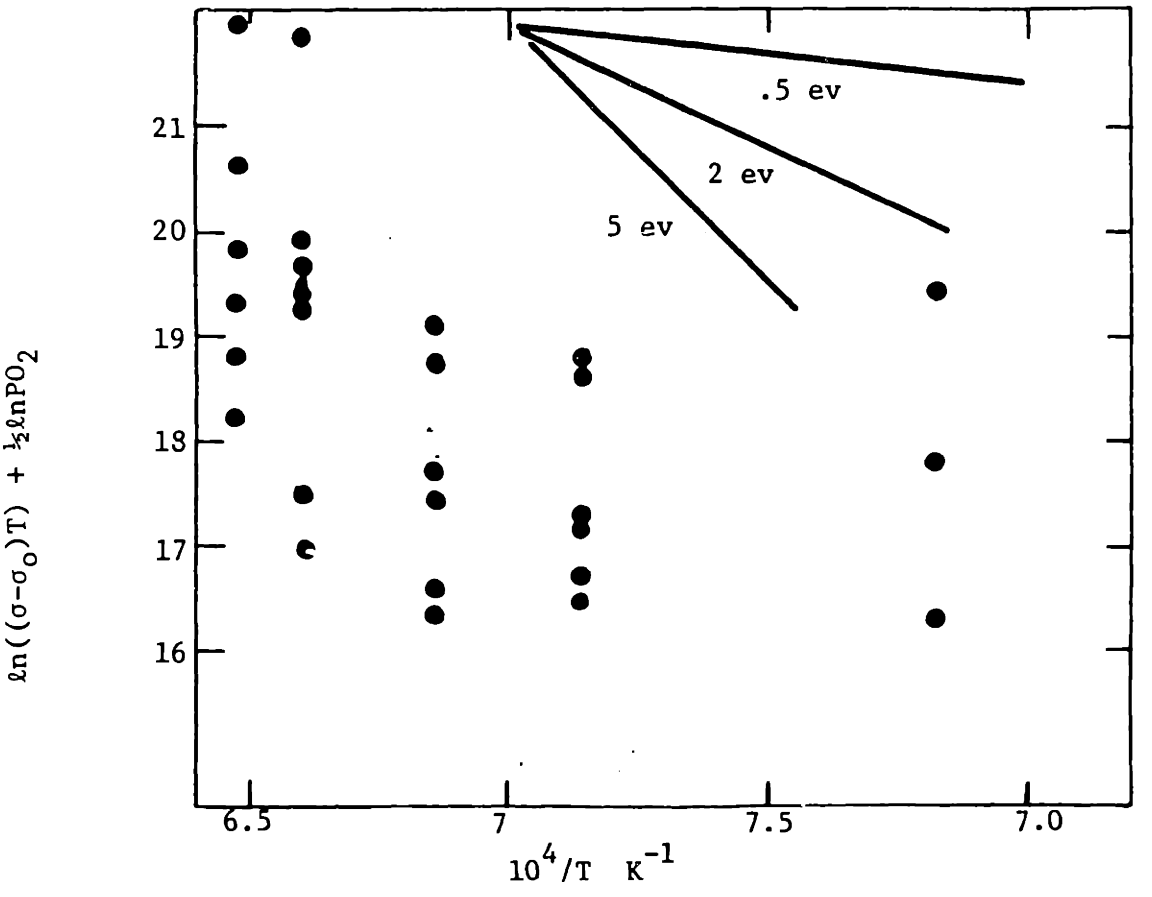

Figure VI.A.7 $\ln((\sigma-\sigma_o)) + 1/2\ln PO_2$ vs 1/T.

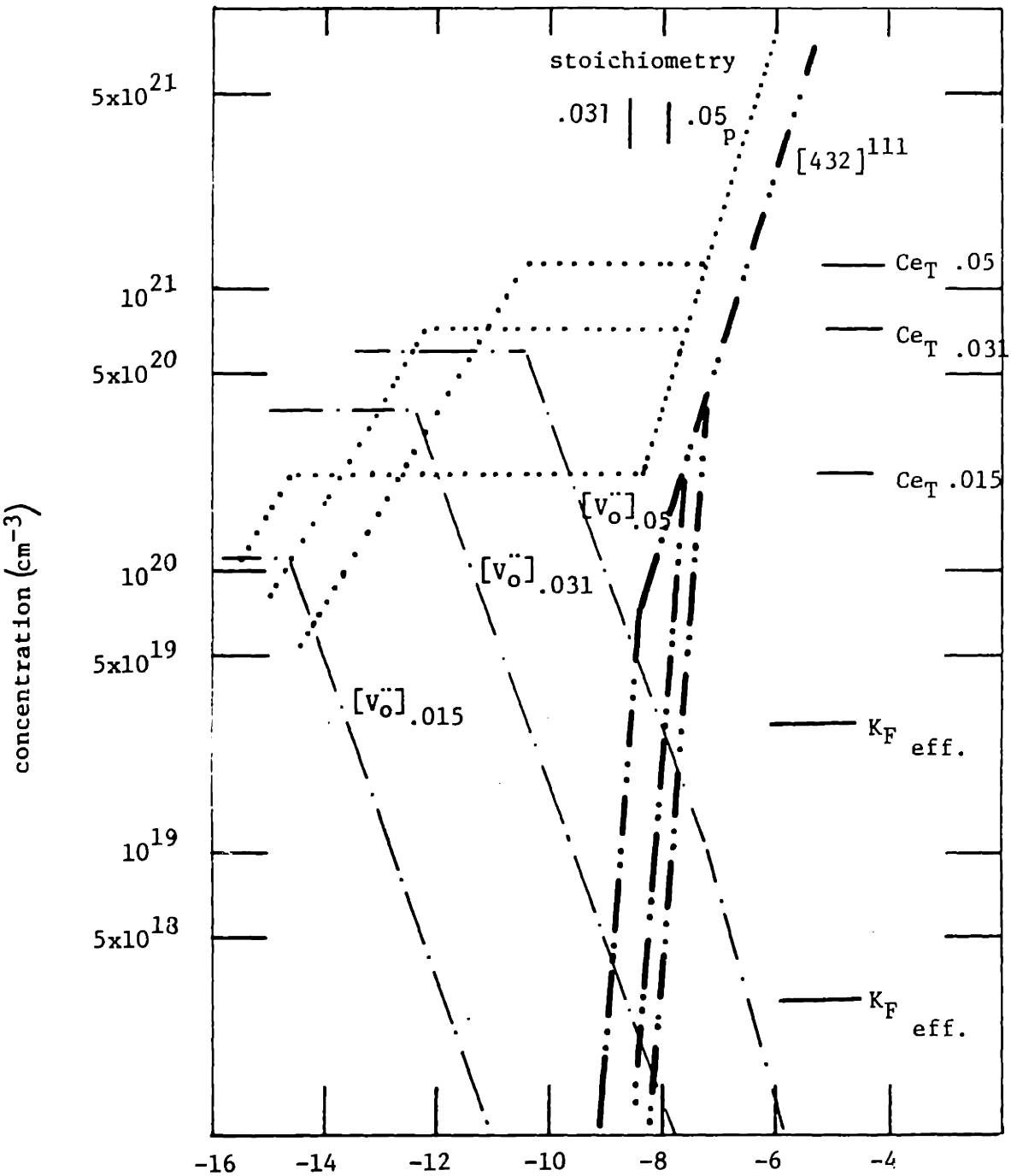

Figure VI.A.8 Defect concentrations in ceria doped $UO_{2\pm x}$ at 1134 °C.

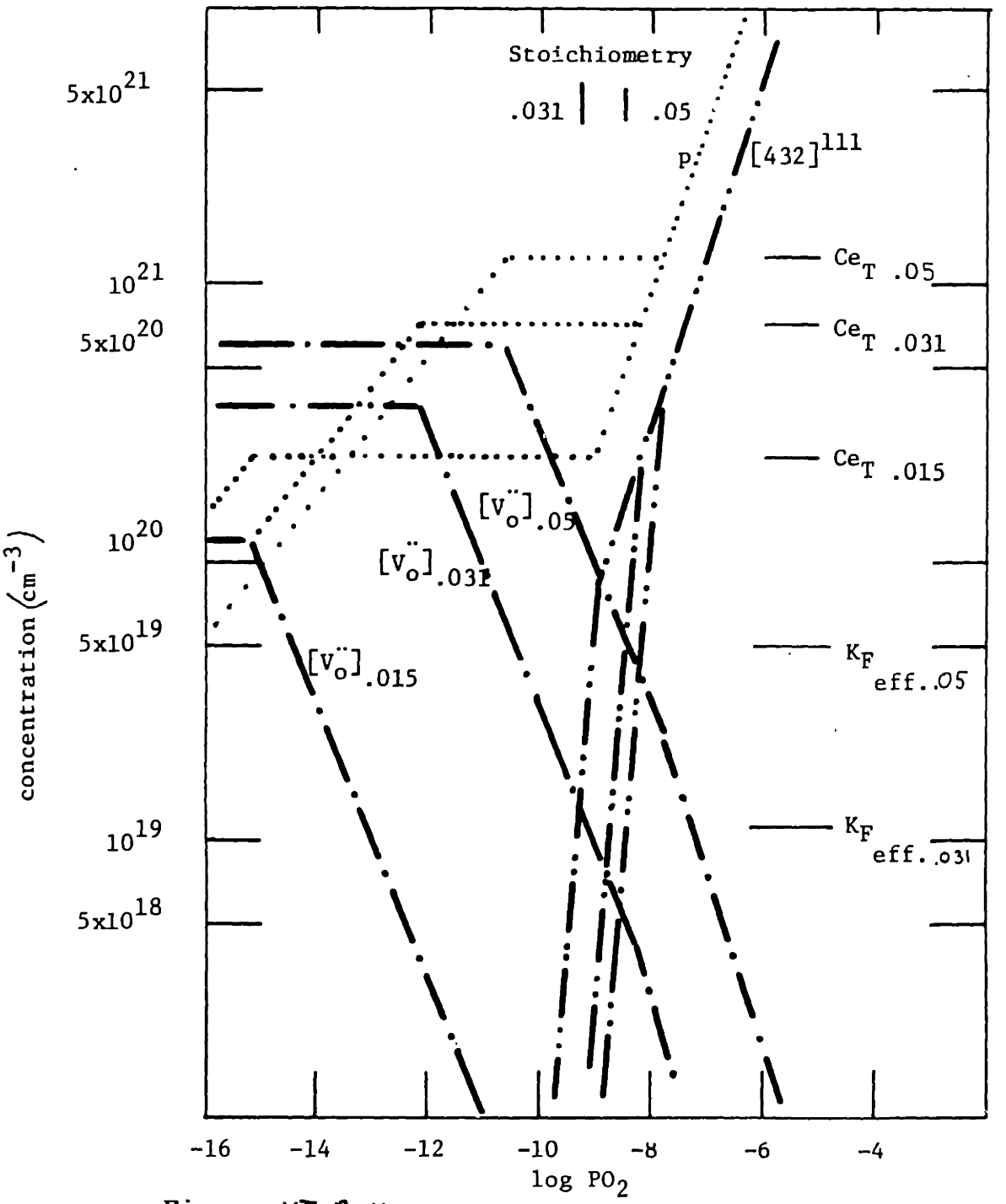

Figure VI.A.11 Defect Concentration in UO_2 1230 C

VI.B DISCUSSION OF THE TRANSPORT MECHANISMS

There is good deal of controversy in the literature as to the relative importance of small versus large polaron conduction in solids. Both urania and ceria exhibit conduction in narrow f bands which makes them both likely to exhibit small polaron conduction. However, due to coupling between the electron density and the defect structure, a simple derivation of the mobility is somewhat more difficult in these systems. This study makes use of the following special aspects to obtain more direct evidence. First, the regions of PO_2 independent conductivity are also regions of fixed carrier concentration, allowing a determination of the mobility from the conductivity. The conductivity was measured on both sides of stoichiometry so that contributions to mobility from ionic defects can be observed. Second, the density of carriers was varied over a wide range of concentrations. Third, both TEP and conductivity were measured, in principle allowing separation of the mobility and concentration components in the conductivity. Fourth, carrier concentrations close to the half filled band were examined. This information will provide additional evidence for the small polaron conduction mechanism.

TRANSPORT IN CERIA RICH SOLID SOLUTIONS

The rate of change of the conductivity with temperature in the PO_2 independent region allows

determination of the mobility of the charge-carrying species because the concentration of carriers is fixed by the dopant. Figure V.A.2 shows that the activation for mobility in the ceria rich solid solutions is about .31ev. This value is independent of the composition indicating that the uranium does not effect the activation energy. Using this data for 0.1m/o urania, equation III.B.1.3, and equation III.B.1.2 a mobility of

$$\mu = 226 \exp(-0.31 \pm .05 \text{ ev}/kT)/T \quad (cm^2/Vs)$$

is calculated. This value compares well to the value determined by Tuller and Nowick[29] for pure ceria. There is some effect of the uranium on total conductivity as can be seen in Figure V.A.4. This figure shows that at concentrations above 0.1m/o, the uranium tends to decrease the mobility. Because of the dopant independent activation energy, the dopant effect must be limited to the preexponential. As noted in section II.A, Tuller and Nowick also observed a dependence of the mobility on the composition.

The change of composition Tuller and Nowick observed was the result of changes of stoichiometry as the material was oxidized or reduced. They use a model which assumes that electrons become trapped between two adjacent oxygen vacancies. This model, while possibly appropriate for highly substoichiometric materials, is inappropriate in the

case of urania doped ceria in the region in which the conductivity is independent of PO_2, because the material changes from substoichiometric to superstoichiometric as the PO_2 is increased in this region, and mobility should change rapidly if it were due to interactions between vacant oxygens and electrons. Because the mobility does not change as stoichiometry is changed, it may be inferred that for defect concentrations up to about 5m/o, no significant defect-electron interactions take place in the presence of uranium ions.

Another possible explanation for the decrease of the mobility is polaron-polaron repulsion. A polaron on a given lattice site effectively excludes other polarons from occupying the lattice sites for some region around it. This repulsion effect was included as B in equation III.B.1.7. This parameter measures the number of empty polaron sites removed when a dopant is added. For the simple theory B=1, this accounts for the site loss of an empty site due to an additional electron in the material. The presence of a polaron on a site excludes other polarons from occupying that site, but ignores the loss of a site due to the replacement of a cation site by the dopant. To account for this, B=2. Then conductivity is proportional to y(1-2y). Where y is the mole fraction of dopant. If the presence of a polaron on a site effectively excludes other polarons from its own site and some number of other sites,

B will be correspondingly increased. Figure VI.B.1 shows the data for ceria rich solid solutions at 1134°C along with the expected value of the conductivity given B=2,B=8, and B=16. From this figure it is apparent that to account for the effect of uranium on the mobility by this mechanism, B must be somewhat larger than 8. Therefore, the number of excluded sites per electron is about 8, and then an additional site is removed by each dopant ion. If this mechanism is responsible for the effect of uranium on conductivity, then it should occur at any carrier concentration. To determine if this is the case, calculations were made of the expected TEP nose at high carrier concentration. These results are plotted in Figure VI.B.2. and show that the data at high carrier concentration can be accounted for with a site exclusion value of only 2 to 3. Based on this analysis (which is strictly valid only for the one dimensional case), it must be concluded that the effect of dopant cannot be completely accounted for by polaron polaron site exclusion.

GENERAL COMMENTS REGARDING THE NOSE OF THE TEP PLOTS

Having just used the theoretical calculation of the TEP nose, it is appropriate to discuss some implications. First from Figure V.A.5 it is obvious that the extrema of the data all fall below the TEP=0 line. Previous analysis[65] had suggested that such a displacement when

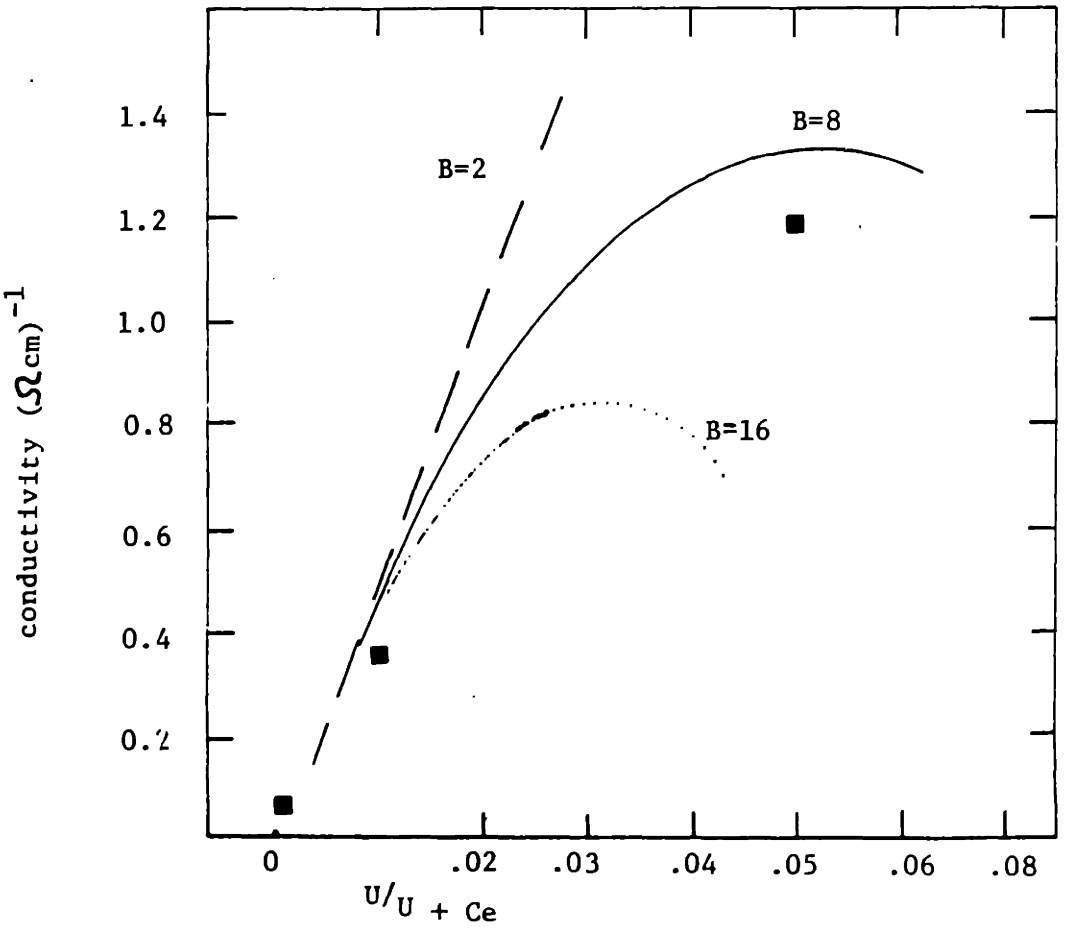

Figure VI.B.1 Conductivity vs composition T = 1134, and theory including polaron-polaron repultion.

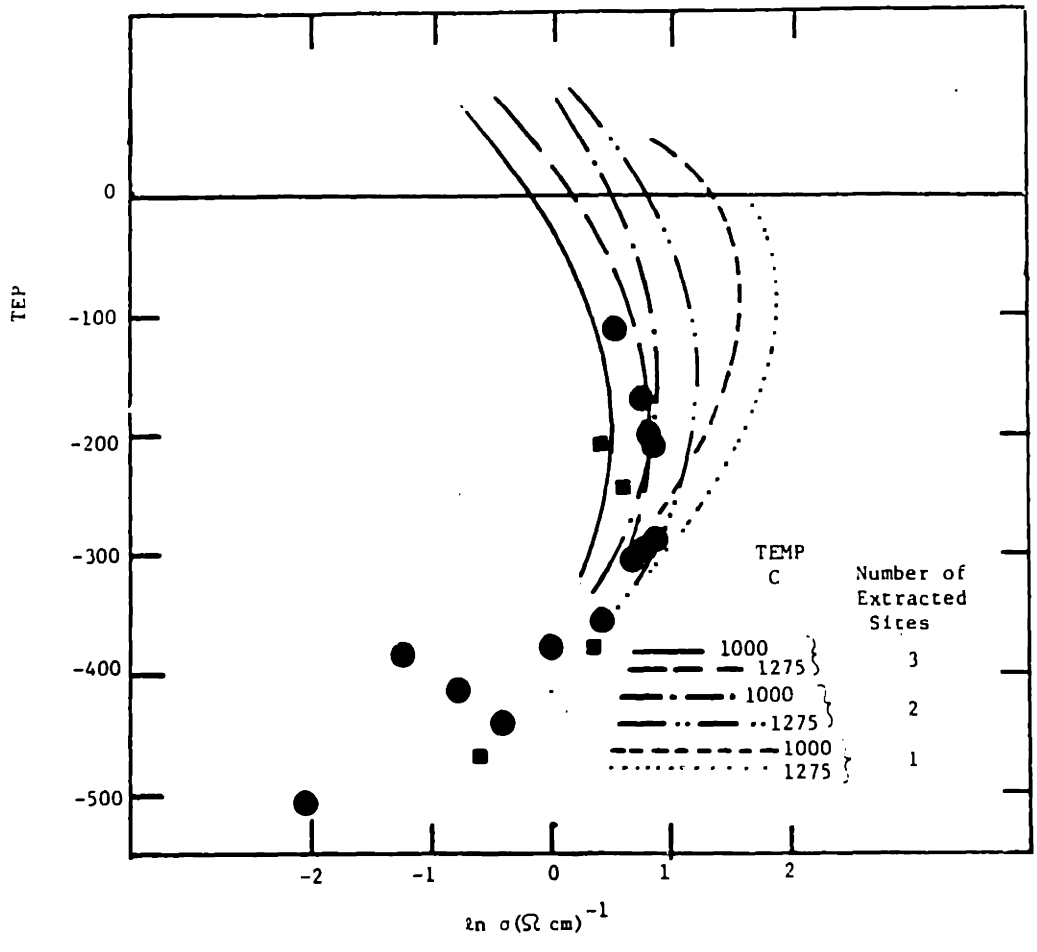

Figure VI.B.2 TEP vs. ln(σ) from figure V.A.5.a and theoretical curves including polaron-polaron repulsion.

analysis[65] had suggested that such a displacement when extrapolated from lower carrier densities, was associated with a difference of the mobilities of the electron and the holes. In this case, the dis lacement is not related to the mobility but to the difference of the carrier entropies.

TRANSPORT IN THE URANIA RICH SOLID SLOLUTIONS

The conductivity TEP relations in the urania rich solid solutions will now be discussed. The conductivity of the urania rich solid solutions was plotted in a $\ln(\sigma T)$ vs $1/T$ in Figure V.B.3. From this the mobility can be determined if the data is from a PO_2independent region. This is the case for the composition of $Ce_{.015}U_{.985}O_{2\pm x}$ but is not the case for the higher doping levels. The mobility of holes is then calculatd to be

$$\mu = (1.462 \times 10^3/T) \exp(-0.31 \pm .05 \text{ ev}/K_b T).$$

The preexponential value calculated here is significantly higher than that predicted from the theory. It is about three times the value determined by Dudney[24] for yttria doped urania.

The compositional dependence of the conductivity (Figure V.B.4) is also very different from that found by Dudney for yttria doped urania, although the conductivity of both yttria doped urania and ceria doped urania is approximately the same at 1.5 m/o dopant. At 3.1 and 5 m/o

yttria concentrations greater than one m/o. However, for ceria doped urania the conductivity is very close to being linearly dependent on the ceria concentration up to at least 5 mole per cent.

There are three differences between the conductivity of yttria doped urania and ceria doped urania. The energy of migration for ceria doped urania is about .1 ev larger than for yttria doped urania. In ceria doped urania the preexpontntial is about 1/2 that of yttria doped urania and the preexponential is much less dependent on the concentration of dopant in the ceria doped urania.

The TEP measurement provides valuable information about the concentration of carriers and about the way the carriers interact with each other. In Figure V.B.5 we see the TEP of urania rich solid solutions. The curve for $Ce_{.015}U_{.985}O_{2+x}$ is a nicely linear plot with a slope very close to k/e. This is consistent with the simple model for polaron conduction.

At higher cerium concentrations, the curves are not so simple. At about the conductivity at which the oxygen partial pressure power law changes from PO_2independent to $PO_2^{1/4}$, the TEP becomes independent of conductivity. One explanation is that some other species becomes important in the conduction process which has a large contribution to the thermoelectric power but has a small enough conductivity that it does not change the observed power

law. One of the major species present in the region is $[V_O^{\cdot\cdot}]$. Based on calculated oxygen vacancy formation energies, Sugisaki et al.[57] have suggested that for plutonia doped urania Q^* of $V_O^{\cdot\cdot}$ is -485 kJ/mole. This is a very large value and results in a large contribution to the TEP, even for a small contribution to the total conductivity from the vacancy. Figure VI.B.3 shows plots of $\ln \sigma$ vs TEP for several values of the mobility ratio for holes and vacancies, μ_{Vo}/μ_p.

The curves were calculated for a doping concentration of 5 m/o using the mobility of holes calculated from the 1.5m/o data. The Brouwer approximation was used so the three defect regions have sharp boundaries. The "glitch" in the curve at about $\ln \sigma = 3$ is a result of this assumption. The curves show that for a mobility ratio of about .015 the general correct shape is produced. At this temperature $\mu_{hole} = .080\ cm^2/Vs$. Therefore, $\mu_{Vo} = 1.2 \times 10^{-3}\ cm^2/Vs$. Table VI.B.1 is a comparison of this value to the ionic mobility of other fluorite materials. The ionic contribution to the total conductivity at this temperature is 0.3 $(ohm\ cm)^{-1}$, which is small enough that it would not markedly change the measured conductivity. The ionic conductivity is about two times the ionic conductivity for $(U,Pu)O_{2-x}$ as calculated from the diffusion data of Bayoglu and Lorenzelli[73] at 1400°C using the Nernst-Einstein relation.

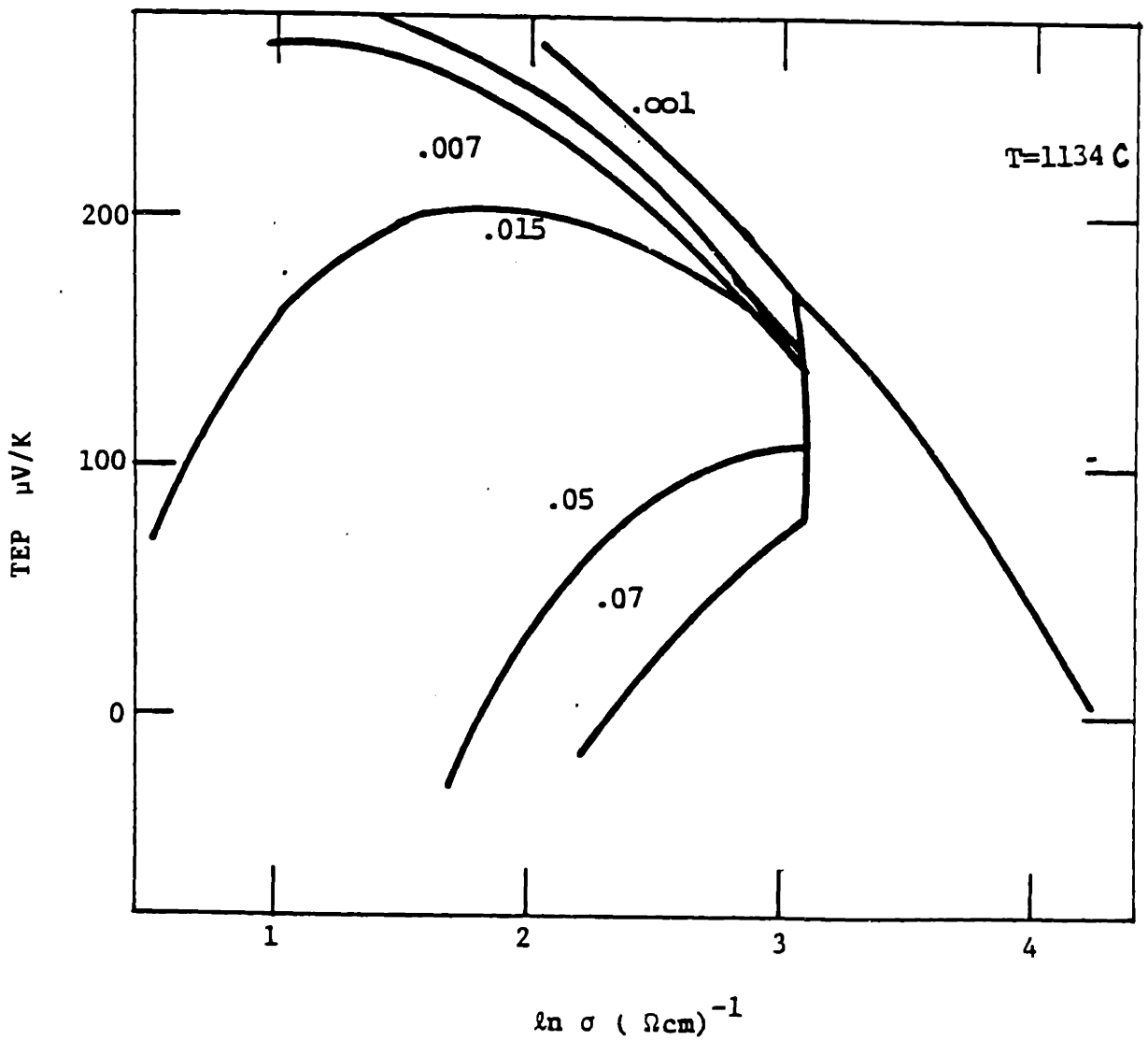

Figure VI.B.3 Theoretical Curves of ln(σ) vs TEP Including Contribution from Oxygen Vacancies
Numbers on curves are μ_{V_o}/μ_p ratio

Table VI.B.1
COMPARISON OF MOBILITIES FOR SEVERAL FLUORITE OXIDES

Material	Moblity
CeO_2 (+5m/o Y_2O_3)[70]	= 1.2 exp(-0.87 ev/kT) = 9.1×10^{-4} (1407 K)
ZrO_2(+12 m/o Y_2O_3)[71]	= 0.42 exp(-0.99ev/KT) = $1.19 \times^{-4}$ (1407 K)
ThO_2(7½m/o Y_2O_3)[72]	= 0.15 exp(-1.0 ev/KT) = 3.9×10^{-5} (1407 K)
UO_2(5 m/o CeO_2) speculative	= $1.23 \times^{-3}$(1407 K)

The above analysis suggests that ceria doped urania is amixed conductor with ionic mobilities close to or higher than the ionic mobility of other oxides with the fluorite structure.

Another possible contribution to the TEP is due to electrons. If the electrons have a large mobility so that there is some contribution to the TEP while the concentration is still low enough that the total conductivity is not significantly changed, a bend of the curve of ln vs TEP similar to the bend suggested from the oxygen vacancies would occur. The conductivity at which the bend occurs is dependent on the ratio of the mobilities of the electrons and holes and on the np product. If neither of these ratios is a function of the cerium concentration, then the conductivity of the bend will be independent of the cerium concentration also. The data (Figure V.B.5.A) shows that the conductivity of the bend decreases with decreasing cerium concentration. Therefore it is unlikely that the electron contribution to the TEP causes the bend in the ln σ vs TEP curves.

VII CONCLUTIONS

This study has used electrical conductivity and thermoelectric power measurements in conjunction with a detailed defect model and a synthesised band digram to examine the defect chemistry and electrical properties of urania ceria solid solutions. We have demonstrated excellent agreement with a detailed defect model and have for the first time obtained reaction equilibria constants for the intrinsic Frenkel ionic disorder. The Frenkel product for ceria rich solid solutions was determined to be

$$K_1(.99) = 2.3\times10^{50}\times10^{\pm1.5}\ \exp(-4.37\ ev/k_bT).$$

In addition to the Frenkel product, a complete set of defect equilibrium reaction constants was determined for the ceria rich solid solutions.

Both urania rich and ceria rich compositions were shown to be both oxygen excess and oxygen deficient in the range of temperatures and oxygen partial pressures studied.

We have confirmed the small polaron conduction mechanism in both urania and ceria rich compositions by observing an activated mobility with a value

$$= (226/T)\ \exp(-0.31\pm.05\ ev/kT)$$

for ceria rich solid solutions and

$$= (1.462E3/T)\ \exp(-0.31\pm.05\ ev/\ kT)$$

for urania rich solid solutions. The magnitude is on the

order of that expected for small polaron conduction.

FUTURE WORK

Future work should focus on the annomouls TEP vs ln conductivity results in urania rich compositions to attempt to disiquish between the oxygen vacancy model suggested here and the posibility of other contributions to the TEP. Two types of experiments would be fruitful: first, more precise TEP measurements and second oxygen diffusion studies at low PO_2.

It would also be usefull to have more reliable data on the band structure of urania ceria solid solutions. This would require fabrication of single crystals of the solid solution. Once crystals are available, standard optical spectroscopy and photo-electrochemical spectroscopy will be useful to study the band structure.

BIBLIOGRAPHY

1. N.J. Dudney "The Electrical Properties of Pure and Yttria Doped Uranium Dioxide" , PhD Thesis , MIT, (1979)

2. H.L. Tuller and A.S. Nowick, "Doped Ceria as a Solid Oxide Electrolyte", J. Electro. Chem. S. 122, 255, (1975)

3. S. Aronson and J. Belle, "Nonstoichiometry in Uranium dioxide", J.Chem. Phys., 29, 151, (1958)

4. L.E.J. Roberts and T.L. Markin, "Thermodynamics of Non-stoicheiometric Oxide Systems",

5. Y. Saito "Nonstoichiometry in Uranium Dioxide", J. Nuc. Mat., 51, 112, (1974)

6. D.J.M. Bevan,J. Inorg. Nucl. Chem., "Ordered Intermediate Phases in the System CeO_2-Ce_2O_3", 1, 49,(1955)

7. D.J.M. Bevan and J. Kordis "Mixed Oxides of the Type MO_2(Fluorite)-M_2O_3 I; Oxygen Dissocation Pressures and Phase Relationships in the system CeO_2-Ce_2O_3 at High Temperatures", J. Inorg. Nucl. Chem., 26, 1509, (1964)

8. R.J. Panlener, R.N. Bluementhal, and J.E. Garnier, " A Thermodynamic Study of Nonstoichiometric Cerium DioxideP", J. Phys. Chem. Solids., 36, 1213, (1975)

9. H.L. Tuller "Electrical Properties and Defect Model of Nonstoichiometric and Impurity-Doped CeO_2", Doctoral Thesis, Columbia University, (1973)

10. L.M. Kovba, Dokl. Akad. Nauk SSSR 194, 98, (1970);Dokl. Chem.(Engl. Transl.)194, 632, (1970); As Sited in Phase Diagrams for Cerimists Fig.5024.(Pub. American Ceramic Society, Columbus Ohio)

11. B.T.M. Willis, "Positions of the Oxygen Atoms in $UO_{2.13}O_2$", Nature, 197, 755, (963)

12. M.R. Thornber and D.J.M. Bevan, Mixed Oxides of the Type MO_2(Fluorite)-M_2O_3. IV. Crystal Structures of the High and Low Temperature. Forms of $Zr_3Yb_4O_{12}$.", J. Sol. Stat. Chem. 1, 536, (1970)

13. F.A. Kroger, "Search for a Defect MOdel for UO_2", Z.Phys. Chem., 49, 178, (1972)

14. C.R.A. Catlow, "Point Defect and Electronic Properties of Uranium Dioxide" Proc. R. Soc. Lond. A., 353, 533, (1977)

15. R.W. Willardson, J.W. Moody and H.L. Goering,"The Electrocal Properties of Uranium Oxides",J. Inorg. Nucl. Chem., 6 19, (1958)

16. L. Nagels, J. Devreese, and M. Denayer, "Electronic Conduction in Single Crystals of Uranium Dioxide", J. Appl. Phys., 35, 1175, (1964)

17. S. Aronson, J.E. Rulli, and B.E. Schaner, "Electrical Properties of Nonstoichiometric Uranium Dioxide", J. Chem. Phus., 35, 1382, (1961)

18. H.P. Myers, T. Jonsson, and R. Wesrin, "Intrinsic Semiconduction in Uranium Dioxide", Sol. Stat. Comm., 2, 321, (1964)

19. S. Iida, "Electrical Properties of Non-Stoichiometric Uranium Dioxide", Jap. J. Appl. Phys., 4, 833, (1965)

20. J. Devreese, R. DeConinck, and H. Pollak,"On the Conduction Mechanism in Uranium Dioxide", Phys. Stat. Sol. 17, 825 (1966)

21. R. DeConinck and J. Devreese, "The Themoelectric Power and the Conduction Mechanism in Nearly Stoichiometric Uranium Dioxide Single Crystals", Phys. Stat. Sol., 32, 823, (1969)

22. T. Ishii, K. Naito, and K. Oshima, "Electrical Conductivity and defect structures in Non-Stoichiometric UO_{2+x}", J. Nuc. Mat., 36, 288, (1970)

23. J.C. Killeen, "The Effect of Niobium Oxide Additions on the Eletrical Conductivity of UO_2", J. Nuc. Mat., 88, 185, (1980)

24. N.J. Dudney, R.L. Coble, and H.L. Tuller, "Electrical Conductivity of Pure and Yttria-Doped Uranium Dioxide", J. Amer. Cer. Soc., 64, 627, (1981)

25. J.L. Bates, C.A. Hinman, and T. Kawada, "Electrical Conductivity of Uranium Dioxide", J. Amer. Cer. Soc., 50, 652, (1967)

26. N.J. Dudney, R.L. Coble, and H.L. Tuller, "Galvanic cell Measurements with Stabilized Zirconia and Platinum Electrodes.", J.Am.Ceram.S., 64, 621, (1981)

27. Tuller and Nowick, "Defect Structure and Electrical Properties of Nonstoichiometric CeO_2 Single Crystals", JECS, 126, 209, (1979)

28. I.K. Naik and T.Y. Tien, "Small-Polaron Mobility in Nonstoichiometric Cerium Dioxide", J. Phys. Chem. Solids, 39, 311, (1978)

29. H.L.Tuller and A.S. Nowick, "Small Polaron Electron Transport in Reduced CeO_2 Single Crystals", J. Phys. Chem. Solids, 38, 859, (1977)

30. I.K. Naik and T.Y. Tien, "Electrical Conduction in Nb_2O_5-Doped Cerium Dioxide", JECS, 126,562, (1979)

31. Sargent Welch Periodic Table

32. T.L. Markin, R.S. Street, and E.C. Crouch, "The Uranium-Cerium-Oxygen Ternary Phase Diagram", J. Inorg. Nucl. Chem. 32, 59, (1970)

33. R. Lorenzelli and B. Touzelin, "Sur le System UO_2-CeO_2;Etude Cristallographique a Haute Temperature", J. Nuc. Mat., (5, 290, (1980)

34. M. Hoch and F.J. Furman, "Non-Stoichiometry of UO_2-CeO_2", Thermodynamics, 2,1965 IAEI,Vienna, 517, (1966)

35. T.L. Markin and E.C. Crouch, "Thermodynamic Data for U-Ce-Oxides", J. Inorg. Nucl. Chem., 32, 77, (1970)

36. I.R. Cox, "Fission Products in Uranium Dioxides, A Preliminary Thermodynamic Study of Urania/Ceria Mixtures", Vacation Training Report(summer 1972) job# VF569, Central Electricity Research Labs.

37. R.C. Brown, "A Thermodynamic Investigation into Urania/Ceria Solid Solutions II", Dragon Project Technical Note, DPTN/728, OECD High Temperature Reactor Project Dragon, AEE, Winfrith, Dorchester, Dorset, England, (1975)

38. R.J. Ackermann, R.J.Thorn, and J. Winslow, "Visible and Ultraviolet Absorption Properties of Uranium Dioxide Films", Optical S. Amer., 49, 1107, (1959)

39. B.W. Veal and D.J. Lam, "X-ray Photoemission Spectroscopy Study of Hexavalent Uranium Compounds", Phys. Rev. B, 10, 4902, (1974)

40. J. Schoenes, "Optical Properties and Electronic Structure of UO_2", J.Appl.Phys. 49,1 463, (1978)

41. J.H.Wood, M. Boring and S. Woodruff, "Relativistic Electronic Structure of UO_2^{++}, UO_2^{+}, and UO_2", J.Chem. Phys.,74,5225,(1981)

42 Y. Baer and J. Schoenes, "Electronic Structure and Coulomb Correlation Energy in UO_2" Sol. State Comm., 33, 885, (1980)

43. P.R. Norton, R.L. Tapping, D.K. Creber, and W.J.L. Buyers, "Nature of the 5f electrons in uranium nitride: A Photoelectron Spectroscopic Study of UN,U,UO_2,ThN, and Th", Phys. Rev. B., 21, 2572, (1980)

44 G. C. Allen, P.M. Tucker and J.W.Tyler, "Oxidation of Uranium Dioxide at 298 K Studied Using X-ray Photoelectron Spectroscopy", J.Phys.Chem., 86 ,224,(1982)

45 G. Hass, J.B.Ramsey, and R.Thun, "Optical Properties and Structure of Cerium Dioxide Films", J. Optical S. Amer.,48, 324, (1958)

46. I.V. Vinokurov, Z.N. Zonn, and V.A. Ioffe, "Electrical Properties of Cerium Dioxide Single Crystals", Sov. Phy. Sol. Stat., 9, 2659, (1968)

47. A.F. Andreeva and Y. Gil'man, "Some Optical Properties of Films of Rare Earth Metal Oxides", Trans. from Zhuranal Prikladnoi Spektroskopii, 28, 895, (1978)

48. J.M. Kowalski, K.H. Johnson, and H.L. Tuller, "Models for the Photo electrolytic Decomposition of Water at semiconducting Oxide anodes", J.E.C.S., 127, 1969, (1980)

49. C. Wagner, and W. Z. Schottky, Z. Phys. Chem. B11, 163, (1931)

50. F. A. Kroger and H. J. Vink, Solid State Physics,3, 310 (1956)

51. D.R. Sempolinski and W.D. Kingery, "Ionic Conductivity and Magnesium Vacancy Mobility in Magnesium Oxide", J. Amer. Cer.Soc. 63,664,(1980)

52. D.R. Sempolinski, W.D. Kingery and H.L.Tuller, "Electronic Conductivity of Single Crysalline Magnesium Oxide", J. Amer. Cer.Soc. 63,669,(1980)

53. H. Fujimoto, "The Electrical Properties and Defect Structure of Doped Thorium Dioxide", PhD thesis, MIT, (1982)

54. A. McHale,"Non-Stoichiometry and Charge Transport in Ta_2O_5", Ph.D thesis, MIT, (1982)

55. Brouwer, Philips Res. Rep., 9, 366 (1954)

56. C. Kittel, Introduction to Solid State Physics, ed.5, John Wiley & Sons, New York, (1976)

57. M. Sugisaki, S. Sato, and H. Furuya, "Solid Phase Thermal Diffusion as a Mechanism for Oxygen Redistribution in $UO_{2\pm x}$ and $(U,Pu)O_{2\pm x}$", J.Nucl. Mat.. 97, 79, (1981)

58. N.N. Greenwood, Ionic Crystals Lattice Defects and Nonstoichiometry, Butterworths, London, (1968)

59. G.L. Sewell, "Model of Thermally Activated Hopping Motion in Solids", Phys.Rev.,129,597, (1963):K.D. Schotte, "The Thermoelectric Properties of the Small Polaron", Z.Phys., 196,393, (1966)

60. D. Emin, "Transport Properties of Small Polarons", J.Sol.St.Chem.,12, 246, (1975)

61. J.D. Hodge, "Thermoelectric Power Measurements in Wustite", Ph.D.Thesis, MIT, (1980)

62. I.G. Austin and N.F. Mott, "Polarons in Crystalline and Non-Crystalline Materials", Adv. in Phys., 18, 41, (1969)

63. P.M. Chakin And G. Beni, "Thermopower in the Correlated Hopping Regime", Phys. Rev. B, 13, 647, (1976)

64. J. Tauc, Photo and Thermoelectric effects in Semiconductors, Pergamon Press, NY, (1962) as referenced in Hodge(Ref. 61)

65. G.H. Jonker, "The Application of Combined Conductivity and Seebeck Effct Plots for the Analysis of Semiconductor Properties", Philips Res. Repts. 23, 131, (1968)

66. Marchant,"Behavior of Uranium Dioxide in a Thermal Gradient", Ph.D. Thesis, MIT, (1974)

67. H. W. Russell, J.Amer. Cer. Soc., 18, 1, (1935)

68. J.S. Anderson, "The Conditions of Equilibrium of 'Non-stoichiometric' cChemical Compounds", Proc. Royal Soc., A185, 69, (1946)

69. Shiun Ling, Columbia University, personal communication

70. H.L. Tuller, "Mixed Conduction in Non-stoichiometric Oxides",Non-Stoichiometric Oxides ed. O. Toft Sorensen, Academic Press

71. T.G. Stratton, D. Reed, and H.L. Tuller, "Study of Boundary Effects in Stabilized Zirconia Electrolytes", Advances in Ceramics Vol #1, Grain Boundary Phenomena in Electronic Ceramics, Amer. Ceram. Soc., (1981)

72 M. Iqbal, E.H. Baker, High Temp. - High Press., 5, 265, (1973)

73. A.S. Bayogulu and R. Lorenzelli, "Diffusion Chimique de l'Oxygen dan $(U,Pu)O_{2-x}$, J. Nucl. Mat., 79, 437, (1979)

BIOGRAPHICAL NOTE:

I was born in Greenville PA and grew up in Cheshire CT. I graduated from Mundelien High School which is located north west of Chicago. Following high school I atter.ded Concordia College in Moorhead MN, majoring in mathematics and physics. After graduation I moved to Cambridge MA.

I was married on the ninth of June in 1979 to Beverly Jean Brokke.

I have accepted a job with Ray Chem corporation in Menlow park CA, and am very excited about the potential contribution I will be able to make to the technology of ceramics with that company.